rec'd 4/20/81
fm Dancer

REPORT NO. FRA/ORD-80/6

PB 80-162266

RESULTS AND ANALYSIS OF THE SWITCHYARD IMPACT TESTS

Oscar Orringer
Pin Tong

U.S. DEPARTMENT OF TRANSPORTATION
RESEARCH AND SPECIAL PROGRAMS ADMINISTRATION
Transportation Systems Center
Cambridge MA 02142

FINAL REPORT

Prepared for
U.S. DEPARTMENT OF TRANSPORTATION
FEDERAL RAILROAD ADMINISTRATION
Office of Research and Development
Office of Rail Safety Research
Washington DC 20590

Technical Report Documentation Page

1. Report No.	2. Government Accession No.	3. Recipient's Catalog No.

4. Title and Subtitle

RESULTS AND ANALYSIS OF THE SWITCHYARD IMPACT TESTS

5. Report Date

6. Performing Organization Code

8. Performing Organization Report No.

DOT-TSC-FRA-79-15

7. Author(s)

Oscar Orringer, Pin Tong

9. Performing Organization Name and Address

U.S. Department of Transportation
Research and Special Programs Administration
Transportation Systems Center
Cambridge MA 02142

10. Work Unit No. (TRAIS)

RR928/R0206

11. Contract or Grant No.

13. Type of Report and Period Covered

Final Report
Dec 1975 - Dec 1978

12. Sponsoring Agency Name and Address

U.S. Department of Transportation
Federal Railroad Administration
Office of Research and Development
Office of Rail Safety Research
Washington DC 20590

14. Sponsoring Agency Code

15. Supplementary Notes

16. Abstract

This report presents the results and analysis of series 3 through 7 and series 10 of the FRA/RPI/AAR Switchyard Impact Tests. The test results and analysis are used to evaluate the head shield and the shelf-E coupler as protective devices for hazardous-materials tank cars.

17. Key Words	18. Distribution Statement
Crashworthiness; Hazardous Materials, Safety Impact Tests, Tank Car	DOCUMENT IS AVAILABLE TO THE PUBLIC THROUGH THE NATIONAL TECHNICAL INFORMATION SERVICE, SPRINGFIELD, VIRGINIA 22161

19. Security Classif. (of this report)	20. Security Classif. (of this page)	21. No. of Pages	22. Price
Unclassified	Unclassified	146	

Form DOT F 1700.7 (8-72) Reproduction of completed page authorized

PREFACE

As a consequence of a series of major accidents beginning in 1969 and involving DOT class 112A/114A tank cars carrying hazardous materials, the Federal Railroad Administration (FRA) proposed for these vehicles improved safety regulations that were implemented in October 1977. A portion of those regulations concerns the installation of head shields to protect the tank car head against puncture. In a continuous effort, FRA sponsored research to establish the mechanism of tank car puncture and to evaluate the effectiveness of the head-shield and Shelf-E coupler in protecting tank cars from puncture in an actual impact dynamic environment. The research included analytical simulation of vehicle impact and full scale tests. The test program was divided into two phases: low speed impacts for preliminary investigation of vehicle dynamics, and the Switchyard Impact Tests (at higher speeds and including demonstration of the protective devices reviewed in this report).

The low-speed experiment was designed by a Washington University of St. Louis team and conducted by ENSCO, Inc. The Switchyard Impact Tests were guided by a steering committee chaired by Donald Levine (FRA). Earl Phillips and Larry J. Schlink (RPI/AAR), Pin Tong (TSC) and Dave Dancer (FRA) participated as steering committee. Rolling stock for the Switchyard Impact Tests was contributed jointly by the RPI-AAR Tank Car Safety Committee and the Shell Oil Company. The final tests were designed by the DOT Transportation Test Center.

Finally, we wish to acknowledge Mr. William Harris, Vice-President for Research and Development, Association of American Railroads, who gave his time and experience to provide guidance to the test program steering committee. Mr. Harris contributed materially to the complex series of critical decisions that were needed to keep the test program on schedule.

METRIC CONVERSION FACTORS

Approximate Conversions to Metric Measures

Symbol	When You Know	Multiply by	To Find	Symbol
		LENGTH		
in	inches	2.5	centimeters	cm
ft	feet	30	centimeters	cm
yd	yards	0.9	meters	m
mi	miles	1.6	kilometers	km
		AREA		
in^2	square inches	6.5	square centimeters	cm^2
ft^2	square feet	0.09	square meters	m^2
yd^2	square yards	0.8	square meters	m^2
mi^2	square miles	2.6	square kilometers	km^2
	acres	0.4	hectares	ha
		MASS (weight)		
oz	ounces	28	grams	g
lb	pounds	0.45	kilograms	kg
	short tons (2000 lb)	0.9	tonnes	t
		VOLUME		
tsp	teaspoons	5	milliliters	ml
Tbsp	tablespoons	15	milliliters	ml
fl oz	fluid ounces	30	milliliters	ml
c	cups	0.24	liters	l
pt	pints	0.47	liters	l
qt	quarts	0.95	liters	l
gal	gallons	3.8	liters	l
ft^3	cubic feet	0.03	cubic meters	m^3
yd^3	cubic yards	0.76	cubic meters	m^3
		TEMPERATURE (exact)		
°F	Fahrenheit temperature	5/9 (after subtracting 32)	Celsius temperature	°C

Approximate Conversions from Metric Measures

Symbol	When You Know	Multiply by	To Find	Symbol
		LENGTH		
mm	millimeters	0.04	inches	in
cm	centimeters	0.4	inches	in
m	meters	3.3	feet	ft
m	meters	1.1	yards	yd
km	kilometers	0.6	miles	mi
		AREA		
cm^2	square centimeters	0.16	square inches	in^2
m^2	square meters	1.2	square yards	yd^2
km^2	square kilometers	0.4	square miles	mi^2
ha	hectares (10,000 m^2)	2.5	acres	
		MASS (weight)		
g	grams	0.035	ounces	oz
kg	kilograms	2.2	pounds	lb
t	tonnes (1000 kg)	1.1	short tons	
		VOLUME		
ml	milliliters	0.03	fluid ounces	fl oz
l	liters	2.1	pints	pt
l	liters	1.06	quarts	qt
l	liters	0.26	gallons	gal
m^3	cubic meters	35	cubic feet	ft^3
m^3	cubic meters	1.3	cubic yards	yd^3
		TEMPERATURE (exact)		
°C	Celsius temperature	9/5 (then add 32)	Fahrenheit temperature	°F

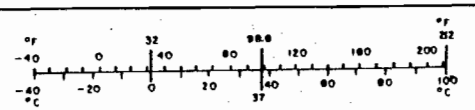

CONTENTS

LIST OF ILLUSTRATIONS

LIST OF ILLUSTRATIONS (CONT.)

LIST OF TABLES

EXECUTIVE SUMMARY

Background

Rail vehicle accidents from 1969 to 1975 included 519 derailments of DOT class 112A/114A hazardous-material tank cars, resulting in 168 ruptures, and catastrophic accidents causing 18 deaths, 832 injuries, and 45 major evacuations involving 40,000 people. The Federal Railroad Administration responded to this serious safety problem with an emergency order aimed at reduction of major switchyard accidents and regulatory actions requiring thermal coating and protection of hazardous-material tank cars against head puncture. The regulatory actions were incorporated in the Code of Federal Regulations in October 1977.

The Switchyard Impact Test Program

During 1975-1976 the Federal Railroad Administration sponsored a major series of tests to establish the baseline puncture resistance of unprotected hazardous-material tank car heads, and to evaluate the effectiveness of two protective devices now required by regulation: the shelf-E coupler and the head shield. These tests simulated accidents of the general type that have been observed to cause catastrophic results in switchyard operations. The Association of American Railroads and the Railroad Progress Institute participated in the test program. The tests were conducted at the Transportation Test Center. The first two series, comprising 19 trials, were carried out under technical direction of a team from Washington University of St. Louis; the final series comprising 13 trials were carried out under technical direction of the Transportation Systems Center.

Test Results

Tank head punctures can occur when one vehicle accidentally overrides another in train makeup operations. The lessons learned about override mechanics from the first two test series

were applied by TSC to design the experiment for the final series. The latter tests achieved the objectives of the test program, and these test results have subsequently been analyzed by TSC to gain an understanding of the distribution of collision-energy dissipation during a typical switchyard impact.

Conclusions

The results of the test program and subsequent analyses have led to the following major conclusions.

1. The presence of a loose light car in a train makeup increases the chances of override, tank head impact, and puncture. The loose light car per se is not able to cause severe damage, but it provides the mechanism whereby sharp objects such as couplers can be placed in contact with the head of a tank car.

2. Backup spacing (caused, for example, by rebound of a car after failure to couple during train makeup) can significantly increase the chances of override. Any amount of spacing is a potential danger for cars equipped with standard-E couplers. Shelf-E couplers can prevent override within a finite envelope of backup spacing, but are ineffective for larger spacings.

3. The tank head can be severely damaged and punctured in the final collision, when one or more heavy striking cars engage a standing consist, after having impacted a loose light car and thrown it into a dangerous position against the standing consist.

4. Override and tank head impact can occur at impact speeds as low as 12 mph. Tank head puncture in unprotected cars is likely at speeds of 14 to 17 mph, the lower limit depending upon the weight of the striking consist.

5. The shelf-E coupler can be an effective protective device either by preventing override of a loose light car or by tearing off the couplers of this car. However, this

effectiveness is limited to situations in which the loose light car is initially positioned close to the standing consist.

6. Those mechanisms that can be relied upon to dissipate collision energy before a tank head is engaged cannot dissipate sufficient energy to prevent a tank head puncture.

7. The head shield is an effective protective device, notwithstanding the foregoing conclusion, because it is able to distribute the tank head impact over a large area, thus increasing the effective resistance to puncture. However, head shields covering only a part of the height of the tank head can be rendered ineffective by extreme overrides.

1. BACKGROUND

The Federal Railroad Administration has been seriously concerned for several years with reduction of major accidents involving DOT class 112A and 114A hazardous-material tank cars. These vehicles are uninsulated cars of 33,000-gallon nominal capacity, consisting of carbon-steel heads and shells with top fittings only (Figure 1). There are approximately 22,000 class 112A/114A cars in service, out of the total national fleet of about 185,000 tank cars. The 112A/114A cars typically transport commodities such as liquefied petroleum gas (LPG), anhydrous ammonia, vinyl chloride, ethyl chloride, butadiene, propylene, flourinated hydrocarbons, and various flammable liquids. Projected usage demand for new hazardous-material tank cars breaks down approximately as follows*: LPG - 60 percent; anhydrous ammonia - 20 percent; vinyl chloride - 10 percent; other - 10 percent. Clearly, tank cars will continue to be a significant mode for the transportation of hazardous materials in the forseeable future.

Since 1969 there have been a series of major catastrophic rail accidents involving 112A/114A tank cars hauling flammable and nonflammable liquefied compressed gases. Accident statistics reported to FRA covering the period January 1, 1969 through December 31, 1975 included 519 derailments of 112A/114A tank cars, of which 168 cars lost part or all of their lading. The consequences of these accidents were 18 deaths, 832 injuries, and 45 major evacuations involving 40,000 persons. The total property loss for four of these accidents was estimated to exceed $100,000,000. Relevant accident history subsequent to 1975 is summarized in Table 1. These statistics amply demonstrate the need for improved safety in the transportation of hazardous materials by rail.

*Estimates estimated on Waybill Information Service.

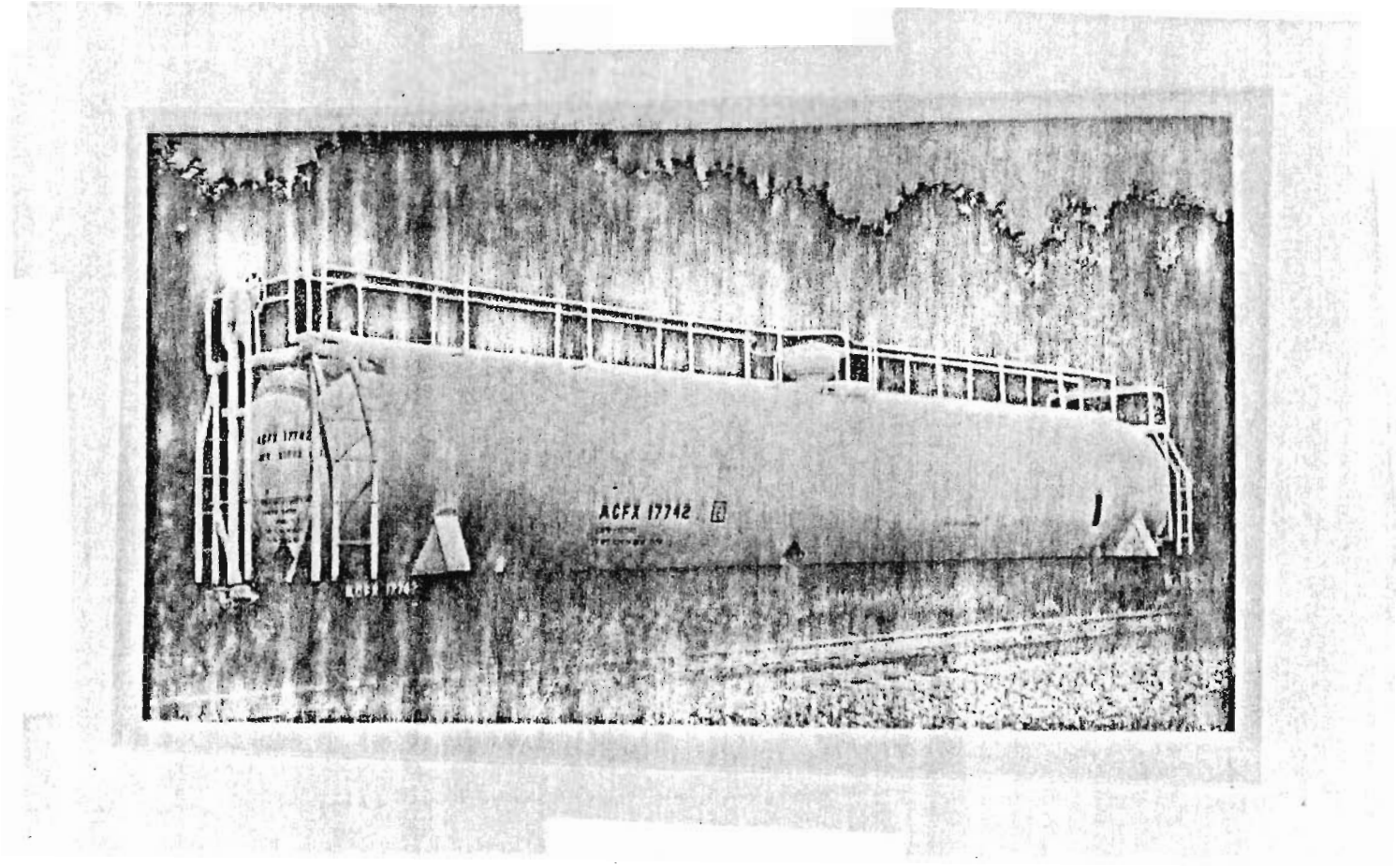

FIGURE 1. TYPICAL DOT CLASS 112A TANK CAR

TABLE 1. MAJOR ACCIDENTS INVOLVING 112A/114A TANK CARS (1976-1978)

DATE	LOCATION	NUMBER OF 112A/114A TANK CARS INVOLVED	REMARKS
11/26/76	Belt, Montana	2	2 deaths; 21 injuries
2/20/77	Dallas, Texas	2	$3.5M third-party property damage
3/16/77	Love, Arizona	3	Also 5 105A cars involved
11/9/77	Pensacola, Florida	2	1 death; 2 permanently disabled; several injuries
2/22/78	Waverly, Tennessee	1	
3/29/78	Lewisville, Arkansas	1	Apparently resulted from vandalism

Major catastrophic accidents involving 112A/114A tank cars often begin with puncture of either the head or shell of one or more cars following a derailment or switchyard collision. In the case of nonflammable cargo, the ensuing spillage can lead to wide dispersion of highly toxic fumes (e.g., Pensacola, 1977). When flammable cargo is involved, spillage is often followed quickly by ignition and major conflagration. In such cases, chain reactions can result from the overheating, overpressurization, and subsequent rupture of adjacent tank cars (e.g., Belt, 1976 and Love, 1977). A large proportion of the initial punctures in both types of accidents are caused by concentrated impact of a vehicle component (usually the coupler of an adjacent car) on the head of the tank car. The impacting component is usually driven as a ram by the residual relative kinetic energy between the impacting, or "hammer" car and the struck car.

Three regulatory actions have already been implemented to reduce the frequency and severity of major accidents involving 112A/114A tank cars. On May 24, 1973 the FRA issued Docket HM-109

as an NPRM for a regulation requiring protective head shields on 112A/114A tank cars. (This announcement was issued through the Hazardous Materials Regulations Board.) On October 25, 1974, FRA issued Emergency Order No. 5 to railroad carriers. This order prohibits the free switching of 112A/114A cars not equipped with protective head shields. Together with requirements for thermal protection, coupler vertical restraint and pressure relief, the 1973 head-shield requirement was incorporated in the Code of Federal Regulations in October 1977 [1]. The 112A/114A tank car fleet is currently being retrofitted in accordance with these regulations.

The new design requirements cited above were the product of a cooperative effort between industry, the academic community, and FRA/TSC. Following a dramatic increase in the tank car accident rate in 1969 (Figure 2) a joint research project in tank car safety improvement was established by the Association of American Railroads (AAR) and five major tank car builders through the Railway Progress Institute (RPI). In the early phases of this project, detailed accident statistics were collected and analyzed to identify the causes of major accidents. The results of the statistical analysis highlighted the uninsulated 112A/114A tank cars, head/shell punctures, and the subsequent thermal effects of pool and torch fires as primary items of concern [2].

Concurrent government work on the thermal insulation of hazardous-material tank cars [3] led to a joint industry-government project to evaluate the fire-resistance capabilities of uninsulated and insulated tank cars. A series of full-scale fire tests were conducted for FRA by the U.S. Army Ballistics Research Laboratories during 1973-74 [4,5,6,7]. A parallel series of over one hundred laboratory fire tests were conducted at the AAR Technical Center [8]. The major conclusions of this work were that: 1) pool and/or torch fires are the primary causes of ruptures of tank cars adjacent to the initially punctured car; 2) uninsulated 112A/114A cars will rupture in less than 30 minutes in a pool fire, while

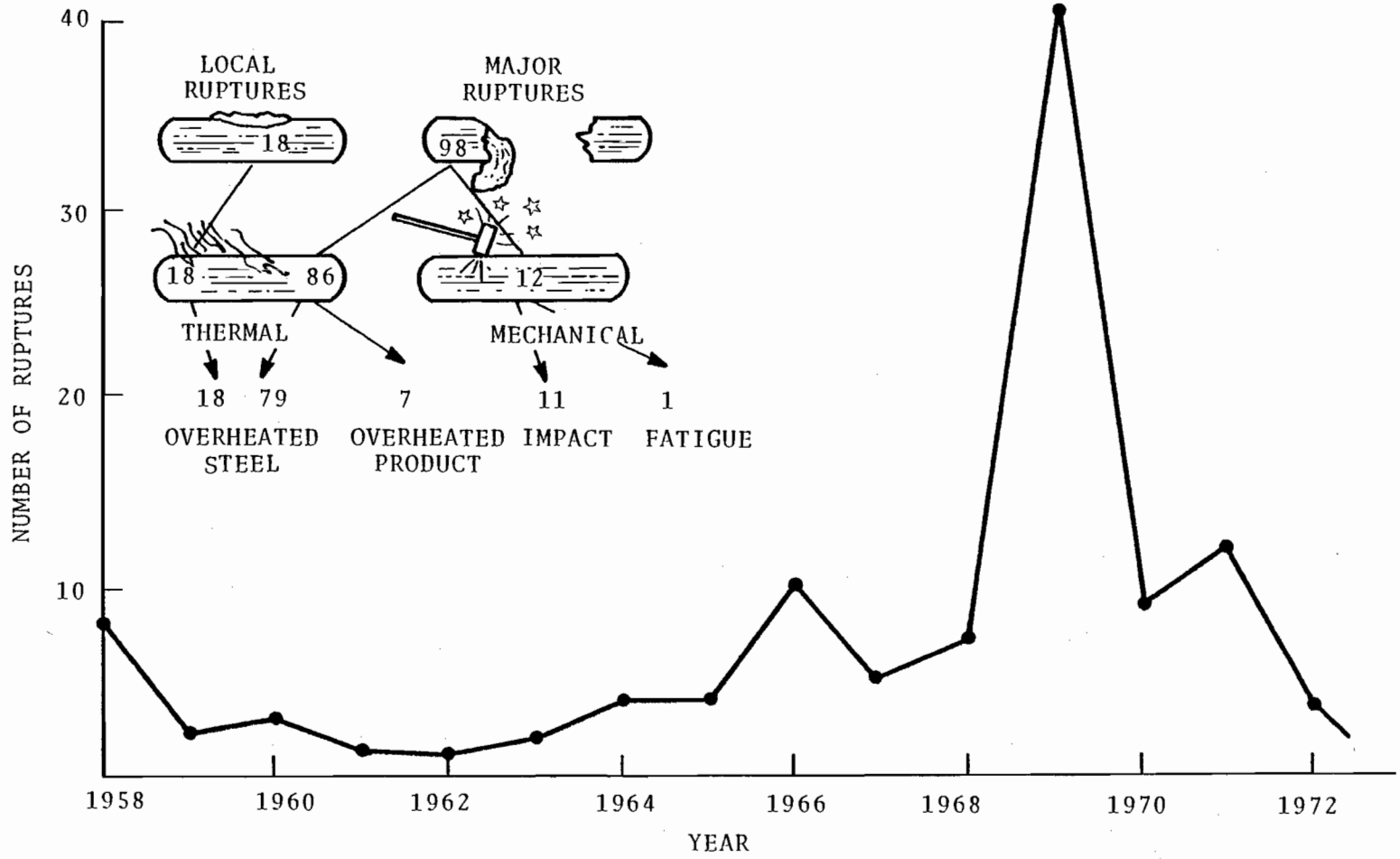

FIGURE 2. TANK CAR RUPTURES BY YEAR

thermal insulation can extend the time-to-rupture to 90 minutes; and 3) uninsulated 112A/114A cars can rupture in less than 4 minutes when subjected to torch fires, while thermal insulation is likely to be able to extend this time to 30 minutes. The thermal protection investigations were concluded with an accelerated life test to evaluate the ability of thermal coating systems to retain their effectiveness in service. The results of that assessment are reported separately [9].

While the thermal insulation requirement is directed toward reducing accident severity by preventing chain-reaction ruptures, independent actions are required to reduce the incidence of initial punctures. The importance of the problem of head puncture by adjacent-car couplers was identified in the RPI-AAR accident statistics phase of its study [10], and attention was then focused on measures for the protection of tank car heads against impact. A preliminary analysis of a variety of protection concepts was conducted by the RPI-AAR, resulting in identification of the 1/2-inch-plate head shield (Figure 3) and the shelf-E coupler (Figure 4) as leading candidates for investigation [2].

Attention was focused on the shelf-E coupler after service experience in 1971-1972 indicated that the type "F" interlocking coupler was not an effective device for prevention of head punctures. The addition of top and bottom shelves to the type "E" coupler (Figure 4) provides a mechanism for restraining the relative vertical motion between the couplers of a tank car and adjacent cars. A total of 225 shelf-E couplers were immediately placed in service to gain operational experience, and their vertical-restraint capabilities were verified in two derailment incidents [2].

Development of the head shield concept actually started in 1970, and an initial version was published in 1971 [11]. It is apparent from Figure 3 that the primary purposes of the head shield are to provide increased material thickness for better resistance against local penetration, and to provide a mechanism for increasing the impact bearing area.

An experimental study of the tank car head impact phenomenon

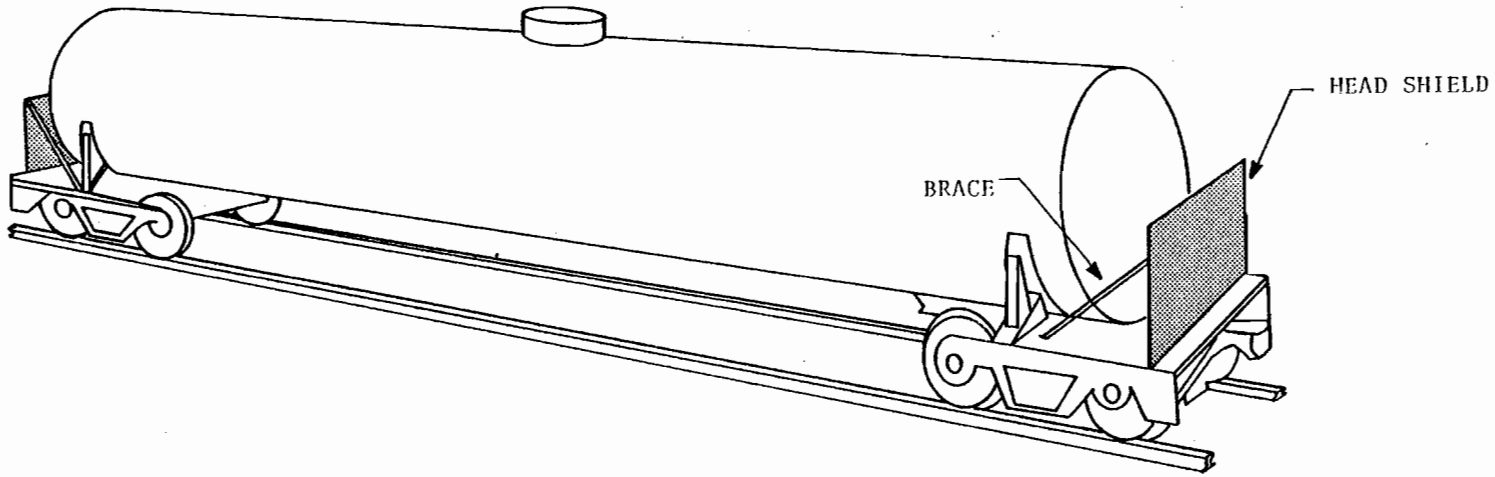

FIGURE 3. HEAD SHIELD PROTECTION CONCEPT

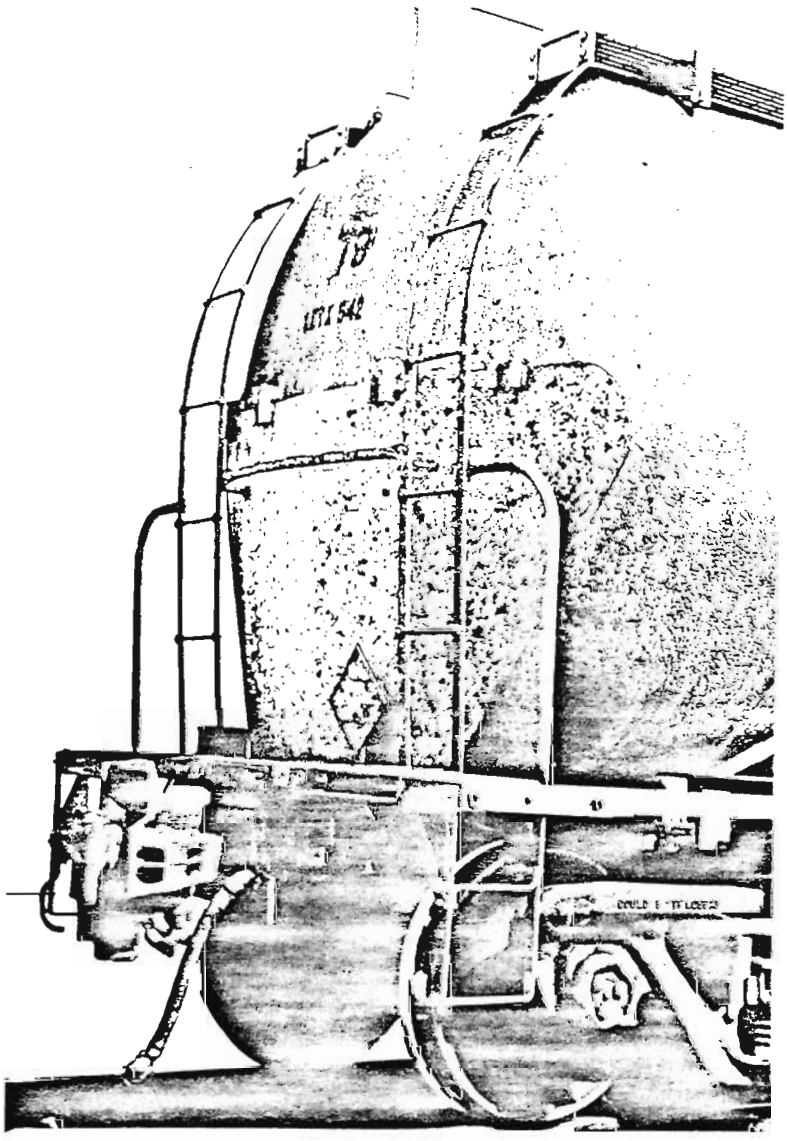

FIGURE 4. SHELF-E COUPLER

was conducted from 1970 to 1972 [12]. This study included 15-scale model tests, as well as some full-scale tests with elevated ran- couplers impacting the heads of new pressure cars. The 1/2-inch- plate head shield was tested as a part of this experiment series, and was found to increase the threshold speed for tank head puncture.

The head shield design was subsequently refined in the 1973 FRA regulatory action mentioned previously. In 1974 the Federal Railroad Administration and the RPI-AAR agreed to jointly sponsor an extensive series of full-scale tests to investigate the mechanisms of tank car puncture and to seek the most effective counter measures.

The accident statistics indicated that switchyard impact incidents had led to several major accidents in the past. Therefore, it was decided that the full-scale tests would simulate the general conditions of switchyard impact, but would not attempt to reproduce any specific accident. FRA thereupon designated this effort as the Switchyard Impact Test Program, and the RPI-AAR named its participation the Phase 15 Project [13].

In late 1975, management of this test series was delegated to the Phase 15 Sterring Committee, which was chaired by FRA and included representatives from the RPI-AAR, Washington University of St. Louis, TSC, and TTC. The Switchyard Impact Tests investigated mechanisms that led to tank head impact, and resistance of unmodified 112A/114A tank cars to head puncture. These tests also provided realistic assessments of the effectiveness of both modified head shields and shelf-E couplers as protective devices. Initial tests (series 1 and 2) were carried out from December 1975 through March 1976, with the primary responsibility for experiment design vested in the Washington University Team.

Based on lessons learned from series 1 and 2, the test was redesigned by the Transportation Systems Center (series 3 through 7 and series 10), and was completed by November 1976. This report summarizes analysis of the test data conducted at the Transportation Systems Center, and focusses attention primarily upon the later

(series 3 through 10) tests. A separate report documenting the test results was also issued by the RPI-AAR [14].

2. TEST PLANS AND OBJECTIVES

Earlier full-scale tests [12] simulated tank car head impacts by collision between two tank cars, one of which was equipped with a specially mounted elevated ram coupler (Figure 5). Although such tests can reproduce the type of head puncture experienced in service, they do not represent the specific energy-absorption characteristics of service collisions involving other types of freight cars, actual support conditions for coupler and draft gear, and the dynamics associated with derailments or switchyard impacts. Also, it was not apparent whether the ram tests might have provided a too conservative or a too optimistic assessment of head puncture in service.

Hence, the Switchyard Impact Tests were designed to simulate generically the switchyard impact phenomenon to increase test realism. The scope was also broadened to include assessment of the shelf-E coupler, as well as the headshield.

Analyses of accident statistics had previously brought to light a correlation between certain initial conditions and the occurrence of major switchyard accidents. Briefly, the critical initial conditions appeared to be creation of a standing consist during train makeup, in which the last car is an unloaded car that has failed to couple to the remainder of the consist (Figure 6). This loose light car can place one or both of its couplers above still height by a combination of pitching and vertical motions, after it is struck by the next car to be fed into the consist. The likelihood of such an override event is increased when the striking car is heavy, and head punctures can occur if either or both of the cars adjacent to the loose light car are loaded tank cars. Hence, coupler override dynamics is an important aspect of tank car head puncture in service.

In a separate FRA/TSC sponsored program [15] and its subsequent study, TSC determined that there were basically four mechanisms which led to coupler override in impact. These are:

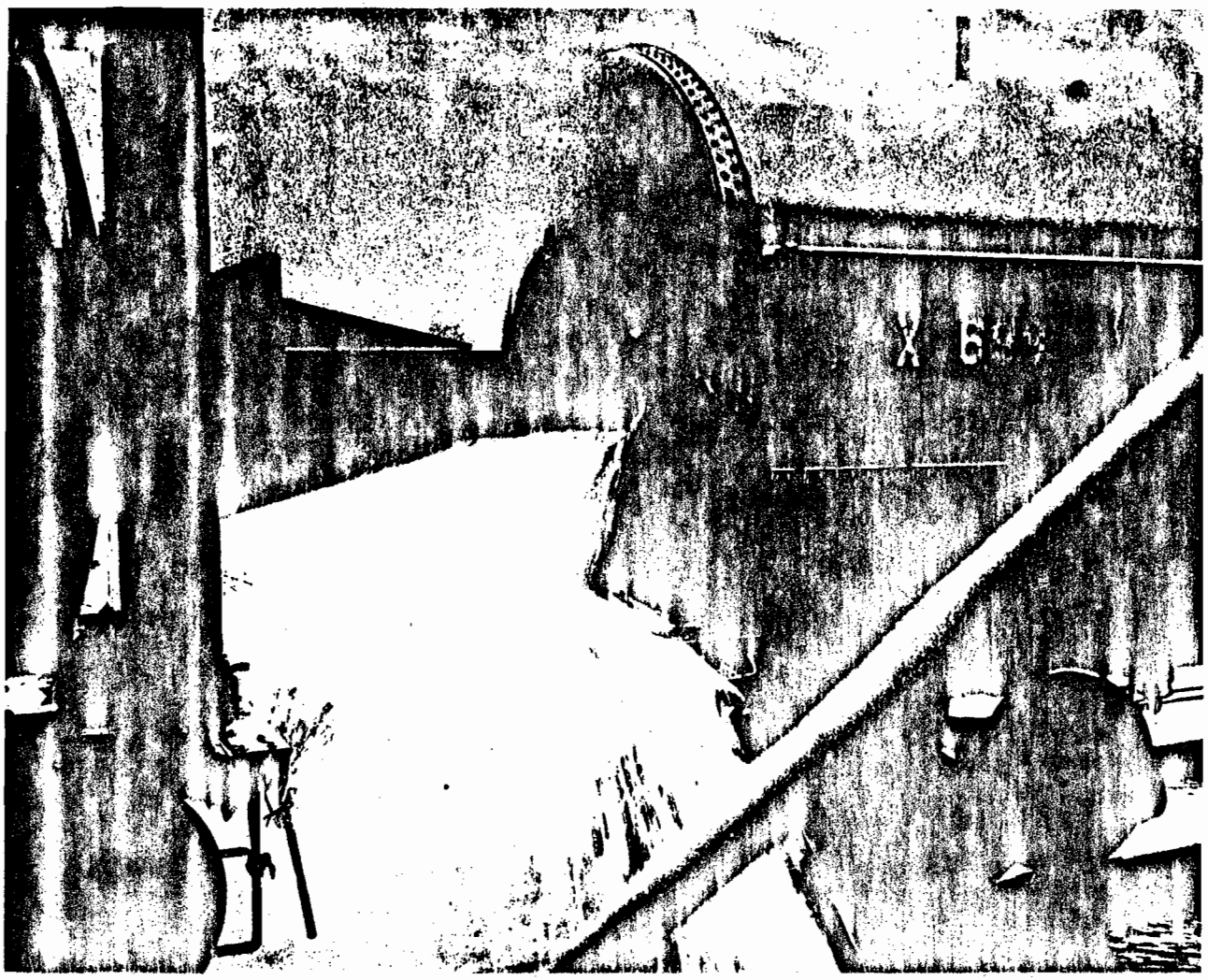

FIGURE 5. TANK CAR HEAD IMPACT BY ELEVATED RAM COUPLER

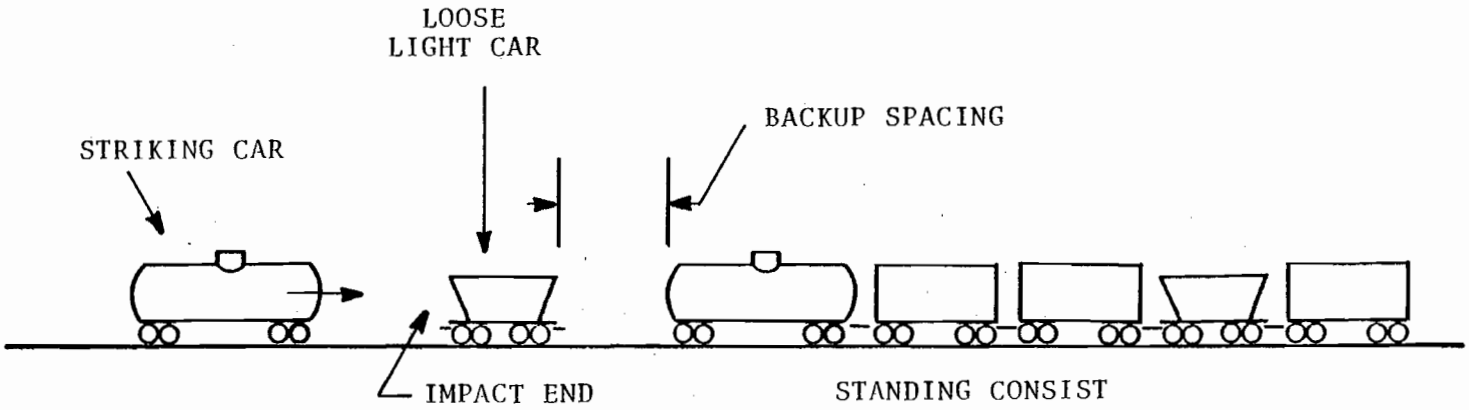

FIGURE 6. TYPICAL PRECURSOR CONFIGURATION FOR SWITCHYARD ACCIDENT INVOLVING TANK CAR HEAD PUNCTURE

1. Pitching motion induced by impact - for a rail vehicle having center of gravity (c.g.) above the height of its couplers, an impact on the coupler at one end will cause the carbody to pitch upward at the opposite end. The vertical height of the upward motion can be as much as several feet, depending on impact speed, carbody weight, moment of inertia and the c.g. height of the impacting cars, etc.

2. Misalignment of coupler heights - if the heights of the impacting couplers of two colliding cars are different, the impact force will produce bending in the coupler shanks. This can cause the coupler faces to incline and result in one coupler sliding above the other.

3. Buckling of the center sill - if the compressive force generated by impact is large enough to buckle the center sill or the coupler shank elastically or plastically, the coupler faces can rotate and cause the sliding of one coupler above the other.

4. Rotation of truck bolster - the truck bolster at the impact end generally rotates during impact. Due to the constraint of the truck frame and the suspension sprungs, the bolster can push the impact end of a vehicle upward and enhance the change of override.

One or a combination of the foregoing mechanisms can cause override during a collision. Depending on the circumstances and parameters involved, override can occur at either end of the loose light car. The following terminologies are used to describe the scenario of an override:

1. First-impact mechanism (Figure 7). Override occurs at the impact and immediately after collision. This is likely to happen when there is sufficient misalignment of the impacting couplers.

2. Second-impact mechanism (Figure 8). The loose light car, after impact by a striking car, pitches upward at its

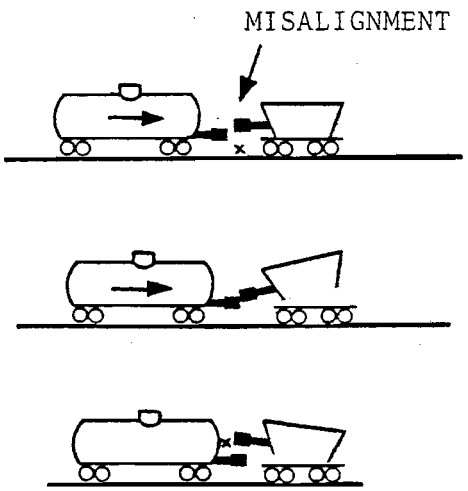

FIGURE 7. FIRST-IMPACT MECHANISM

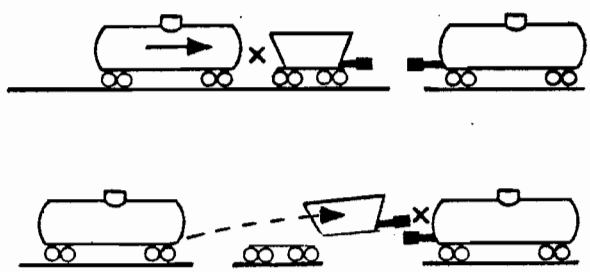

FIGURE 8. SECOND-IMPACT MECHANISM

forward end. With proper backup spacing available, the pitch motion can produce enough coupler misalignment to cause an override on the standing consist as the loose light car strikes the latter.

3. Third-impact mechanism (Figure 9). This mechanism involves the following sequence of events. The loose light car pitches upward initially at its forward end after impact by a striking car. With sufficient backup spacing available, the loose car's forward end can fall back to original height (due to gravity) as it encounters the standing consist. This second impact will cause the light car to pitch its initial impact end upward. Thus, the impact-end coupler is elevated and can override the sill of the striking car as the latter engages the consist. The elevation of the impact-end coupler can sometimes be caused by detrucking (Figure 10) at the forward end of the light car as it moves away after the initial impact.

4. Buckling mechanism. This is more likely to occur when the impacted car is backed up by another car with little or no spacing. The buckling of the impacted car can result in override at either one or both ends.

To achieve realism of simulating some of the typical major switchyard accidents in the test, the experiment was designed to have one or more heavy tank cars strike a loose light hopper car backed by other cars. Backup spacing (between the loose light car and standing consist) was identified as a key parameter governing the occurrence or absence of override. Hence, the primary objective of test series 1 was to measure the motions of a light hopper car after impact by a single moving tank car. A secondary objective was to simulate head punctures caused by the detrucking mechanism. The objective of test series 2 was to investigate the characteristics of a third-impact mechanism that had been observed in actual switchyard accidents, using the series 1 information to establish the proper backup spacing. The results of the initial

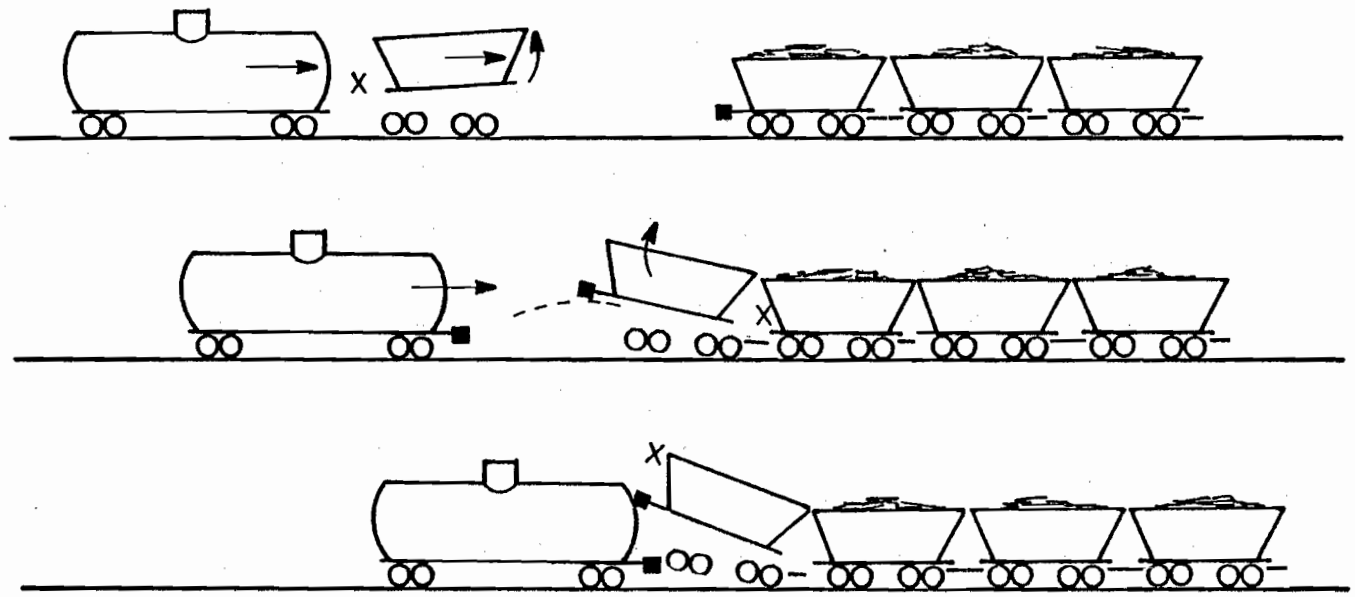

FIGURE 9. THIRD-IMPACT MECHANISM

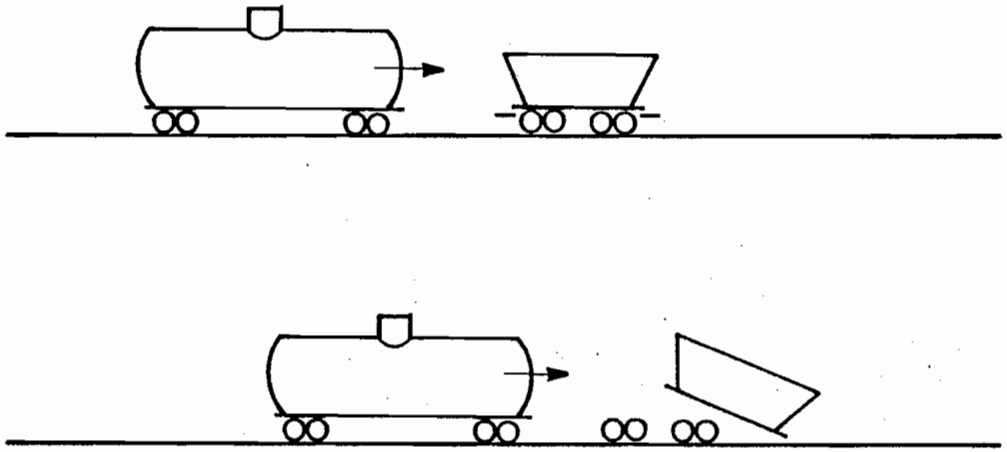

FIGURE 10. TEST SERIES 1 CONFIGURATION AND DETRUCKING MECHANISM

tests will be reviewed briefly in terms of their effects on planning of subsequent series.

Test series 1 comprised twelve tests at speeds ranging from 5.4 to 16.9 mph. This series achieved the objectives of defining the motion of a loose, unloaded hopper car after first impact and using the results to estimate backup spacings for test series 2 [16]. However, no overrides occurred in series 1 because the hopper cars did not detruck at their forward ends.

Series 2 comprised seven tests at speeds ranging from 7.8 to 13.7 mph. A standing consist of 5 loaded hopper cars was used, with backup spacing ranging from 2.875 to 16 feet. Achievement of a tank car head puncture thus depended on achievement of the third-impact mechanism (Figure 9), since only the striking car was tank car. Unfortunately, the variabilities inherent in testing of this type presented a number of difficulties [18,19,20]. As a result, only one override and no tank head punctures were achieved in this series.

A major problem was thought to be associated with tank car lading simulation. Since maintenance of test safety required that water be substituted for flammable or toxic liquefied cargo, it was not possible to simultaneously match the rail weight and volume "innage" of a service-load tank car. (The greater density of water compared with hazardous cargo densities is the source of this difficulty.) The first fourteen tests were run with tank cars loaded to match service rail weight, resulting in about 63 percent innage. Under this low innage condition, it was found that the moving tank car initial speed was extremely difficult to control and measure [20,21], and that only about 25 percent of the tank car mass was effective in impact [20], due to sloshing of the water lading. Consequently, the tank cars in the last two series 1 tests, the last three series 2 tests, and in subsequent series were loaded to match typical service innage (about 93 percent), in order to reduce the severity of sloshing.

The third-impact tests were assessed at TSC based on results obtained in related studies of crashworthiness and the mechanics

of train-to-train collisions [15, 22]. This assessment highlighted the sensitivity of the desired outcome to precise timing of the sequence of events involved, and the high probability of nonrepeatable testing [23]. Consequently, a revised test plan was adopted for the remainder of the Switchyard Impact Tests, with the following specific objectives:

1. Investigate other override mechanisms and evaluate the puncture resistance of existing 112A/114A tank cars (series 3).
2. Evaluate the effects of a 1/2-inch-plate, part-height head shield on collision dynamics and on puncture resistance (series 4).
3. Evaluate the ability of tank-car mounted shelf-E couplers to prevent puncture (series 5).
4. Investigate the effects of striking mass on collision dynamics and puncture, i.e., by a striking consist of more than one car (series 6).
5. Investigate the effects on override and puncture when the light hopper car is initially coupled to the standing consist (series 7, 8 and 9).*
6. Evaluate the combined effect of shelf-E couplers and a full-height head shield on puncture resistance under severe (upper-limit) impact conditions (series 10).

*Series 8 and 9 were scheduled to repeat series 7, except with interlocking F and shelf-E couplers in place of standard-E couplers on the tank cars. These two series were subsequently eliminated from the test program because no head punctures were achieved in series 7.

3. TEST DESCRIPTION

Thirteen tests in all were run after the completion of the initial series: five in series 3, two in series 4, two in series 5, one in series 6, two in series 7 and one in series 10. Eleven of these thirteen tests (where wayside camera data were available) are analyzed in this report. GATX, UTLX and SOEX tank cars of DOT 112A class and L&N hopper cars of 50 and 60 tons capacity were used in the test. All the test vehicles were inspected and shopfit to meet industry interchange standards prior to testing. There was no attempt to control tank car lading temperatures. Since the test period extended from December 1975 through November 1976, the tests were conducted with lading temperature ranging from 40 to 79°F.

3.1 PRETEST ACTIVITIES AND MEASUREMENTS

3.1.1 Test Organization

The tests were managed by the Steering Committee, which was chaired by FRA and included representatives from the RPI-AAR, TSC and Washington University of St. Louis. The detailed planning and design, and the technical direction of the series 1 and 2 tests were delegated to Washington University. For series 3 through 10, these responsibilities were delegated to TSC. The Transportation Test Center, supported by Kentron-Hawaii, actually carried out the tests and recorded all the test data. TSC conducted the analysis of the test data.

3.1.2 Experimental Determination of Typical Car Properties

Properties of the tank cars and the loose light hopper car, such as masses, rotary inertias, spring rates and key dimensions are required as inputs to analytical models that seek to describe the test results. These properties were determined by a series of pre-test measurements made on one L&N hopper car and one GATX tank

car [24,25,26]. Although the measurement reports refer to a 50-ton hopper car, it should be noted that the serial number (130954) places this car in the 60-ton class, according to L&N engineering drawings [27]. Since all light hopper cars in test series 3 through 10 were in the same class, the measured properties are assumed to be typical. The measured properties of tank car GATX 91883 are also assumed to be typical of the cars used in the tests, although other sources of data indicate that this assumption may not be completely justified [28]. Also, coupler heights above the rail were measured just prior to each test.

Only the masses, rotary inertia and key dimensions of the hopper cars are relevant to the fundamental physical analysis models presented in Section V. The typical data obtained from L&N hopper car 130954, together with derived dimensions, are summarized in Figure 11. Some assumptions have also been made, and are so indicated in the figure.

In regard to the tank cars, light weight is the only property required for the analyses in Section V. This value was recorded as 84.2 KIPS during experimental assessment of the inertial properties of GATX 91883 [26]. However, tank car light weights can vary considerably, and values up to 90.5 KIPs have been reported [28]. Consequently, light weights were established individually by RPI/AAR for most of the test cars, and these values are used together with measured rail weight to estimate innage and effective impact mass. Details of the innage calculations are summarized in Appendix A.

Coupler height above rail at the impact end of the light hopper car is used to estimate the offset of the first impact below the center of gravity of the hopper carbody. The offset is estimated from the average of the hopper and tank car coupler heights. The measurements and calculated offsets are summarized in Table 2. The results of the calculations indicate that an average offset, $\ell \cong 2.04$ ft, can be used in the analytical model.

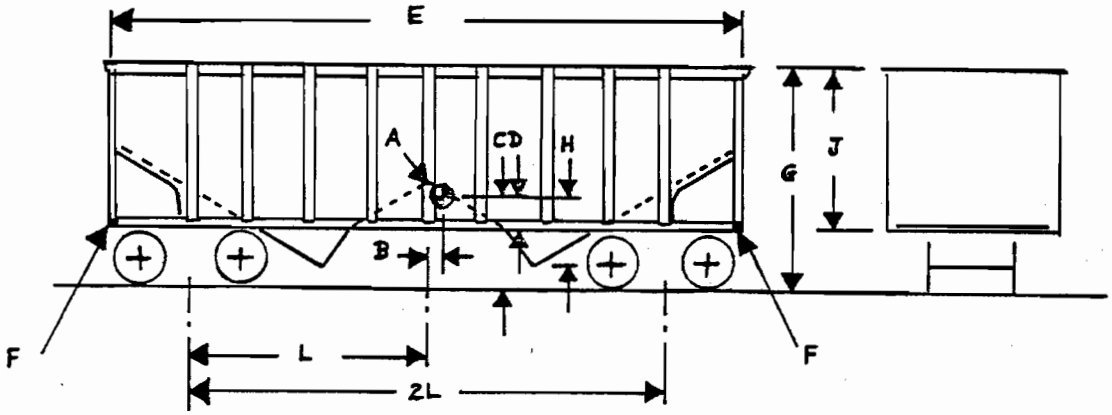

DIMENSIONAL DATA AND REFERENCES

KEY	DESCRIPTION		
A	Carbody C.G. Location		
B	C.G. offset from carbody C.L.	8.25"	Neglected in Analysis
C	C.G. height above rail	4.759'	Derived
D	C.G. height above bottom of angle section	15.875"	
E	Carbody length	33.0'	
F	Visual reference points		
G	Carbody height above rail	11' 11"	
H	Truck C.G. offset below carbody C.G.	3.384'	Derived; truck C.G. assumed 16.5" above rail
J	Carbody height	8' 5 3/4"	
L	Offset: carbody C.G. to truck center	12.0'	

MASS PROPERTIES

ITEM	MASS UNITS	FORCE UNITS
Carbody	.0591 KIP $sec^2 in^{-1}$	22.84 KIPS
Trucks (2)	.0386	14.92
Total	.0977	37.76
Carbody rotary inertia	896.5 KIP $in.sec^2$	2405.6 KIP-ft^2

FIGURE 11. PROPERTIES OF L&N HOPPER CAR NO. 130954

TABLE 2. COUPLER HEIGHT AND IMPACT OFFSET

SERIES AND TEST NUMBER	HOPPER CAR	TANK CAR	CALCULATED IMPACT OFFSET, ℓ^* (ft)
3.2	33.5	32.0	2.030
3.3	32.75	31.375	2.087
3.4	33.125	31.625	2.061
3.5	33.875	31.75	2.025
4.1	33.0	31.5	2.071
4.2	33.125	32.0	2.045
5.1	32.75	31.9375	2.064
5.2	32.875	31.625	2.071
6.1	34.0	31.75	2.019
7.1	33.75	31.5	2.040
10.1	34.1875	32.75	1.970
AVERAGE			2.044
STANDARD DEVIATION			0.033

$$*\ell = 4.759 - \frac{1}{2}\left(\frac{\text{HOPPER+TANK}}{12}\right) \text{ ft}$$

3.2 TEST CONFIGURATIONS, INSTRUMENTATION AND DATA REDUCTION

Test series 3, 4 and 5 were conducted using a single loaded tank car as the striking car. Test series 6, 7 and 10 employed a striking consist of three cars. The general arrangements are illustrated Figure 12. In the figure, and subsequently in this report, the notations "B"-end and "A"-end are used to refer to the impact end and forward end of the empty hopper car, respectively.* Series 7 departed from the arrangement shown in Figure 12 by having the empty hopper car initially coupled to the standing consist.

The empty hopper car in each test was instrumented with strain gages at various locations and one accelerometer near the "B" end (Figure 13). In addition, both the "A" and "B" end couplers were instrumented with strain gate pairs to pick up net compression and net vertical bending of the coupler shanks (Figure 14). The strain and acceleration data were post-processed through filters having either 50 or 100 Hz breakpoint frequency, and the filtered data were then digitized for plotting.

In addition to the onboard instrumentation, wayside cameras recorded the car motions in each test. The locations of these cameras are illustrated in Figure 15. Of most interest in the present case are the high-speed closeup cameras, which operated successfully during eleven of the thirteen series 3-10 tests. The closeup camera films were read on an automatic digitizer to obtain position-time histories, using the reference points "F" shown in Figure 11 and similar reference points on the adjacent tank cars.

An independent measurement of the initial speed of the lead tank car in the striking consist was made with an electronic speed gate developed by TTC [29]. The speed-gate measurements are used to correct the velocities estimated from the position-time history plots.

---

*For convenience in notation. This convention departs from the standard nomenclature of "B"-end for the handbrake and of the car, such as has been used in Ref. 14.

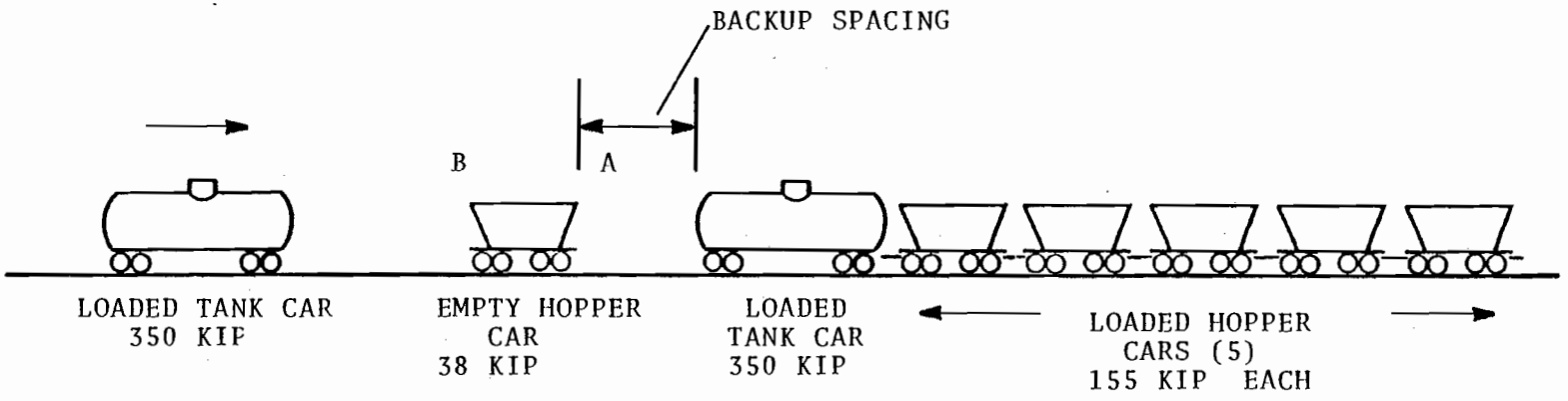

(A) CONFIGURATION FOR SERIES 3, 4 AND 5

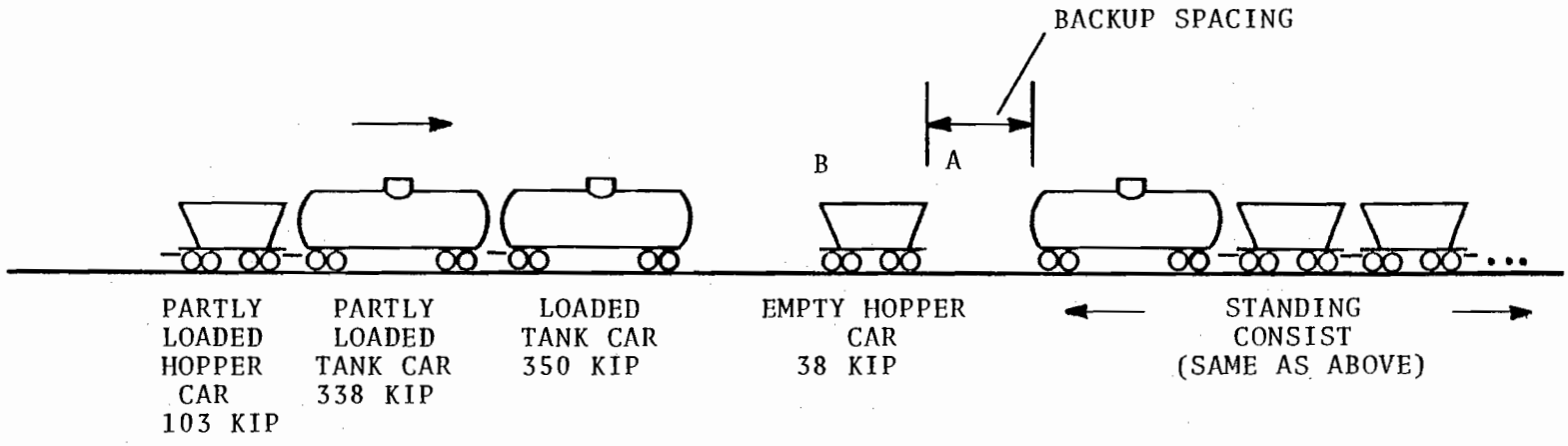

(B) CONFIGURATION FOR SERIES 6, 7 AND 10

FIGURE 12. TEST CONFIGURATION FOR SERIES 3 THROUGH 10 (NOMINAL RAIL WEIGHTS SHOWN)

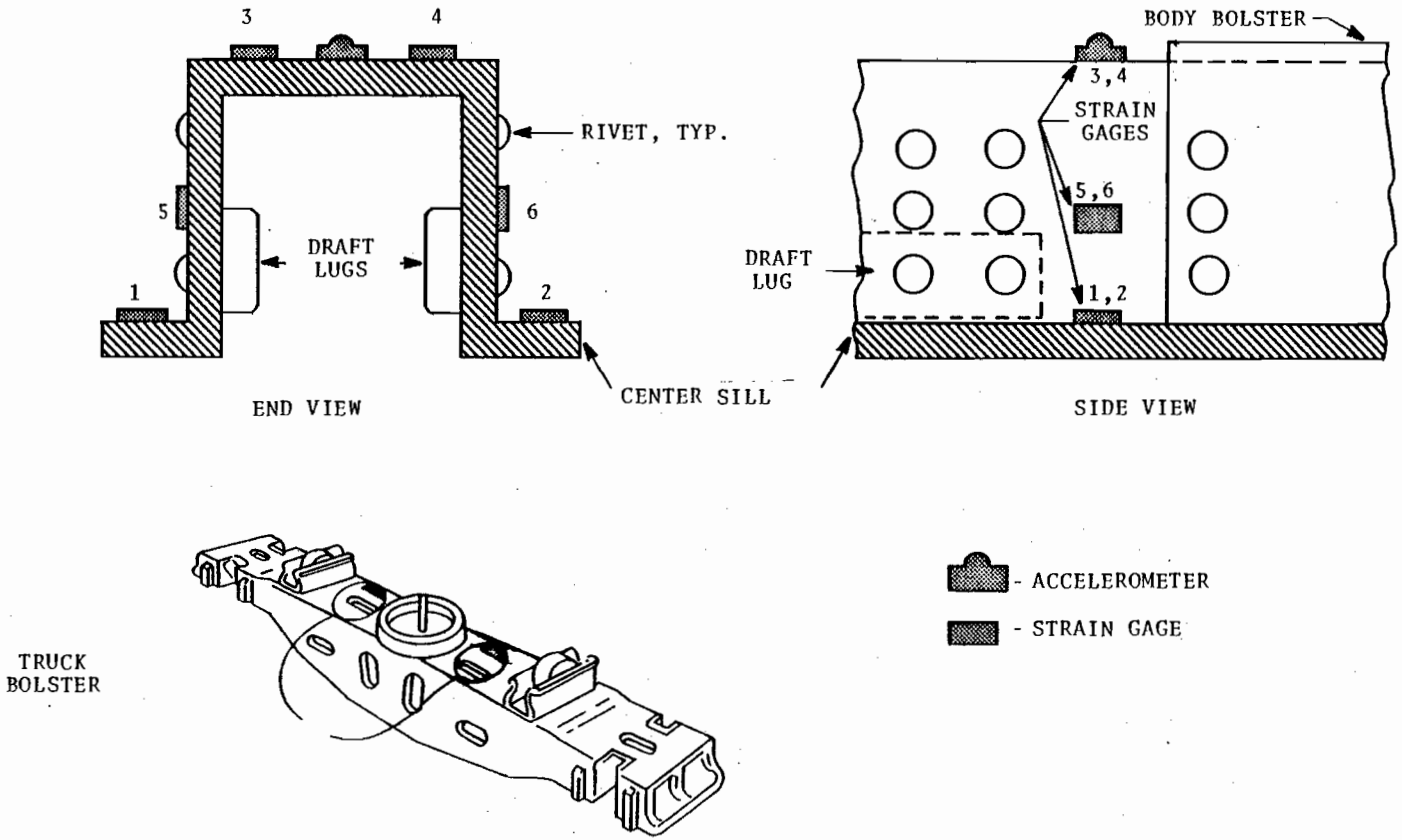

FIGURE 13. STRAIN GATE AND ACCELEROMETER LOCATIONS AT IMPACT ("B") END OF HOPPER CAR

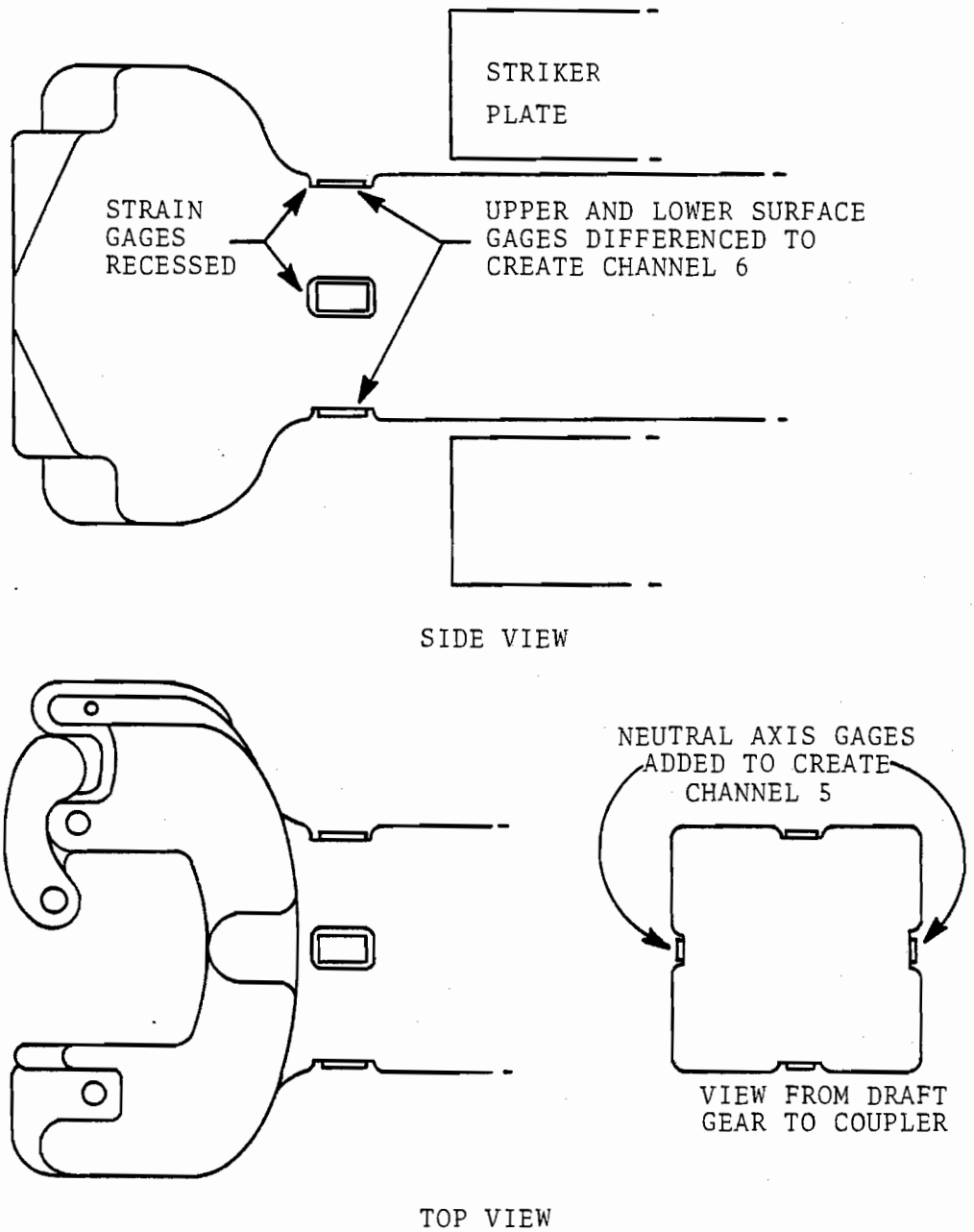

FIGURE 14. LOCATION OF STRAIN GAGES ON COUPLER SHANK

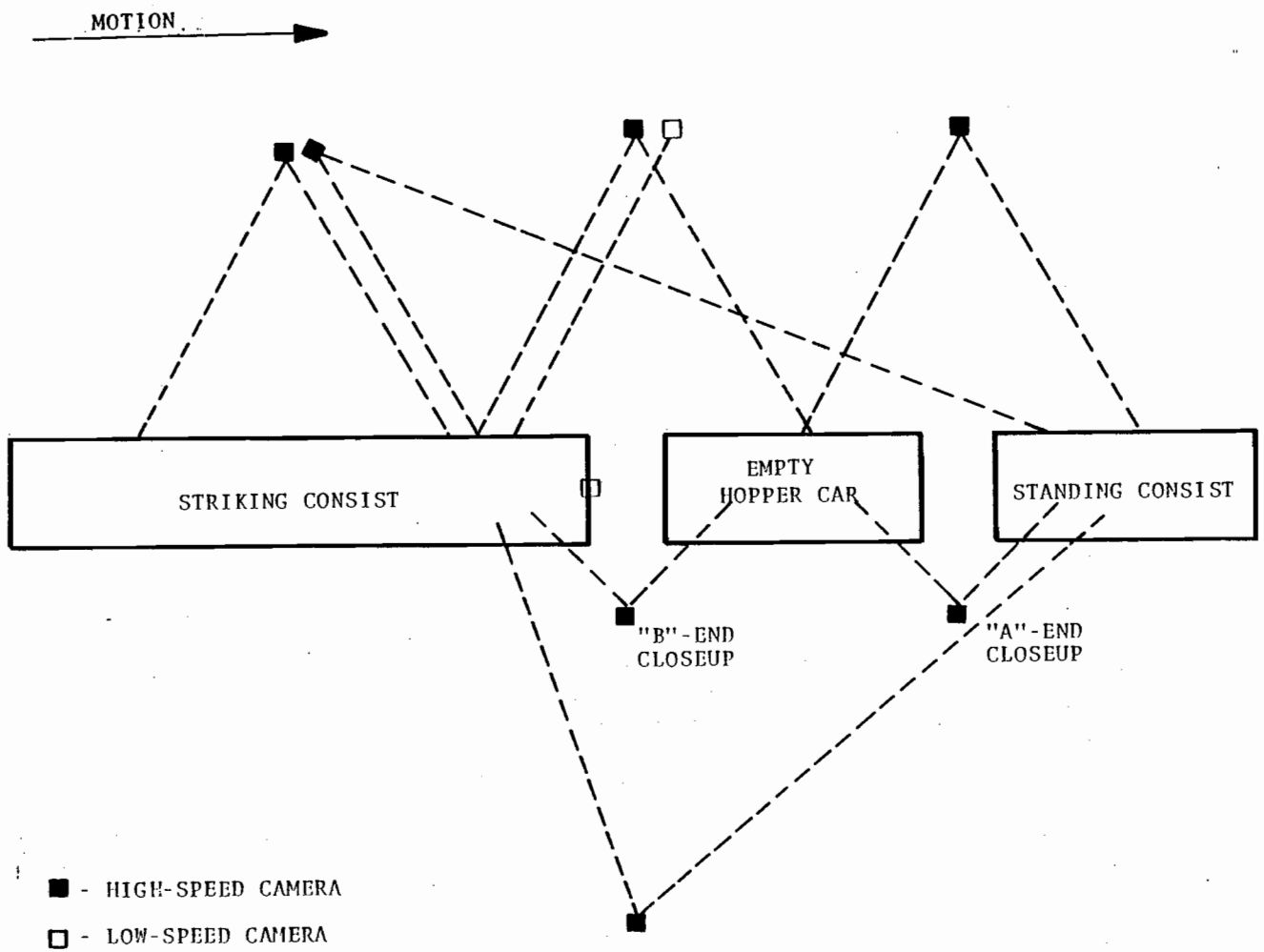

FIGURE 15. WAYSIDE CAMERA LOCATIONS

3.3 TEST MATRIX

A summary of test series 3 through 10 is given in Table 3. Thirteen tests were run at speeds ranging from 12.7 to 19.4 mph, and with backup spacing ranging 2.5 to 3.75 feet in the uncoupled-car tests. High-speed closeup films of both ends of the empty hopper car were obtained in eleven tests, which are the subject of the analysis presented in Section V.

TABLE 3. SWITCHYARD IMPACT TEST MATRIX (SERIES 3-10)

TEST SERIES AND NUMBER	INITIAL SPEED AT GATE (MPH)	BACKUP SPACING (FT)	LADING TEMPERATURE (^{o}F)	RAIL WEIGHTS (KIPS)				COUPLER TYPE INSTALLED ON ADJACENT TANK CARS	HEAD SHIELD TYPE INSTALLED	REMARKS
				EMPTY HOPPER CAR	STRIKING CONSIST					
					LEAD TANK CAR	SECOND TANK CAR	HOPPER CAR			
3.1	12.7	2.50	58	37.5	344.00			std E		"B" end closeup camera failed
3.2	14.9	3.50	52	37.5	344.00			std E		
3.3	16.5	3.50	55	37.5	344.00			std E	Part height	Head shield on striking tank car only
3.4	15.4	2.50	68	37.5	343.36			std E		
3.5	16.9	2.50	74	37.5	343.36			std E		
4.1	18.7	2.50	UNK	37.5	348.52			std E	Part height	
4.2	19.2	3.50	78	37.5	350.68			std E	Part height	
5.1	19.4	2.50	66	37.5	350.00			shelf E		
5.2	19.0	3.75	79	37.5	350.00			shelf E		
6.1	14.2	2.92	72	40.4	350.14	337.78	103.28	std E		
7.1	18.1	0.00	71	40.1	351.58	337.78	103.28	std E		Empty car coupled
7.2	15.0	0.00	48	39.9	347.26	338.00	103.00	std E		Empty car coupled; "B" end closeup camera failed
10.1	17.1	3.75	40	37.8	353.78	337.78	103.28	shelf E	Full height	

4. TEST RESULTS

Test series 3 through 10 generally achieved the objectives stated in Section II. The couplers of the empty hopper cars overrode and impacted the heads of adjacent tank cars in all tests; override at both ends occurred often. Head punctures occurred in four tests. The test results are reviewed in detail in the following subsections.

4.1 DESCRIPTION

The sequence of events in the Switchyard Impact Tests can be described in terms of the typical sequence illustrated in Figure 16. The nomenclature in the figure is consistent with that used in earlier analyses [15], but the actual sequence is more complicated.

First impact is defined as the initial impact between the striking tank car and the empty hopper car. The hopper carbody is always observed to move forward, leaving behind the striking tank car. The hopper car trucks also roll forward, but at a slower speed than the carbody. The carbody also rises (creating coupler misalignment as its forward end) and pitches following first impact.

At second impact, the hopper carbody strikes the standing tank car. In all test cases except series 7, the "A"-end coupler has almost always overridden the standing tank car platform and impacted the tank head. The pitch attitude of the hopper carbody may be positive, negative or zero at this point. Also, "second impact" is sometimes observed to consist of two or more individual impacts whose locations on the tank head may vary, and the hopper carbody may continue to change its pitch attitude.

At third impact, the striking tank car catches up with and engages the standing consist at the "B" end of the empty hopper car. This engagement often occurs with the "B"-end coupler having overridden the striking tank car platform. The third impact is

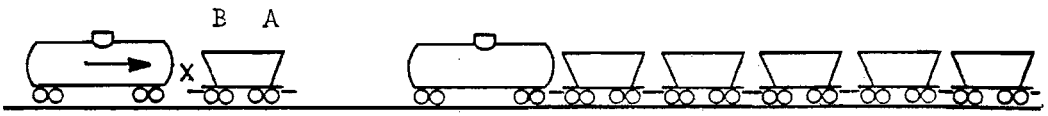

(A) FIRST IMPACT

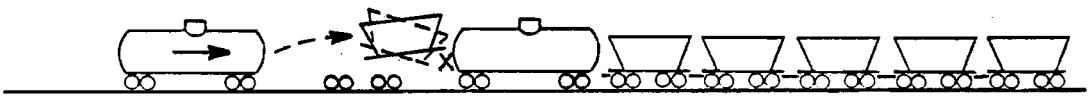

(B) SECOND IMPACT

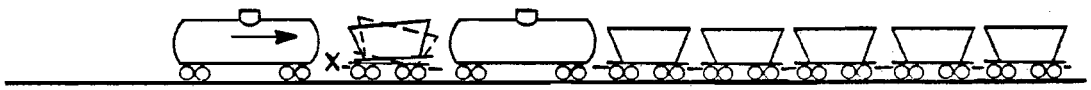

(C) THIRD IMPACT

FIGURE 16. GENERIC SEQUENCE OF MAJOR EVENTS

almost always observed to be a multiple-impact sequence, with impacts from the striking car being transmitted through the hopper carbody and thus translated into additional impacts of the standing tank car.

Under the foregoing conditions, punctures can occur in the head of either the striking or the standing tank car. Of the four punctures actually obtained, two occurred in the head of the striking car (tests 4.1 and 6.1) and two in the head of the standing car (tests 3.5 and 5.2). It is important to note that, in test 4.1, the puncture resulted from the hopper carbody and coupler overriding a part-height head shield and that, in test 5.2, the puncture occurred in spite of the shelf-E coupler installation. Complete narrative descriptions of each test appear in Appendix B.

4.2 COUPLER FORCES

Coupler compression forces were estimated from the strain gage data obtained from the hopper car "A" and "B"-end couplers. The strains commonly exhibited a prominent peak, but did not return to zero after the test, indicating that the coupler shanks had undergone severe plastic deformation. A typical example is shown in Figure 17. Post-test inspections often revealed permanent local buckling of the hopper car sill and coupler shanks at the strain-gage locations. These local bending effects further hampered the estimation of forces from the strain-gage outputs.

Hence, peak compression forces were estimated by applying an approximate elastic-plastic analysis to the coupler shank. The estimates are summarized in Table 4, but these data should not be taken too seriously. Also, it is important to note that the times of occurrence of the individual force peaks listed for each test are different.

4.3 WAYSIDE CAMERA MEASUREMENTS

Figure 18 illustrates the measurements made by digitization of the high-speed closeup camera films. Each camera contained one end of the empty hopper car and the adjacent end of a tank car in

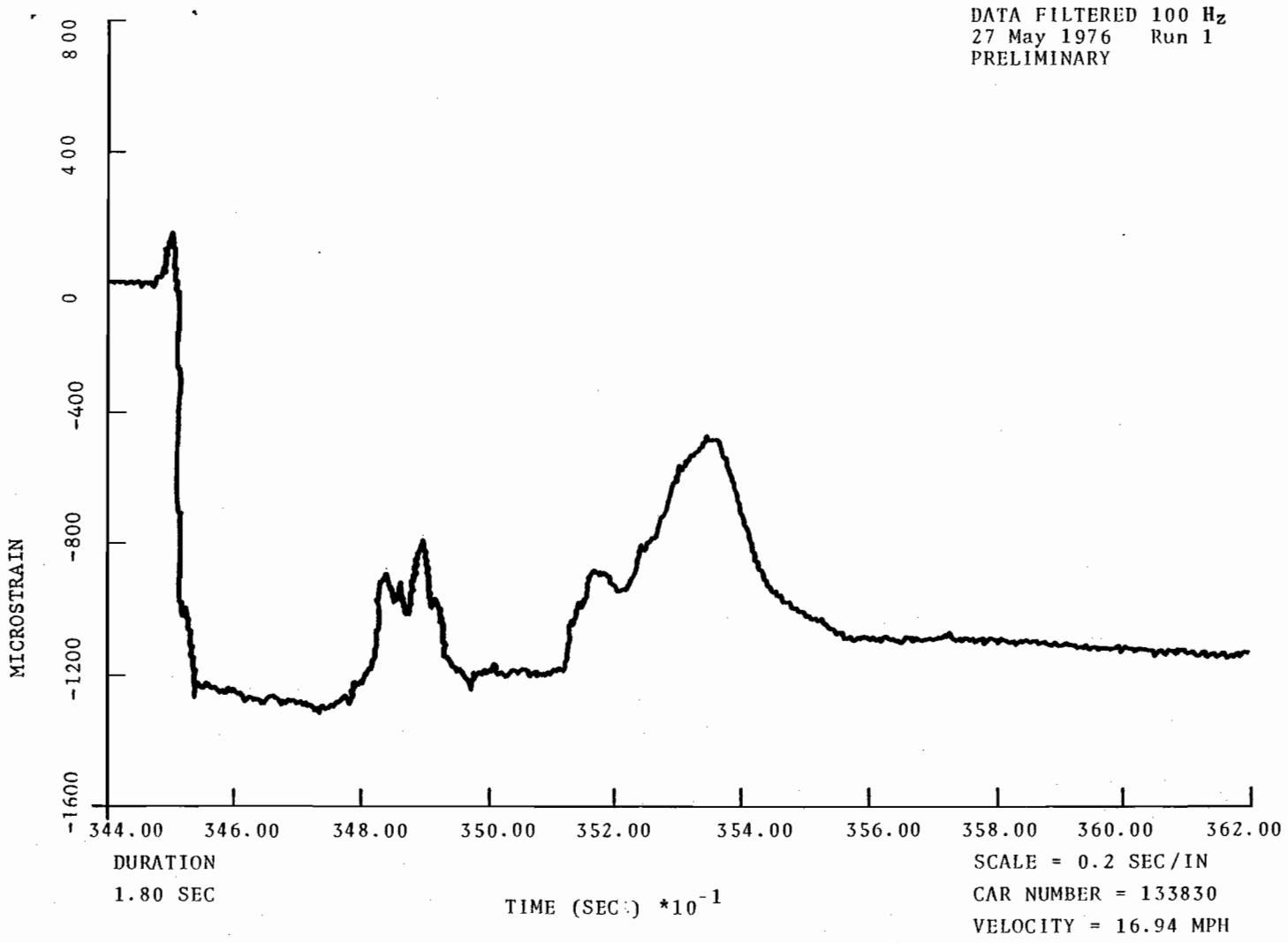

FIGURE 17. TYPICAL STRAIN-TIME HISTORY AT COUPLER SHANK

TABLE 4. ESTIMATED PEAK COUPLER COMPRESSION FORCES

Series and Test Number	HOPPER CAR "A" END		HOPPER CAR "B" END	
	Force (KIP)	Location Code*	Force (KIP)	Location Code*
3.1	530	H	880	C
3.2	520	H	1,140	C
3.3	540	H	1,130	C
3.4	525	H	1,040	C
3.5	610	HP	1,040	C
4.1	800	H	1,120 unknown	C HP
4.2	1,140	C	650	H
5.1	1,200	C	660	
5.2	650	HP	1,180	C
6.1	610	H	1,150 520	C HP
7.1	1,050	C	1,260	C
7.2	1,200	C	1,200	C
10.1	625	H	1,250	C

*C - Force measured while tank car coupler engaged
H - Force measured while tank car head or head shield engaged
P - Force associated with head puncture

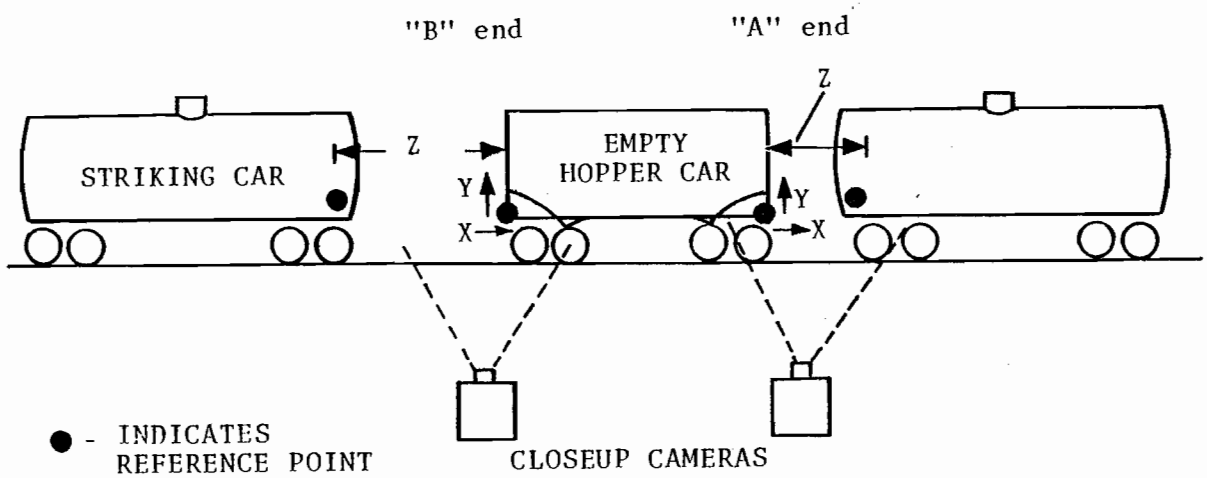

FIGURE 18. CLOSEUP CAMERA MEASUREMENT SCHEMATIC

its field of view. The reference points on the vehicles generally remained in the view fields long enough to provide position-time plots from times just before first impact until part way into third impact. Hopper carbody horizontal displacement, X, and vertical displacement, Y, together with horizontal tank car/hopper car separation, Z, were digitized and plotted at both the "A" and "B" ends for eleven of the thirteen tests in series 3 through 10. The resolutions of these plots were approximately ± 4 inches in position.

First impact is of most importance for the subsequent analysis, and its appearance on typical position-time plots is illustrated schematically in Figure 19. The actual plots for each test appear in Appendix C.

Beginning with the "B" end, separation Z is observed to decrease linearly* with time as the striking tank car approaches. First impact is characterized by reversal of the Z-plot, coincident with increases of X and Y with respect to time. A short nonlinear region at this point (usually of about 0.05 sec duration) is observed in many cases, indicating the time span during which energy and momentum are being transferred from the striking tank car to the hopper car. The X, Y, and Z-plots subsequently increase linearly with time, indicating that the vehicles are once again in free motion. The slope of the X-plot exceeds the slope of the Z-plot in this region, reflecting the fact that the hopper carbody has a greater horizontal velocity than the striking tank car after first impact. The position-time plots exhibit nonlinearities again when second and third impact occur.

The "A"-end plot is generally similar to the "B"-end plot, except that the behavior of Z reflects separation between the hopper carbody and the standing tank car. Hence, no change in Z is observed until first impact, after which the slope of Z is just the negative slope of X.

*A slight nonlinearity appears in some cases, indicating sloshing action in the tank car.

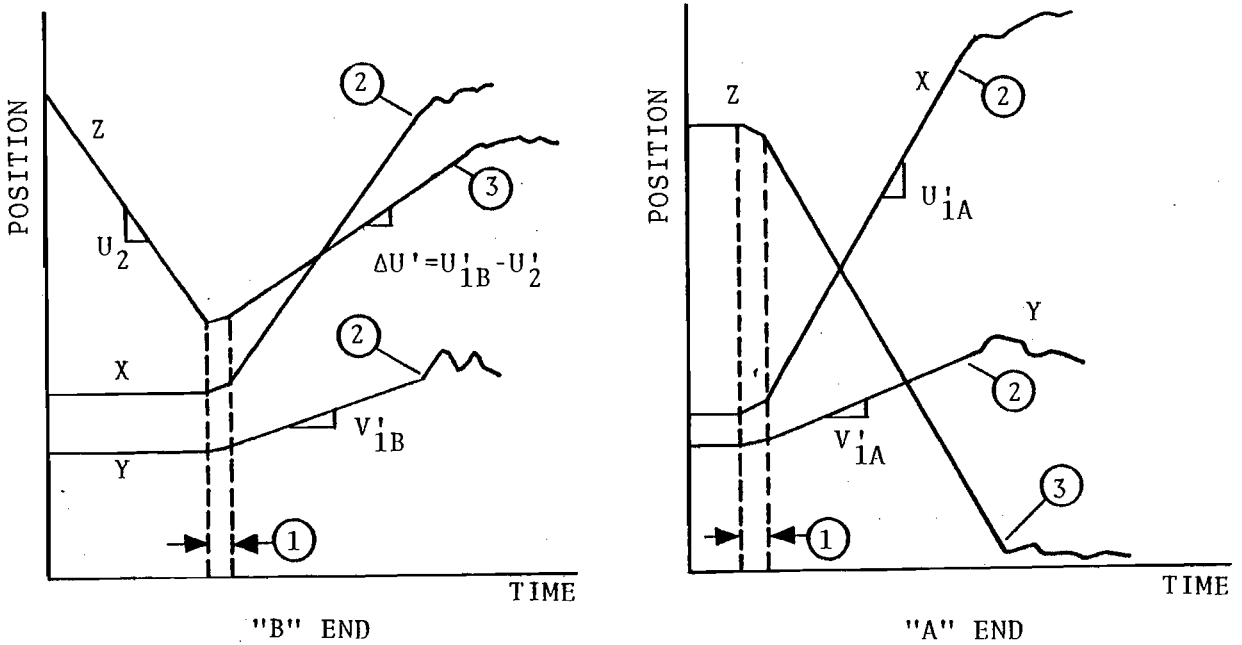

1 - Duration of first impact
2 - Beginning of second impact
3 - Beginning of third impact

FIGURE 19. TYPICAL APPEARANCE OF POSITION-TIME PLOTS

Figure 19 also indicates how slope measurements in the free-motion regions are used to estimate the following velocities:

U'_{1A}, V'_{1A} = Horizontal and vertical velocities of hopper carbody "A" end after first impact.

U'_{1B}, V'_{1B} = Horizontal and vertical velocities of hopper carbody "B" end after first impact.

U_2 = Striking tank car horizontal velocity before first impact.

$\Delta U' = U'_{1B} - U'_2$ Separation speed after first impact.

These raw data are summarized in Table 5, together with the independent speed-gate measurement for U_2. Examination of these results indicates that camera calibration errors are present.* This conclusion is reached because the apparent horizontal velocities U'_{1A}, U'_{1B} at the two ends of the hopper carbody are unequal in most cases. Such a result is physically possible only if the hopper carbody is stretching or compressing by a large amount (several feet in about one second), a hypothesis that is patently ridiculous.

A discrepancy is also observed between the camera and gate measurements of initial tank car velocity, U_2. This may be due in part to camera calibration error, and in part to a real difference in the tank car velocity at the two measurement points, which were separated by an unknown distance along the test track.

Based on the available information and an assumption that calibration errors are the only significant sources of discrepancy in tank car initial speed, the raw data have been adjusted by scaling to make U'_{1A} equal to U'_{1B}, and to make U_2 (camera) equal to U_2 (gate). The adjusted velocities, summarized in Table 6, will be used in subsequent analyses. The adjusted velocities are reported in terms of:

*Camera calibrations were based on nominal frame speed settings because time-interval markers were not included in the film.

TABLE 5. RAW VELOCITY DATA*

SERIES AND TEST NUMBER	U_{1A}'	V_{1A}'	U_{1B}'	V_{1B}'	$\Delta U'$	CAMERA U_2	GATE
3.2	19.6	4.95	20.2	3.33	3.85	21.5	21.9
3.3	22.8	5.93	23.8	6.73	6.76	20.4	24.2
3.4	21.4	5.58	21.3	3.86	3.90	17.8	22.6
3.5	22.9	6.40	22.3	6.16	2.91	24.8	24.8
4.1	26.7	5.03	24.6	6.40	3.44	25.8	27.3
4.2	36.9	10.40	24.9	4.92	10.20	25.5	28.2
5.1	26.7	5.65	26.7	8.72	7.60	26.7	28.5
5.2	25.3	8.00	23.4	4.00	2.55	20.4	27.9
6.1	22.4	6.66	20.0	6.81	3.49	20.8	20.6
7.1	21.6	17.80	22.8	12.20	4.11	26.2	26.6
10.1	24.8	5.33	27.1	2.91	5.62	20.0	25.1

*All speeds in units of ft/sec; 1 mph $\cong$ 1.47 ft/sec. Estimated measurement error $\pm$ 0.7 ft/sec due to plot resolution limits.

$U_1' = U_{1A}' = U_{1B}'$ = Horizontal velocity of hopper carbody center of mass after first impact.

$V_1' = \frac{1}{2}(V_{1A}' + V_{1B}')$ = Vertical velocity of hopper carbody center of mass after first impact.

$\omega_1' = (V_{1A}' - V_{1B}')/E$ = Angular velocity of hopper carbody about center of mass after first impact.**

U_2 = Initial horizontal velocity of striking tank car (value measured at speed gate).

U_2' = Horizontal velocity of striking tank car after first impact.

TABLE 6. ADJUSTED VELOCITY DATA*

SERIES AND TEST NUMBER	U_1'	V_1'	ω_1'	U_2	U_2'
3.2	20.6	4.30	.0547	21.9	16.67
3.3	28.2	7.66	-.0194	24.2	20.18
3.4	27.05	5.98	.0650	22.6	22.10
3.5	22.3	6.20	.0024	24.8	19.39
4.1	26.0	5.84	-.0564	27.3	22.36
4.2	27.5	6.59	.0703	28.2	16.23
5.1	28.5	7.67	-.0994	28.5	20.39
5.2	32.0	7.79	.1408	27.9	28.52
6.1	19.8	6.32	-.0258	20.6	16.34
7.1	23.15	15.73	.2030	26.6	18.98
10.1	34.0	5.48	.1107	25.1	26.95

*Linear velocities in ft/sec; 1 mph ≅ 1.47 ft/sec. Angular velocities in rad/sec.

** Where E = distance between reference points "F" = 33 ft; see Figure 11. Note that $\omega_1' > 0$ means that the carbody pitches "A"-end up.

5. DATA ANALYSIS

Preliminary analyses of the Switchyard Impact Tests and other rail vehicle collision test results have been conducted with complicated dynamic models that seek to represent the detailed behavior of each vehicle and coupling at the component level [15, 22, 30, 31, 32]. While there is a laudable intent of using such models to predict the absorption of collision energy by various inelastic deformation modes arising from the component properties, the attempt to attain this goal tends to disappear in a welter of detailed assumptions that must be made about the initial conditions and the elastic and inelastic behavior of each component of the model. Consequently, interpretation of test results with such models tends to emphasize adjustment of the many input parameters to match observed behavioral details (e.g., a complete position-time or coupler force-time plot from first through third impact), which may not shed much light on understanding of the fundamental physical behavior of vehicle collision.

This report takes the opposite approach by restricting the analysis to fundamental physical models that allow attention to be focussed on model validity and physical interpretation of the test data. It will appear, of course, that such an approach leads to an empirical estimate of energy absorption from the test data, rather than a prediction from component properties. However, such estimates are still useful, and it is hoped that the associated physical interpretation of the data will provide useful guidelines for refinement of detailed dynamic models in the future.

The following analyses treat the apparent motions of the vehicles immediately after first impact, i.e., in the time interval for which the motion measurements are the most reliable. It should be noted that, while the analysis of first impact provides some estimates for inelastic energy absorption, it does not address all of the possible inelastic mechanisms.

5.1 ONE-DIMENSIONAL ANALYSIS OF FIRST IMPACT

The data in Table 6 provide a concise kinematic description of first impact; it remains to be seen what type of model will be required to provide dynamical behavior consistent with the kinematics. The inadequacy of linear or quasi-linear models can be demonstrated by a one-dimensional analysis of the horizontal energy and momentum transfer. For this purpose the tank car and hopper car are treated as point masses m_2 and m_1, respectively (Figure 20). Based on this model, we expect intuitively that the striking tank car will be slowed down by the impact ($U_2' < U_2$). However, contrary results appear in the kinematics of tests 5.2 and 10.1 (see Table 6). While these results can be accounted for in part by presumed $\pm$ 0.7 ft/sec errors in the velocity estimates, the range of the observations for U_2' still indicates some deficiency in the model.

The deficiency is confirmed by examining the limiting cases of energy absorption of which the two-mass model is capable. The appropriate momentum and energy conservation laws for the model can be expressed as:

$$m_2U_2 = m_1U_1' + m_2U_2' \tag{1}$$

$$m_2(U_2)^2 = m_1(U_1')^2 + m_2(U_2')^2 + 2\varepsilon \tag{2}$$

where ε represents the energy absorbed inelastically. The absorbed energy is bounded by $0<\varepsilon<\varepsilon_c$, where ε_c is the standard collision energy for two masses impacting in one-dimensional motion:

$$\varepsilon_c = \frac{1}{2}\left(\frac{m_1m_2}{m_1 + m_2}\right)(U_2 - U_1)^2 = \frac{1}{2}\left(\frac{m_1m_2}{m_1 + m_2}\right)(U_2)^2 \tag{3}$$

Equations 1 and 2 can be solved to obtain the following expressions for the post-impact velocities (see Appendix D):

$$U_1' = \frac{m_1\varepsilon}{m_1 + m_2}\ U_2 \tag{4}$$

$$U_2' = \left[1 - \frac{m_1\varepsilon}{m_1 + m_2}\right]\ U_2 \tag{5}$$

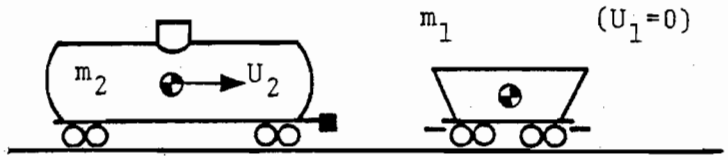

(A) Before impact

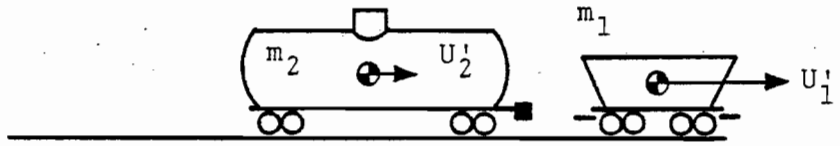

(B) After impact

FIGURE 20. TWO-MASS MODEL OF FIRST IMPACT

where

$$\varepsilon = 1 + \sqrt{1-e} \qquad e = \varepsilon/\varepsilon_c \tag{6}$$

are convenient parameters associated with inelastic energy absorption. The limiting cases are e=0 (ε=2) to represent a perfectly elastic collision, and e=1 (ε=1) to represent a completely inelastic collision.*

The limiting cases contain implicitly between them all possible one-dimensional, two-mass models incorporating any conceivable collection of detailed quasi-linear sub-models for inelastic components. Thus, the applicability of this entire class of models to the test results can be assessed by examining the limiting cases.

Figures 21 and 22 compare the observed velocities with bounds obtained from Eqs. 4 and 5 by using average values of the vehicle rail weights.** While the behavior of the hopper car (Figure 21) seems to confirm the validity of the two-mass model, the behavior of the tank car (Figure 22) fails to do so. At most, five of the eleven tests can be considered to fall within the bounds of the model in the latter figure.

These conflicting interpretations can be reconciled by a hypothesis that a small part of the tank car mass m_2 does not participate in the impact with the hopper car. Note that since $m_2 >> m_1$, the bounds obtained from Eq. 4 are not sensitive to small changes in the effective value of m_2, but that the bounds obtained from Eq. 5 can be sensitive to such changes. Two physical mechanisms can be invoked to explain the differences between rail-weight mass and effective mass. In the cases involving single

---

*Note that $U_1' = U_2' = m_2 U_2/(m_1+m_2)$ for the completely inelastic collision i.e., the two masses remain together after impact, and no additional momentum or energy can be transferred between them.

**See Table 3. The averages of eleven weights (unfilmed tests 3.1 and 7.2 excluded) are 38.03 KIPS for the empty hopper cars and 348.13 KIPS for the lead striking tank cars. Thus, $m_1/(m_1 + m_2) = \omega_1/(\omega_1 + \omega_2) = 0.0985$.

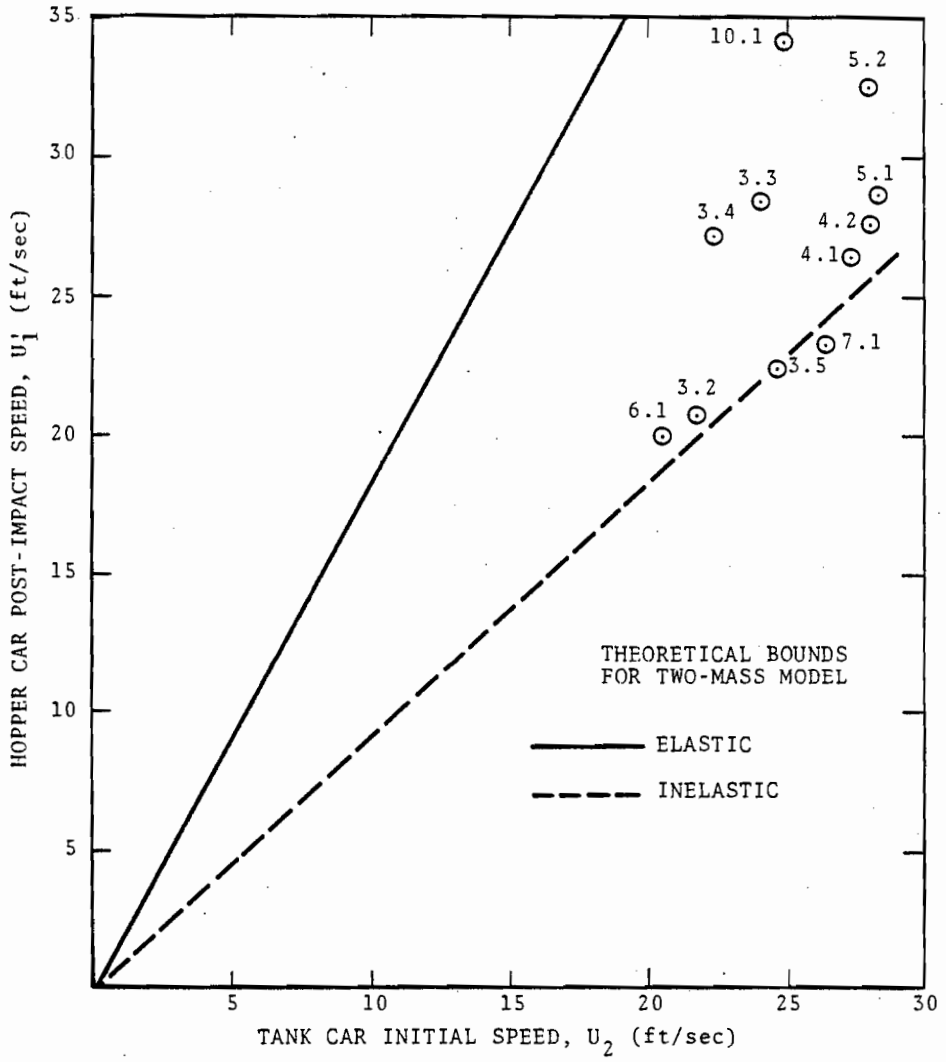

FIGURE 21. ASSESSMENT OF TWO-MASS MODEL BY COMPARISON WITH HOPPER CAR BEHAVIOR

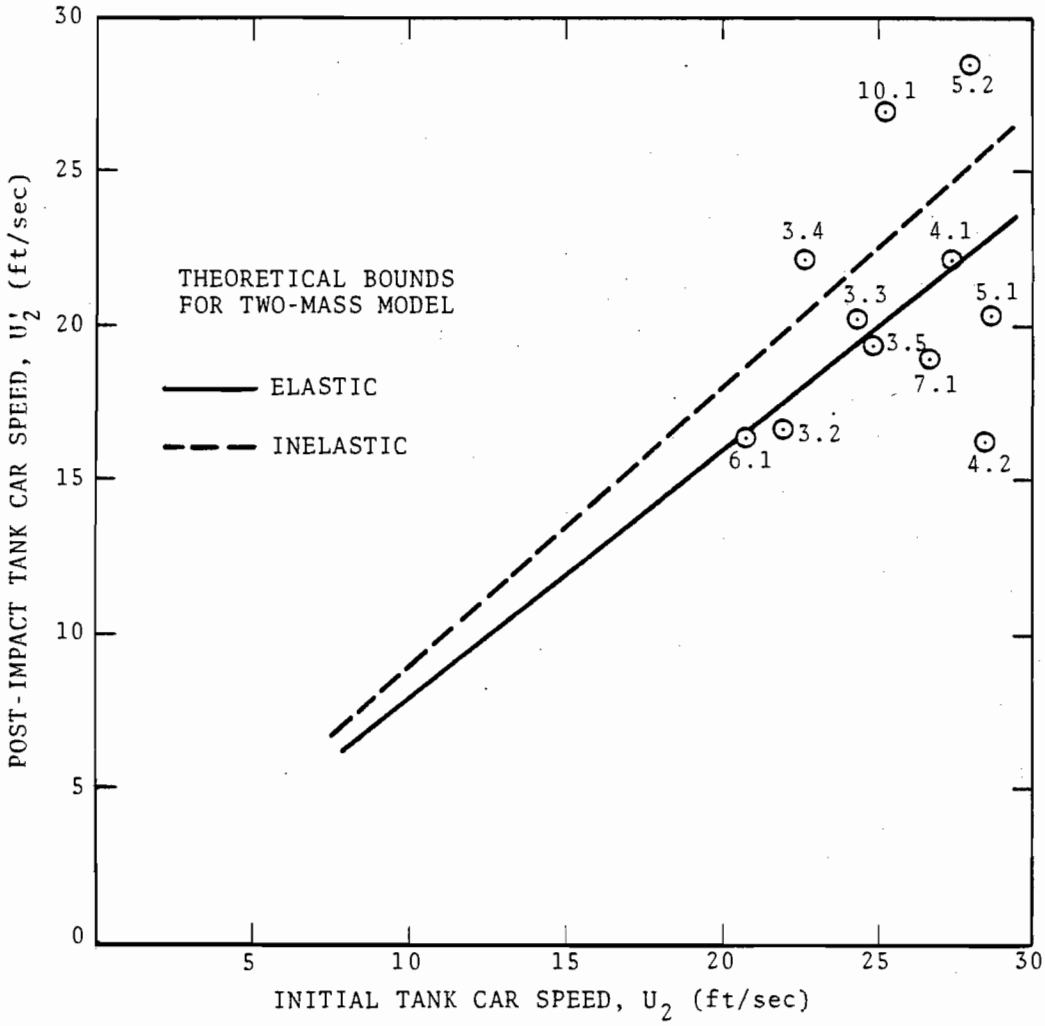

FIGURE 22. ASSESSMENT OF TWO-MASS MODEL BY COMPARISON WITH STRIKING TANK CAR BEHAVIOR

striking tank cars, a part of the lading may be ineffective due to sloshing. For three-car striking consists, the second and third vehicles may be almost completely ineffective due to dynamic slack action. Indeed, since the data have been compared with bounds based on a one-car striking mass, the position of test point 6.1 in Figure 22 strongly suggests the presence of slack action in that test.

5.2 SLOSHING/SLACK-ACTION MODEL

The effects of sloshing and slack action must be highly nonlinear to account for the observed horizontal kinematics of first impact. Linearized formulations are available to predict the frequency of small-amplitude sloshing for simple configurations (e.g., rectilinearly shaped tanks) and experimental data are available for cylindrical configurations applicable to tank car sloshing [33]. However, although the equivalent mass-spring models for small amplitude sloshing predict a reduced effective mass, they cannot account for impacts that result in either very small decrease or any magnitude of increase in the post-impact speed of the striking tank car. Furthermore, the weight of the other experimental evidence [35] and the fact that the tank cars are almost full point to a highly nonlinear phenomenon known as dome impact.

Under such conditions, it is possible for a portion of the lading to act as a nearly independent mass, which can be visualized to travel back and forth within the tank car. Momentum and energy exchange then occur periodically between the independent mass and the observed mass (tank carbody, trucks and remainder of lading). We may think of such exchanges as being confined to short periods during which the independent mass is close to one of the ends of the tank. As a conceptual model, we may assume the limiting case of instantaneous, perfectly elastic impacts illustrated in Figure 23. Prior to first impact with the hopper car, the momentum/energy exchanges taking place within the tank car system cause the velocity of the observed tank car mass to oscillate between two values: U_2 and

$$U_2'' = U_2 + \frac{2m_4}{m_2+m_4} (U_4 - U_2) \qquad (7)$$

Visual observations of this phenomenon (with a period between 2 and 3 seconds for tank cars with about 93 percent image) were mentioned previously. Speed-time plots qualitatively reflecting the visual observations and corresponding to the conceptual model are compared schematically in Figure 24.

It is reasonable to expect that slack action in the three-car striking consists should exhibit nonlinear characteristics similar to those associated with dome-impact sloshing. In the case of slack action, the periods of car-to-car momentum/energy transfer will be restricted to time intervals during which the couplers are close to full buff or full draft position. Slack action can be treated conceptually in the same manner as sloshing, with the understanding that the observed and independent masses are to be taken respectively as the lead tank car and the remaining cars in the striking consist. However, it must be recognized that the ability of the model shown in Figure 23 to represent slack action will be limited to consists of a few cars. For longer consists, more detailed models will be required to account for distributions of buff and draft conditions and for elastic wave effects.

The apparent anomalies that resulted from analyzing the test results with the two-mass model can now be explained by replacing the point-mass tank car with the sloshing/slack-action model of Figure 23. First impact is now a light impact, in the sense that the striking mass m_2 is less than the total mass of the striking consist. However, first impact must be treated as a compound sequence consisting of an observed impact (m_2/m_1) and a subsequent sloshing/slack-action impact (m_4/m_2).

Two possible sequences are illustrated in Figures 25 and 26. In Figure 25, the observed tank car mass m_2 is traveling at its lower speed U_2 when the hopper car is engaged. Consequently, the observed mass is slowed to speed U_2''', which is less than the speed U_2', predicted by the two-mass model. However, when the

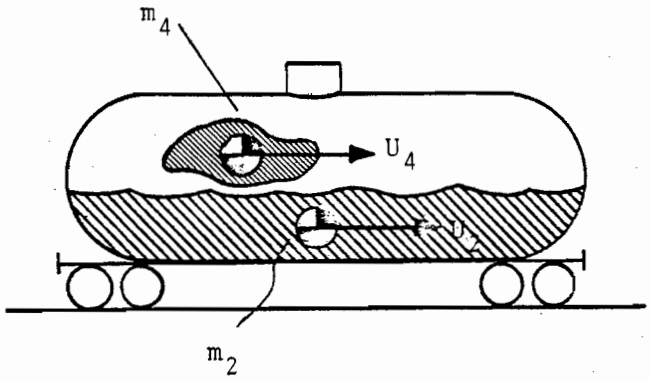

m_2 = Observed mass

m_4 = Independent mass

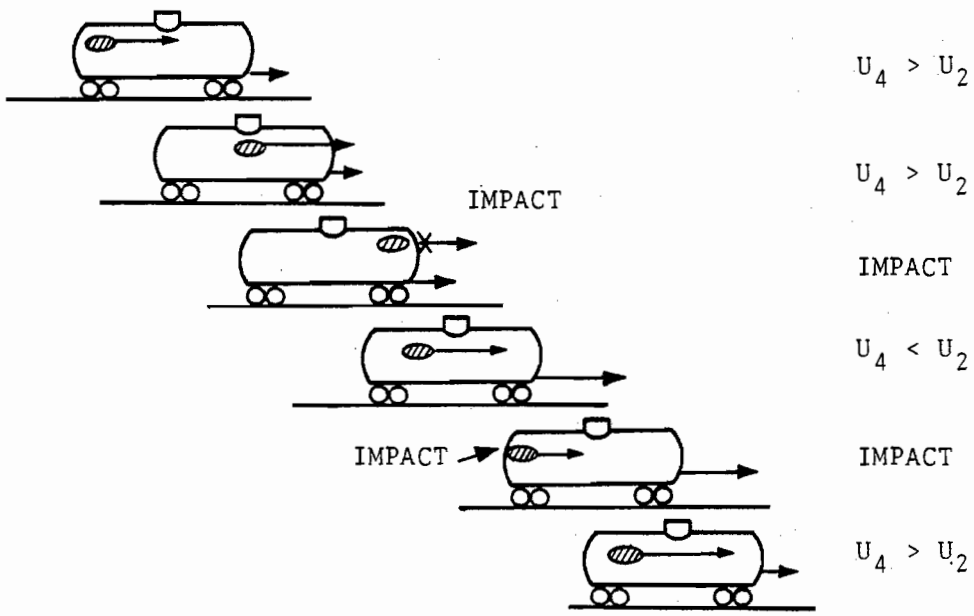

FIGURE 23. SLOSHING MODEL

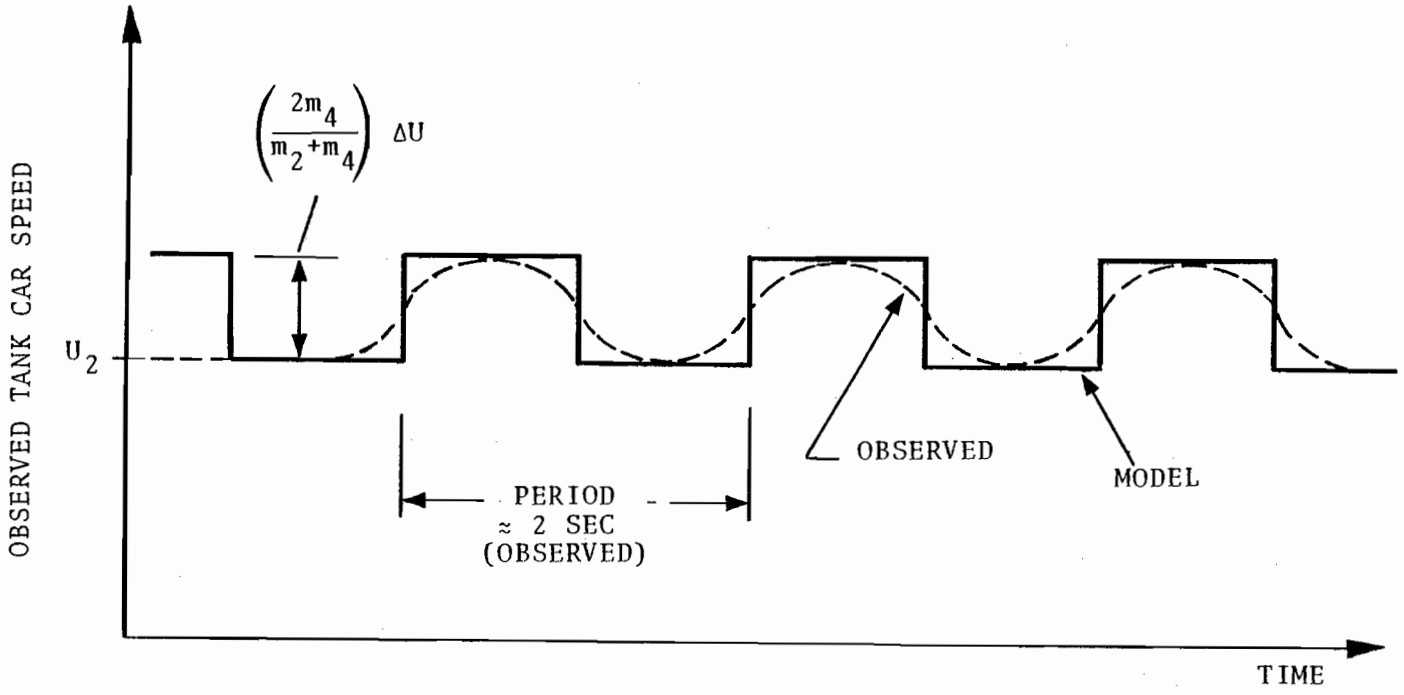

FIGURE 24. KINEMATIC BEHAVIOR OBSERVED DURING SLOSHING ACTION

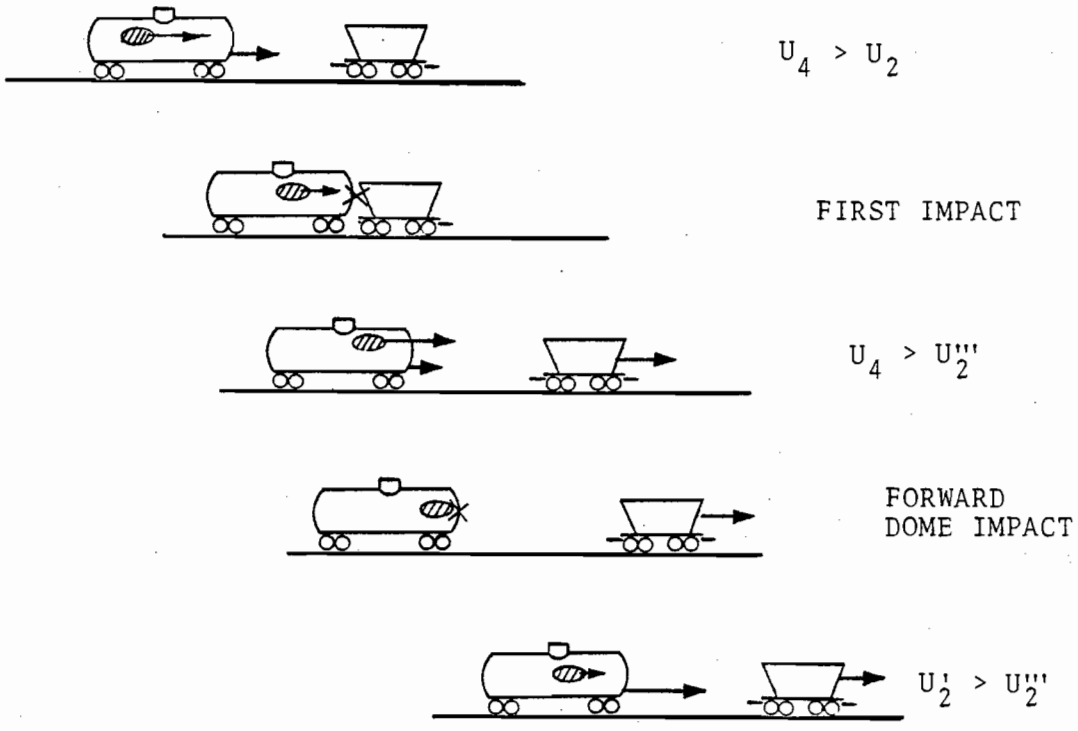

FIGURE 25. LIGHT SLOW IMPACT

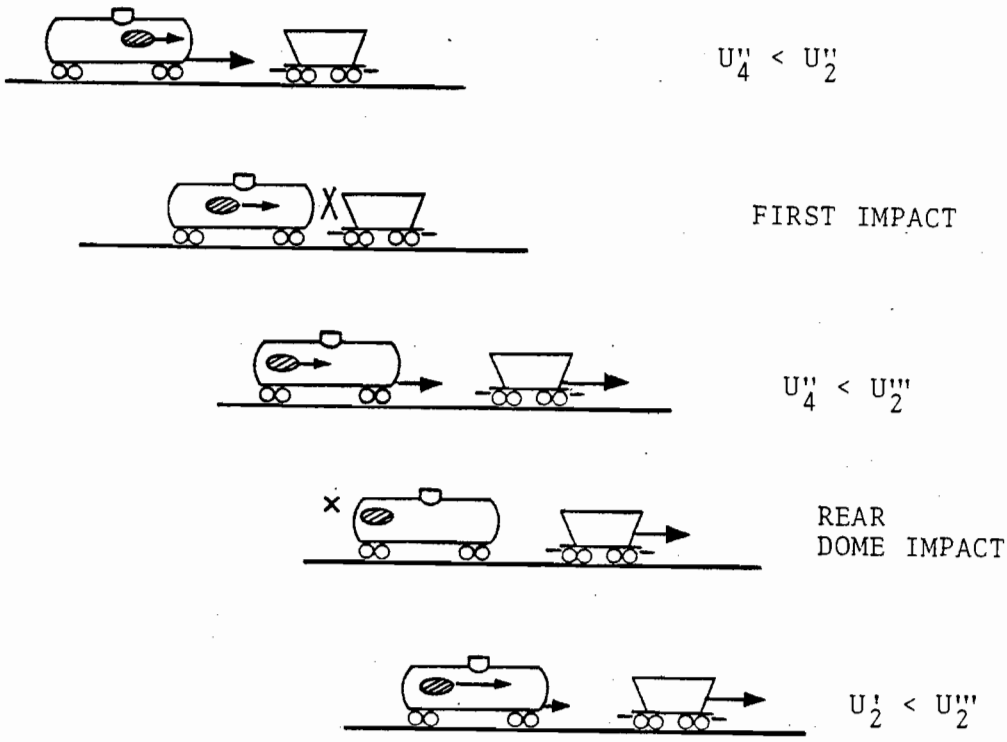

FIGURE 26. LIGHT FAST IMPACT

independent mass m_4 engages the forward end of the tank car, the observed mass is accelerated to a higher speed U_2'. The value of U_2' will generally be different from the U_2' predicted by the two-mass model, and under some conditions the result of the compound sequence is $U_2' > U_2$. Hence, this sequence is able to account for both anomalously low and anomalously high post-impact speeds. Figure 24 illustrates the opposite case, in which the observed tank car mass is traveling at its higher speed where it engages the hopper car. In this case, the independent mass subsequently impacts the rear end of the tank car and the final post-impact speed is always less than U_2.

The apparent anomalies in the observed speeds can now be explained by a hypothesis that the m_4/m_2 impact can occur either very quickly or with some delay after the m_2/m_1 impact. Thus, high values of U_2' can result from a "quick" version of the light slow impact (Figure 25) in which the position plotting resolution has missed a short time interval of reduced tank car speed. On the other hand, low values of U_2' can result from a delayed version of the light slow impact or from the light fast impact.

Predictions of the sloshing/slack-action model are again based on the formulation and solution of momentum and energy conservation laws and a hypothesis that an amount of energy, ε, is absorbed inelastically by the tank car/hopper car impact. For the case of light slow impact the solutions of immediate interest are:

$$U_2''' = \left[1 - \frac{m_1 \varepsilon}{m_1 + m_2}\right] U_2 \qquad (8)$$

$$U_2' = \left[1 + \left(\frac{m_4 - m_2}{m_2 + m_4}\right)\left(\frac{m_1 \varepsilon}{m_1 + m_2}\right)\right] U_2 + \left(\frac{2m_4}{m_2+m_4}\right)(U_4 - U_2) \qquad (9)$$

where ε is the energy-absorption parameter defined previously (see Eqs. 3 through 6), except in terms of the observed mass m_2. Details of the formulation and solution appear in Appendix D.

To assess the sloshing/slack-action model, the observed data for U_2 and U_2' have been replotted in Figure 27, where they

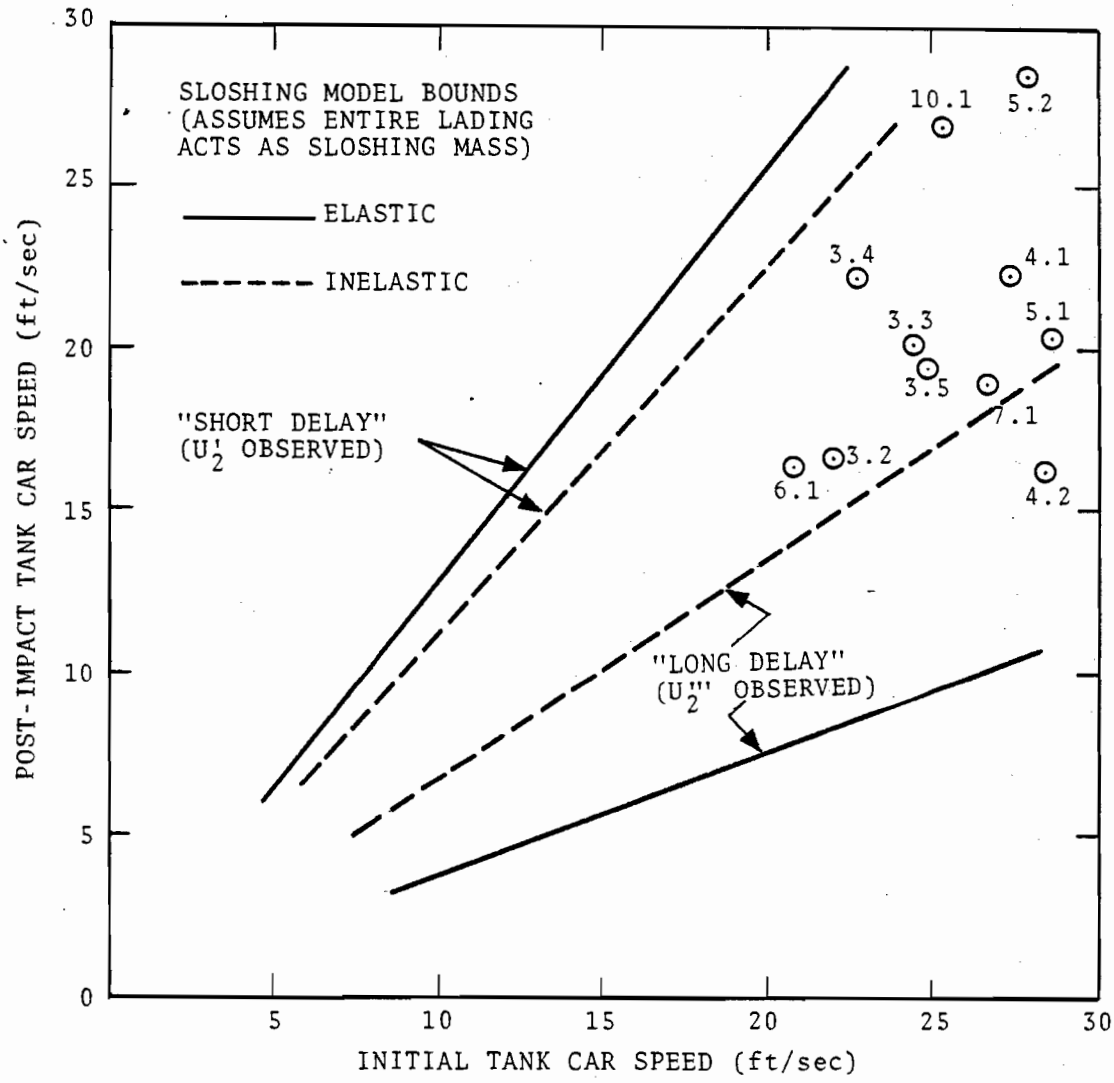

FIGURE 27. ASSESSMENT OF SLOSHING/SLACK-ACTION MODEL

are compared with bounds derived from limiting cases of Eqs. 8 and 9. The following assumptions were used to derive the bounds:

1. Average properties for a single tank car to represent the striking consist.
2. Entire tank car lading assumed to act as independent mass m_4.
3. Limiting case to represent small amount of initial sloshing ($U_4=U_2$).

Also, note that the inelastic short-delay bound is not completely accurate because m_4/m_2 impact should actually be $m_4/(m_2+m_1)$ impact for this case.

It is apparent from the figure that the sloshing/slack-action model is able to account for the horizontal kinematics observed in the tests. However, it is of more interest to conduct a detailed analysis of the data with the model to estimate the actual amounts of mass involved in sloshing or slack action. The results of a trial-and-error analysis with the short- and long-delay versions of the light slow impact are summarized in Table 7. The trial-and-error procedure involved successive assumptions for the independent mass, with the objective of bounding as many of the observations as possible. The results indicate that the single striking tank car appears to be reasonably represented by assuming a sloshing mass equivalent to twice the outage. (Note, however, that tests 4.2 and 5.1 were not fit well by this assumption.) In the three-car consist cases, test 6.1 is reasonably represented by slack action nor sloshing,* and test 10.1 appears to have been intermediate between slack action and full buff condition.

5.3 TWO-DIMENSIONAL ANALYSIS OF FIRST IMPACT

First impact must be analyzed in at least two dimensions to

*The results of test 7.1 may have been affected by the standing consist.

TABLE 7. RECONCILIATION OF OBSERVATIONS WITH SLOSHING/SLACK-ACTION MODEL

SERIES AND TEST NUMBER	NUMBER OF HAMMER CARS STRIKING CARS	SLOSHING OR SLACK MASS ASSUMPTION	TYPE OF DELAY	SPEED RATIO U_2 (AFTER)/U_2(BEFORE)		
				PREDICTED		
				ELASTIC COLLISION	INELASTIC COLLISION	OBSERVED
3.2	1	2X OUTAGE	LONG	0.777	0.889	0.762
3.3	1	2X OUTAGE	LONG	0.777	0.889	0.832
3.4	1	2X OUTAGE	SHORT	0.870	0.953	0.978
3.5	1	2X OUTAGE	LONG	0.777	0.889	0.782
4.1	1	2X OUTAGE	LONG	0.780	0.890	0.819
4.2	1	2X OUTAGE	LONG	0.782	0.891	0.575
5.1	1	2X OUTAGE	LONG	0.780	0.890	0.715
5.2	1	2X OUTAGE	SHORT	0.900	0.981	1.021
6.1	3	2 REAR HAMMER CARS IN DRAFT	LONG	0.793	0.896	1.793
7.1	3	2 REAR HAMMER CARS IN DRAFT	LONG	0.833	0.916	0.713
10.1	3	2X OUT/REAR IN BUFF REAR CARS IN DRAFT	SHORT	0.958 1.168	0.996 1.158	1.072

make a complete estimate of the energy absorbed by various kinematic as well as inelastic modes. The general requirements for the two-dimensional model can be derived from examination of Table 6. The effects of sloshing and slack action are most important for study of the striking consist, but the two-dimensional model emphasizes the role of the hopper car. Hence, it is appropriate to treat the striking consist as a point mass again, but with an effective mass m_2 out of a total rail-weight mass m_2+m_4. However, the simplest model, which treats the hopper car as a single rigid mass, is inconsistent with the test results, in that it predicts angular velocities one order of magnitude larger than the observations, and that it cannot predict the observed vertical velocities. (For details, see Appendix E.)

A two-dimensional model consistent with the test results is illustrated in Figure 28. The dimensions ℓ, h, L and the inertial properties m_2, m_3, I_1 are taken from Table 2 and Figure 11. The second part of the figure illustrates the detail of carbody/truck interaction. The impact between the centerplate and bowl can be treated as a sliding surface contact at a characteristic angle $90°-\theta$, and it is then easily shown that the changes in carbody velocity resulting from this impact must obey the relation:

$$-\Delta V''/\Delta U'' = \tan\theta \qquad (10)$$

The carbody/truck interaction supplies the mechanism by which the carbody can acquire a vertical velocity and reduce its angular velocity. The mass of both trucks is treated as if it were located at the "B" end of the hopper car, but this treatment preserves the angular momentum-transfer characteristics between the carbody and the trucks. Since the trucks can be assumed to interact with the earth immediately after carbody/truck impact, the vertical mass $m_3 \to \infty$ can be adopted to simplify the predictions.

First impact is now treated as the compound sequence shown in Figure 29. The striking consist is treated as a point mass, m_2, traveling horizontally and with its center of mass located on the first-impact line of action shown in Figure 28. (This simplified treatment ignores a small amount of angular momentum that

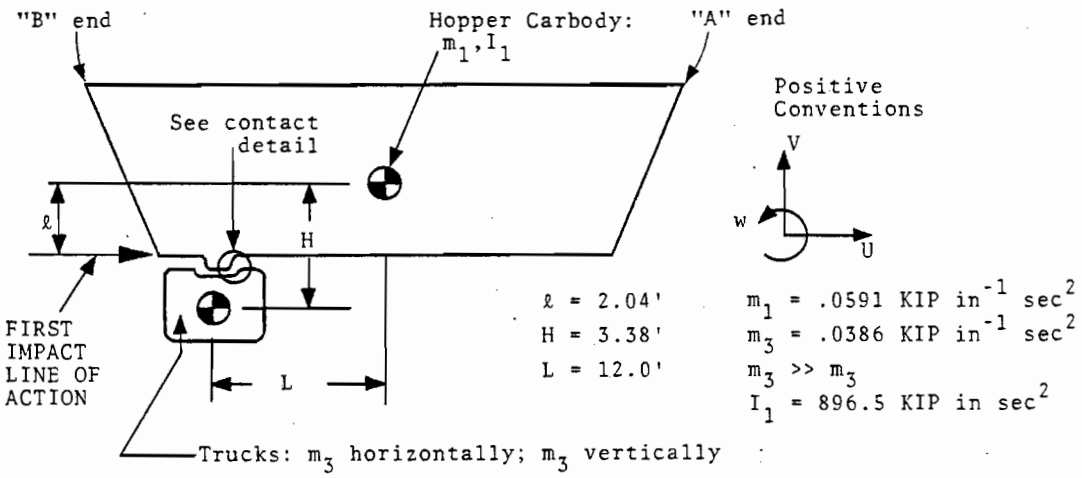

(A) Model Characteristics

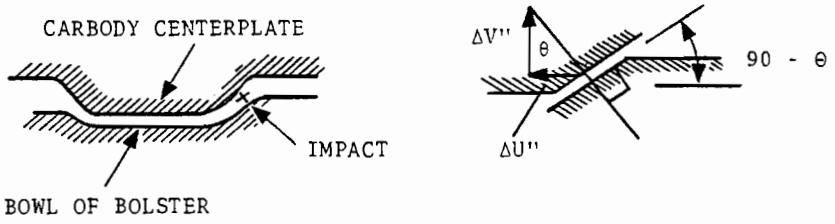

(B) Contact Detail

FIGURE 28. CARBODY/TRUCK INTERACTION MODEL

(A) Initial Conditions

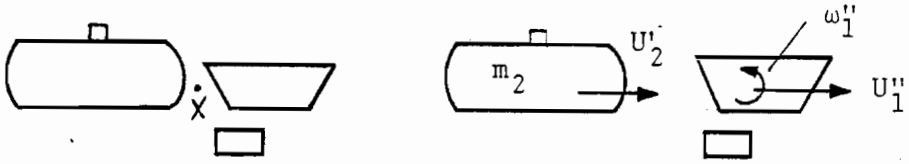

(B) Impact Between Tank Car and Hopper Carbody

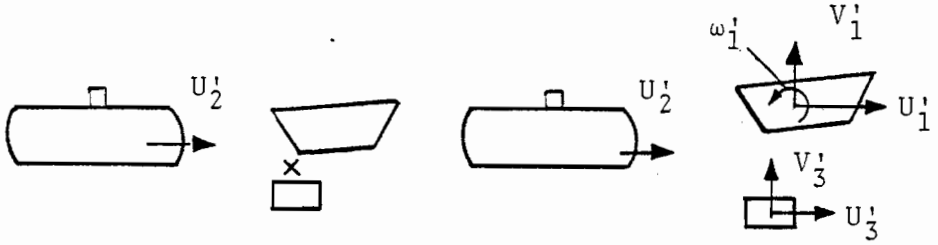

(C) Carbody/Truck Interaction

FIGURE 29. COMPOUND SEQUENCE FOR FIRST IMPACT

may be acquired by the striking consist.) The tank car/hopper car impact causes the hopper carbody to acquire velocities U_1'' and ω_1'', the latter representing upward pitch of the "A" end, while the striking consist is slowed to its final velocity U_2'. An amount of energy E is assumed to be absorbed inelastically by this impact. Carbody/truck interaction then occurs, such that the carbody attain velocities U_1', V_1', ω_1' and the truck mass acquire velocities U_3', V_3' (the vertical velocity V_3' is, of course, zero in the limiting case $m_3 \to \infty$), As amount of energy E'' is assumed to be absorbed inelastically in this impact.

Momentum and energy conservation laws can be formulated for each of the impacts described above, these equations can be solved in combination with the contact constraint (Eq. 10) to obtain expressions for the final velocities in terms of the initial conditions. The complete formulation and solution appears in Appendix E. Of most interest in the present case are the predictions for the hopper carbody, which can be expressed as:

$$\frac{U_1'}{U_2} = \frac{E}{A}\left[\frac{I_1}{m_1 \ell^2} - \frac{C\ (C-1)}{B}\ E''\right] \tag{11}$$

$$\frac{V_1'}{V_2} = \frac{C\ (C-1)\ EE''}{AB}\ \tan\theta \tag{12}$$

$$\frac{\ell\omega_1'}{U_2} = \frac{E}{A}\left[1 - \frac{CE''}{B}\right] \tag{13}$$

where

$$A = 1 + \frac{(m_1+m_2)\ I_1}{m_1 m_2 \ell^2} \tag{14}$$

$$B = 1 + \frac{I_1}{\bar{m}\ (H+L\tan\theta)^2} \tag{15}$$

$$C = 1 + \frac{I_1}{\bar{m}\ (H+L\tan\theta)} \tag{16}$$

and where $\bar{M}$ is an effective mass defined by

$$1/\bar{M} = \frac{1 + \tan^2\theta}{m_1} + \frac{1}{m_3} \tag{17}$$

The quantities ε and ε are nondimensional energy-absorption parameters bounded by $1 \leq \varepsilon, \varepsilon'' \leq 2$, where the lower and upper limits represent completely inelastic and perfectly elastic collision, respectively.

The energy-absorption coefficients and the contact angle, θ, are the unknowns in Eqs. 11 through 13. Expected values of these quantities can be estimated from the test data by means of a nonlinear regression analysis that leads to the following estimator formulae:

$$\tan \hat{\theta} = \frac{(\Sigma x_i)\ (\Sigma x_i) - \frac{N}{2}\ (\Sigma x_i y_i)}{N\ (\Sigma x_i^2) - (\Sigma x_i)^2} \tag{18}$$

$$\hat{\varepsilon} = \frac{1}{N} \left[(\Sigma x_i) + \frac{1}{\tan \theta}\ (\Sigma y_i) \right] \tag{19}$$

$$\hat{\varepsilon}'' = \frac{B}{C} \left[1 - \frac{\ell A}{N\hat{\varepsilon}}\ \Sigma \frac{\omega'_{1i}}{U_{2i}} \right] \tag{20}$$

where

$$x = \frac{Am_1\ell^2}{I_1} \left(\frac{U'_1}{U_2} \right) \quad y = \frac{Am_1\ell^2}{I_1} \left(\frac{V'_1}{U_2} \right) \tag{21}$$

and where A, B, C are given by Eqs. 14 through 17, N is the number of samples (the eleven test results), and Σ represents summation over the =1,2,...,N observations*. Details of the formulation and solution appear in Appendix F.

Application of the regression model to the test data leads to the following results:

$$\hat{\theta}_{AVG} \cong 83° \quad \hat{\varepsilon}_{AVG} \cong 1.25 \quad \hat{\varepsilon}''_{AVG} \cong 1.02$$

*Mass properties of the typical hopper car (Figure 11) and striking-consist effective masses based on Table 7 were used in the regressior

The result for $\hat{\theta}$ suggests that carbody/truck interaction tends to be a glancing impact, which is consistent with the intuitive picture of a centerplate pitching up and out of its bowl as the carbody moves forward. The results for ε and ε'' suggest that virtually all of the collision energy available for absorption during the first impact is absorbed inelastically.

5.4 ENERGY AVAILABLE FOR HEAD PUNCTURE

The collision energy available for puncture of tank car heads in typical train makeup accidents can be estimated by first accounting for the energy absorbed by other modes. Based on the results discussed in Subsection 5.3, it appears reasonable to assume that all of the collision energy available to the compound first-impact sequence is absorbed inelastically, i.e., $e=e''=1$ where

$$e = 1 - (\varepsilon-1)^2 \qquad e'' = 1 - (\varepsilon''-1)^2 \tag{22}$$

are the nondimensional energy absorption coefficients. However, these coefficients are defined in terms of the energies available for each impact (see derivation in Appendix E):

$$e = \frac{E}{\frac{1}{2}\left[\frac{m_1 m_2 \ell^2 I_1}{m_1 m_2 \ell^2 + (m_1+m_2) I_1}\right] (U_2/\ell)^2} \tag{23}$$

$$e'' = \frac{}{\frac{1}{2}\left[\frac{\bar{M}\, I_1\, (H+L\tan\theta)^2}{\bar{M}\,(H+L\tan\theta)^2 + I_1}\right] \left(\omega_1'' + \frac{U_1''}{H+L\tan\theta}\right)^2} \tag{24}$$

whereas it is of greater practical interest to determine the ratio of $E+E''$ to the total initial kinetic energy of the effective mass of the striking consist, $\frac{1}{2} m_2 U_2^2$. The details of the necessary calculations, reported in Appendix F, show that

$$(E+E'')_{AVG} \cong 0.065 \left(\tfrac{1}{2} m_2 U_2^2\right) \tag{25}$$

In addition to the inelastic mechanism, it is also appropriate to think of the kinetic energies of hopper carbody vertical and rotational motion and truck horizontal motion as energy-absorption mechanisms, in the sense that these kinetic energies cannot be retransmitted to an adjacent tank car in a manner that would contribute to head puncture. A calculation based on the average values of V_1', ω_1' and U_2 shows that these mechanisms absorb about $0.005\ (1/2m_2U_2^2)$.

Thus, out of the initial kinetic energy of the effective mass of the striking consist, about 7 percent can be considered to have been absorbed by the effects of a typical first impact. The remaining 93 percent resides in kinetic energy of horizontal motion of the hopper carbody and the striking consist effective mass, and all of this amount is potentially available for head puncture.

However, two other inelastic energy-absorption mechanisms must be considered: breakage of the couplers by elastic-plastic bending of the shanks, such as was observed to occur in some of the tests with shelf-E couplers, and hopper carbody buckling, which was also observed in one test. Estimates for these modes show that coupler shank bending can absorb at most about 10 percent of the initial kinetic energy of a 16 mph loaded tank car, while hopper carbody buckling can potentially absorb the entire amount.

6. DISCUSSION AND CONCLUSIONS

This report has reviewed the results of the FRA-AAR-RPI Switchyard Impact Test Program, in which full-scale impact tests were conducted to simulate typical switchyard accident situations involving loaded class 112A/114A hazardous-material tank cars. The test results have been analyzed with simplified dynamic models that have provided the basis for rational interpretation of the observed vehicle motions.

The test program and the analyses have led to an understanding of the proximate causes of tank car head puncture in switchyard accidents. Also, the effectiveness of shelf-E couplers and head shields mounted on 112A/114A tank cars for reducing the frequency and severity of head puncture has been evaluated. The following conclusions can be drawn based on the test results and analyses.

The presence of a loose light car in a train makeup increases the chances of override, tank head impact, and puncture in switchyard operations.

The presence of loose cars in a makeup can result from failure to couple during humping operations. An unloaded loose car is susceptible to large-amplitude vertical and pitching motions when struck by the next car to be fed into the makeup. The 50 and 60 ton class hopper cars used int he Switchyard Impact Tests are highly susceptible to such motions because of their low empty weight and high carbody center of gravity. Other types of unloaded freight cars may act in a similar manner, but are less susceptible to the required amplitudes because of heavier empty weight and, in some cases, lower carbody center of gravity (Table 8). In any case, the principal significance of the loose light car lies in its ability to provide the kinematic mechanism for bringing sharp objects (usually its own couplers) into contact with the heads of adjacent tank cars.

TABLE 8. COMPARISON OF FREIGHT CAR EMPTY WEIGHTS

CAR TYPE	EMPTY WEIGHT (KIP)	REMARKS
Hopper Car	37 to 40	Open top, 50 to 60 ton class
Box Car*	50 to 80	
Stock Car*	45 to 50	
Gondola*	55 to 90	Slightly lower C.G.
Flat Car*	50 to 70	Lower C.G.

*Source: Reference 30

Backup spacing is an important parameter, in that it significantly increases the chances of override.

Backup spacing can result when a car being humped onto the end of a standing makeup fails to couple and rebounds before coming to rest. Various backup spacings, up to the order of several feet, have been observed in switchyard operations. For cars equipped with standard-E couplers, override is encouraged even by small spacings. For example, the Switchyard Impact Tests have demonstrated that light-car override occurs consistently at 2.5-ft. backup spacing. Tests 5.1 and 5.2 have also indicated that, while the shelf-E coupler can prevent override at short spacings, the effective range is limited by light-car dynamics. On the basis of the test results, this limit appears to lie between 2.5 and 3.5 ft.

Override and tank head impact can occur at impact speeds as low as 12 mph.

Two such instances of override, one with tank head impact, were observed in the test program (test 2.1 at 11.7 mph and test 3.1 at 12.7 mph). Occurrences of 112A/114A tank car head punctures

at impact speeds as low as 4 mph in switchyard operations have been reported [14]. Occurrences at such low speeds apparently involve unique kinematic situations, and the reported occurrences may have involved effects of low temperature on the ductility of tank head materials.

Tank head puncture is likely to occur at impact speeds above 17 mph if the striking car is a single loaded tank car (e.g., test 3.5). If there is a striking consist of more than one heavy car, puncture is likely at impact speeds above 14 to 15 mph (e.g., test 6.1).

Severe head impact damage is caused by one or more heavy striking cars.

The loose light car merely activates the override mechanism; it does no significant damage to the tank head at second impact. Severe damage occurs when the heavier striking consist collides with the standing consist. The effective weights of both consists must be considered in evaluating the potential severity of the final collision. As has been shown by analysis of the test results, sloshing in a single striking tank car may reduce the effective weight slightly below the rail weight when the car is loaded to 93 percent or more innage. However, the effective weight of a string of cars may be considerably less than the sum of their rail weights because of slack action. This applies to both striking and standing consists.

In any case, the potential for tank head puncture during the final collision is much greater than at first or second impact because the final collision occurs between two large and essentially equal masses. At a minimum, these masses are one heavy car plus the light carbody (standing) and one heavy car (striking). Thus, the kinetic energy available for absorption during the final collision is much larger than the energy available at first or second impact.

The potential for tankhead puncture increases as cars are added to either consist, since the effective collision mass is

increased thereby. However, the increase cannot be indefinite, but rather will be limited by loss of ability of a long consist to behave as a rigid mass.

Severe tank head damage may occur at either the standing or striking consist. The actual location is highly variable, and is determined by the dynamic behavior of the loose light car between first and third impact.

Inelastic energy absorption by mechanical components and kinematic dissipation is not able to prevent tank head punctures in severe accidents.

Energy available for head puncture is proportional to the square of the impact speed. Thus, comparing switchyard accidents that caused punctures at reported speeds of 4 mph with a moderately severe (say, 12 mph) accident, and assuming that no inelastic absorption occurred at 4 mph, it appears that about 10 percent of the energy available at 12 mph is all that is required to puncture a tank head.

Hence, components must absorb more than 90 percent of the available energy to prevent puncture. Analysis has shown that the absorption mechanisms in the draft gear and suspension are typically completely inelastic, and in such state can absorb about 6.5 percent of the available energy at first impact. Another 0.5 percent is typically lost in pitching and vertical motions of the loose light car, this energy being dissipated at some location other than the tank head at second impact. Also, one might reasonably assume that at second impact the kinetic energy stored in horizontal motion of the loose light car is dissipated at locations other than the puncture site on the tank head. This will amount to another 5 to 10 percent, according to the analysis. Finally, it has been shown that the severe bending of coupler shanks can absorb about 10 percent. Thus, all of these components and kinematic dissipation mechanisms together are able to absorb at most only about 30 percent of the available energy. Hence, about 70 percent of the initial energy remains available for the final collision: far more than apparently required to puncture a

tank head.

Carbody buckling is an effective but unreliable energy absorption mechanism.

A crude calculation has shown that the carbody of a 60 ton class hopper car may be able to absorb by inelastic buckling an amount of energy of the same order of magnitude as the collision energy. However, carbody buckling is an imperfection-sensitive and therefore highly unreliable mechanism, i.e., it cannot be depended upon to absorb sufficient energy, given the variations that may be expected in carbody conditions. It is noteworthy in this connection that a tank head puncture occurred in the one test case where extensive carbody buckling was observed (Test 5.2).

The shelf-E coupler is a useful device for reduction of accident severity, but cannot be relied upon alone as a preventive measure.

The principal effectiveness of the shelf-E coupler, as observed in the Switchyard Impact Tests, lies in its ability to prevent override or to tear off the coupler of the loose light car if override occurs. When the coupler is torn off, the likelihood of a tank head puncture is reduced by the increased bearing area (usually the end sill) that impacts the tank head.

However,to the effective, the shelf-E coupler must fully engage the opposing coupler. Otherwise, the top shelf is typically torn off without preventing override and without seriously damaging the opposing coupler or absorbing any significant amount of energy. Whether or not full engagement occurs will be highly variable, depending upon loose light car weight, C.G. height, and backup spacing. Again, test 5.2 can be cited as a case in point. In that test, a partial engagement by the shelf-E couplers failed to tear the couplers off the loose car, while override and a tank head puncture occurred, even with some energy having been absorbed by carbody buckling.

Head shield designs influence the mechanism of tank head impact and puncture.

The head shield per se does not appear to absorb any significant amount of collision energy. However, after being torn from its mountings the head shield acts as a bearing plate between the impacting coupler and the tank head, thus effectively blunting the coupler and distributing the impact energy over a greater area. The effectiveness of the head shield concept was demonstrated by tests 4.2 (one striking car, 19.2 mph, part-height head shield) and 10.1 (three striking cars, 17.1 mph, full-height head shield). The latter test represents severe upper-limit conditions that might be encountered in switchyard accidents.

On the other hand, part-height head shields may be rendered ineffective by the kinematics of override. This was demonstrated by test 4.1 (one striking car, 18.7 mph, part-height head shield). In that test, the loose light car underwent pitching and vertical motions with amplitudes large enough to cause its impact-end coupler to override the head shield and puncture the upper half of the tank head.

REFERENCES

1. Code of Federal Regulations, Title 49 "Transportation," Part 179, Section 105, October 1977.

2. Phillips, E.A., "RPI-ARR Railroad Tank Car Safety, Research and Test Project," paper presented to the Rail 76 Conference, Basle, Switzerland, June 3-4, 1976.

3. Levine, D. and D. Dancer, "Fire Protection of Railroad Tank Cars Carrying Hazardous Materials - Analytical Calculations and Laboratory Screening of Thermal Insultation Candidates," U.S. Naval Ordnance Laboratory, NOL-TR-72-142, July 1972.

4. Anderson, C. et al., "Railroad Tank Car Fire Test: Test No. 6," U.S. Army Ballistics Research Laboratories, FRA-OR&D-75-36, August 1973.

5. Anderson, C. et al., "Railroad Tank Car Fire Test: Test No. 7," U.S. Army Ballistics Research Laboratories, FRA-OR&D-75-37, December 1973.

6. Anderson, C. et al., "The Effects of a Fire Environment on a Rail Tank Car Filled with LPG," U.S. Army Ballistics Research Laboratories, FRA-OR&D-75-31, September 1974.

7. Townsend, W. et al., "Comparison of Thermally Coated and Uninsulated Rail Tank Cars Filled with LPG Subjected to a Fire Environment," U.S. Army Ballistics Research Laboratories, FRA-OR&D-75-32, December 1974.

8. Phillips, E.A. and A.M. Skogsberg, "Phase 11 Report on Specifications for Insulation-Jacket Type Thermal Shield Systems on DOT 112A(114A) Tank Cars," RPI-AAR Tank Car Safety Research Project, RA-11-7-34 (AAR-R-196), November 1975.

9. Johnson, M.R., "Results of the Accelerated Life Testing of Hazardous Materials Tank Cars," IIT Research Institute, Chicago, IL, in preparation.

10. Anon., "Final Phase 01 Report on Accident Review," RPI-AAR Report No. RA-01-4-16, June 1972.

11. Everett, J.E. and E.A. Phillips, "Hazardous Materials Tank Cars - Tank Shield or Bumper Design," Association of American Railroads, FRA-RP-72-01, August 1971.

12. Phillips, E.A. and L. Olson, "Final Phase 05 Report on Tank Car Head Study," RPI-AAR Tank Car Safety Research Project, RA-05-1-17, July 14, 1972.

13. Phillips, E.A., "Phase 15 Switchyard Impact Test Program," memorandum to RPI-AAR Tank Car Safety Research Project Review Committee, February 18, 1975.

14. Schlink, L.J., "Phase 15 Report on Switchyard Impact Tests," RPI-AAR Tank Car Safety Research Project, RA-15-1-40 (AAR R-304), August 2, 1978.

15. Tong, P., "Mechanics of Train Collision," DOT Transportation Systems Center, FRA-OR&D-76-246, April 1976.

16. Peters, D.A. (Washington University, St. Louis, MO), Letter to D. Levine (FRA/RA-42), January 20, 1976.

17. Diboll, W.B. (Washington University, St. Louis, MO), "Trip Report; Phase 15, Series 2 (3 Impact) Tank Car Impact Tests," Memorandum to B.A. Szabo (Washington University), February 6, 1976.

18. Peters, D.A. (Washington University, St. Louis, MO), Letter to D. Levine (FRA/RA-42), March 8, 1976.

19. Diboll, W.B. (Washington University, St. Louis, MO), "Trip Report, Tank Car Impact Tests, 2-4 March 1976," Memorandum to B.A. Szabo (Washington University), March 12, 1976.

20. Anon., "Minutes of the Phase 15 Subcommittee of the Tank Car Safety Project Review Committee," Transpoint Building, Washington, DC, February 13, 1976.

21. Anon., "Minutes of Meeting/FRA-AAR-RPI Tank Car Safety Research Project/Phase 15 Meeting," AAR Technical Center, Chicago, IL, February 20, 1976.

22. Tong, P. and J.N. Rossettos, "Modular Approach to Structural Simulation for Vehicle Crashworthiness Prediction," DOT Transportation Systems Center, HS-801-475, March 1975.

23. Tong, P. (TSC/610), "Tank Car Impact Tests," Memorandum to D. Levine (FRA/RRD-33), March 25, 1976.

24. Nintzel, A.J., "Experimental Determination of the Mass Properties of a 50 Ton Louisville & Nashville Hopper Car, Serial No. 130954," Kentron Hawaii, Ltd., September 30, 1975.

25. Nintzel, A.J., "Experimental Determination of the Natural Frequency and Damping of a 50 Ton Louisville & Nashville Hopper Car, Serial No. 130954," Kentron Hawaii, Ltd., November 12, 1975.

26. Reimers, J.J., "Experimental Determination of Body Characteristics of Tank Car GATX 91883 and Louisville & Nashville Hopper Car Serial No. 130954," Kentron Hawaii, Ltd., November 20, 1975.

27. Anon., "60=Ton Hopper Cars," L&N R.R. Co., Mechanical Engineer's Office, Louisville, KY, Engineering Drawing, Sheet No. H-17 for Serial Nos. 130000-131699 and 131700-132499, Undated.

28. Combes, C.L. (ed.), Car and Locomotive Cyclopedia of American Practice, Simmons-Boardman Publishing Corp., New York, NY, 1970, p. 256, 526.

29. Stauffer, J.B., et al., "Test Specification #7115 for Switchyard Impact Tests (RPI-AAR Phase 15)," DOT Transportation Test Center, September 19, 1975. (Revised November 4, 1975.)

30. Hohenemser, K.H. et al., "Computer Simulation of Tank Car Head Puncture Mechanisms," Washington University, St. Louis, MO, FRA-OR&D-75-23, February 1975.

31. Peters, D.A. et al., "Tank Car Head Puncture Mechanisms," Washington University, St. Louis, MO, FRA-OR&D-76-269, June 1976.

32. Peters, D.A. and S.K. Yin, "Non-Destructive Impact Between Railroad Cars: Experimental and Analytical Study," Washington University, St. Louis, MO, FRA-OR&D-76-247, January 1977.

33. Abramson, H.N. (ed.), "The Dynamic Behavior of Liquids in Moving Containers with Applications to Space Technology," National Aeronautics and Space Administration, NASA SP-106, 1966.

34. McClintock, F.A. and A.S. Argon, Mechanical Behavior of Materials, Addison-Wesley, Reading, MA, 1966, p. 186, 196.

APPENDIX A

INNAGE CALCULATIONS

Innage calculations have been made for eleven lead striking cars whose light weights and capacities, as well as rail weights, were recroded. The calculation procedure is as follows: Let W_R = measured rail weight, W_L = light weight and W_C = lading capacity in KIPS. Then:

$$\text{INNAGE} = (W_R - W_L)/W_C \qquad \text{(A-1)}$$

A factor of 8.39 lb_f/gal is used for water density to convert lading capacity from gallons to KIPS.

Results of the calculations are summarized in Table A-1. The largest innage is 94.2% (test 10.1). The average innage is 92.3%, with a standard deviation of 1.4%.

TABLE A-1. SUMMARY OF INNAGE CALCULATIONS

Test No.	Car No.	W_R (KIP)	W_L (KIP)	Capacity, W_C (Gal)	W_C (KIP)	INNAGE (%)
3.1	GATX-57688	344.0	86.3	33,661	282.42	91.2
3.2	GATX-57688	344.0	86.3	33,661	282.42	91.2
3.3	UTLX-38547	344.0	86.0	33,894	284.37	90.7
3.4	UTLX-38493	343.36	85.5	33,905	284.46	90.6
3.5	ULTX-38493	343.36	85.5	33,905	284.46	90.6
4.1	GATX-93412	348.52	86.4*	33,657	282.38	92.8
4.2	UTLX-38102	350.68	85.8*	33,884	284.29	93.2
5.1	GATX-92588	350.0	84.35	33,664	282.44	94.1
7.1	SOEX-3084	351.58	88.65	33,639	282.23	93.2
7.2	GATX-91768	347.26	84.7	33,620	282.07	93.1
10.1	UTLX-38311	353.78	87.1**	33,942	284.77	93.6

*Including weight of partial head shield (815 lb.)

**Including weight of full-height head shield (1600 lb., estimated)

APPENDIX B

NARRATIVE SUMMARIES OF VISUAL OBSERVATIONS

The following are summaries of visual impressions noted by observers both during the tests and from post-test viewing of the wayside films. Since such impressions tend to vary with different observers, the impressions of both TSC personnel and AAR personnel are included here for completeness. The latter summaries have been reproduced from Ref. 14.

Test 3.1

TSC

"A"-end coupler overrides, hitting tank car end platform. Coupler subsequently impacts tank car head twice. The second impact of the tank head was the result of the reengagement of the tank car at the initial impact end. No override at "B" end; no head puncture.

AAR

After first impact, the hopper car coupler hit the top of the coupler and the end platform on GATX-91883 (standing car)* and then struck the head at the shoe and head reinforcing pad.

---

*Bracketed words added by present authors for clarity.

Test 3.2

TSC

"A"-end coupler overrides, almost clearing standing tank car end platform. Coupler subsequently impacts tank car head twice. Second impact of head observed to be much more severe than first.

AAR

L&N-133950 (hopper) and GATX-57688 (striking car) coupled on impact. The hopper car coupler struck GATX-92571 (standing car) causing a severe head dent. After hitting the head, the coupler dropped approximately nine inches, coming to rest on top of the head shoe.

Test 3.3

TSC

"A"-end coupler overrides, almost clearing tank car end platform. Coupler subsequently impacts platform and support structure twice and tank head (lightly) as a third event. "B"-end coupler overrides and impacts head shield twice (second time severely).

AAR

The hopper car coupler overrode the draft sill of GATX-57688 (standing car) and dented the head. At impact, the hopper was completely lifted off its trunks. Following the impact, the draft sills at each end of the hopper car were supported on the draft sills of both tank cars. The bottom of the hopper car coupler was on top of the head block on GATX-57688 approximately 3 inches from the reinforcing pad. The coupler on the opposite end of the hopper car struck the shield of UTLX-38547 (striking car) forcing the shield into the head and down against the top of the lead wheel (AL side).

Test 3.4

TSC

Empty hopper car caught between standing and striking tank cars, but "A"-end coupler overrides after three impacts. "A"-end coupler impacts tank head lightly and then heavily (fifth impact). Empty hopper car sill buckles over body bolster at fifth impact. "B"-end coupler held initially, but overrides at fifth or seventh impact.

AAR

On impact, the hopper car was caught and squeezed between the two tank cars high on their couplers, the eccentric load forcing the hopper car up. After impact, the hopper car was suspended by its couplers between the heads of both tank cars. The hopper "A"-end ("B"-end in present notation) draft sill was bent down about 30°. Coupler identations showed that the length of coupler engagement on impact was 2-5/8" at UTLX-38482 (standing) and 4" at UTLX-38493 (striking).

Test 3.5

TSC

"A"-end coupler overrides, almost clearing tank car end platform. Coupler subsequently impacts standing tank car head twice, puncturing head the second time. Striking tank car engagement of standing consist appears to be associated with second impact of standing tank car head.

AAR

At impact, the hopper car was lifted completely off its trucks, overrode the draft sill of UTLX-38498, [standing] and struck low on the head. The coupler punctured the head at the intersection of the head and the head reinforcing pad. The head of UTLX-38493 [striking] was dented but not punctured. The "A" end ["B" end in present notation] coupler of the hopper car broke behind the head and was hanging beneath the car.

Test 4.1

TSC

"A" and "B"-end couplers override almost simultaneously, "A"-end coupler engaging tank car coupler partially and briefly. Multiple impacts observed at both ends, all on head shield of standing tank car. "B"-end of empty hopper car continues to pitch up, overrides part-height head shield, and impacts upper half of striking tank car head twice. Head punctured on second impact.

AAR

Immediately after impact, the hopper car "B"-end ("A"-end in present notation) lifted and hit the coupler and the head shield on UTLX-38094 (standing). The hopper car body piveted about this point. The hopper car "A"-end ("B"-end) then lifted and the bottom of the coupler struck the incoming tank car at the top of the head shield and punctured the head.

Test 4.2

TSC

"A" and "B"-end couplers override. "A"-end coupler overrides first, barely touching end platform of standing tank car. Coupler subsequently impacts head shield twice. First impact breaks head shield supports, and shield acts as a bearing plate on tank car head at second impact. "B"-end coupler, almost broken off during override, subsequently impacts head shield of striking tank car.

AAR

Hopper car rose vertically with coupler striking head shield on UTLX-38755 (standing). On opposite end, coupler head broke off and remaining stub impacted head shield of UTLX-38102 (striking). Hopper car trucks rolled forward and car came to rest suspended horizontally between tank cars.

Test 5.1

TSC

"A"-end coupler impacts standing tank car coupler three times, but tank car shelf-E coupler prevents override. "B"-end coupler is bent and broken off during override of striking tank car.

AAR

Following impact of the struck hopper car into UTLX-38102 (standing), the hopper car rotated upward at the "A"-end, pivoting around its "B"-end coupler which was restrained by the shelf coupler on UTLX-38102. The "A"-end couplers on the hopper car and GATX-92588 (striking) broke off at their shanks (but remained coupled) permitting vertical movement of the "A"-end of the hopper car. As it rotated up, the striker and the protruding broken coupler shank on the hopper car scraped and dented the head of GATX-92588. The hopper continued rotating upward through approximately 75 degrees, and then fell out from between the tank cars.

Test 5.2

TSC

"A"-end coupler knocks off the top shelf of the coupler of the standing tank car, overrides and impacts standing tank head. Car body of empty hopper car twists, delaying override of "B"-end coupler. Coupler subsequently breaks off top shelf of striking tank car coupler and overrides. Sequence of multiple impacts occurs, with hopper car sill buckling near "B"-end body bolster at fifth impact. Standing tank car head cracked by "A"-end coupler, causing leakage of lading.

AAR

Hopper car was lifted off its trucks, held momentarily, then fell off to one side at 15° angle at end facing SOEX-3007 (standing); hopper car coupler rose over shelf coupler, breaking off top shelf and impacting head 18" above sill and 12" off vertical centerline. At end facing SOEX-3066

(striking), side of hopper car buckled, causing lateral force and separation of couplers. Top shelf of coupler on SOEX-3066 bent back 5°.

Test 6.1

TSC

"A"-end coupler overrides after brief partial engagement of standing tank car coupler and impacts the head of the standing tank car. "B"-end coupler overrides cleanly when the striking tank car catches up. Sequence of multiple impacts on standing tank car head. Striking tank car head impacted twice and punctured at second impact.

AAR

The impact lifted both ends of the hopper car off its trucks and the "B"-end ("A"-end) dented the head of GATX-91881 (standing) where the head block and reinforcing pad are welded to the tank. The hopper car coupler did not contact the coupler on GATX-91881. The "A"-end ("B"-end) of the hopper car lifted about 6 inches when the moving train squeezed it between GATX-91881 and SOEX-3112 (striking). The hopper car coupler shot up into the head of SOEX-3112 about 1 foot above the sill. The coupler punctured the head and continued on until the entire end of the sill was caught inside the head. The train came to rest with the hopper car suspended between both tank cars.

Test 7.1

TSC

No report available.

AAR

Hopper car struck head of UTLX-38497 (standing) about 2 feet above sill. Opposite end coupler struck SOEX-3084 (striking) just below horizontal centerline of head. Hopper sill at struck end buckled 90°, and car was then thrown clear of tracks. The two tank cars came to rest almost coupled.

Test 7.2

TSC

No report available.

AAR

The hopper car sill buckled on initial impact. The "B"-end ("A"-end) jumped up and dented the head of SOEX-3008 (standing) and then the "A"-end ("B"-end) dented GATX-91768 (striking) directly on the handrail bracket pad. GATX-91768 continued to bend the hopper car sill into a 90-degree bend and the train stopped with the hopper car suspended between the two tank cars.

Test 10.1

TSC

"A"-end coupler breaks off top shelf of standing tank car coupler and overrides end platform. Coupler subsequently impacts head shield lightly, then severely. "B"-end coupler overrides at delayed third impact, hitting head shield. No puncture occurs.

AAR

Hopper car coupler struck bottom of head shield on UTLX-38120 (standing) just above sill. At struck end, hopper car coupler engaged with coupler on UTLX-38311 (striking), then both couplers broke off at shanks and shank on hopper car impacted head shield on UTLX-38311 near horizontal centerline. Hopper car came to rest supported between the two tank cars at about a 20-degree angle.

APPENDIX C

POSITION-TIME PLOTS FROM WAYSIDE CAMERAS

The following plots cover only those tests in which wayside cameras operated at both ends of the hopper car. (Thus, tests 3.1 and 7.2 are absent.) Each plot is identified by computer printout documenting the test number and camera location. For example, test 3.2 at the "A" end of the hopper car is indicated by (see page 87): "TEST NO. 2A ... SERIES 3." When comparing plots, note that both the position and time scales may change from one plot to another.

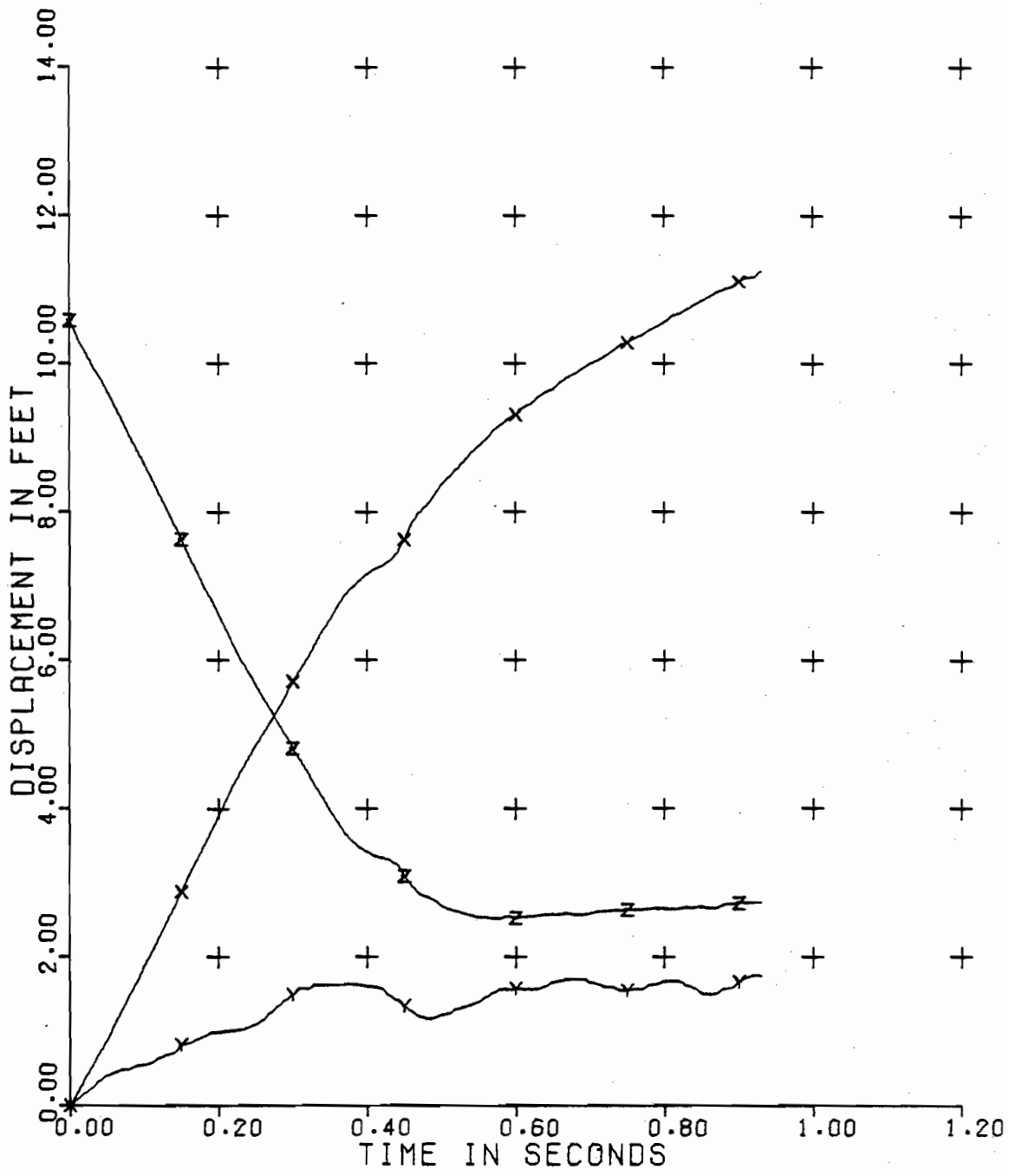

TEST NO. 2A APR 29, 1976 SERIES 3

BACK-UP DISTANCE 3.5 FT

SPEED AT IMPACT 14.9 MPH

KEY

X = HORIZONTAL DISPLACEMENT

Y = VERTICAL DISPLACEMENT

Z = HORIZONTAL DIFFERENCE

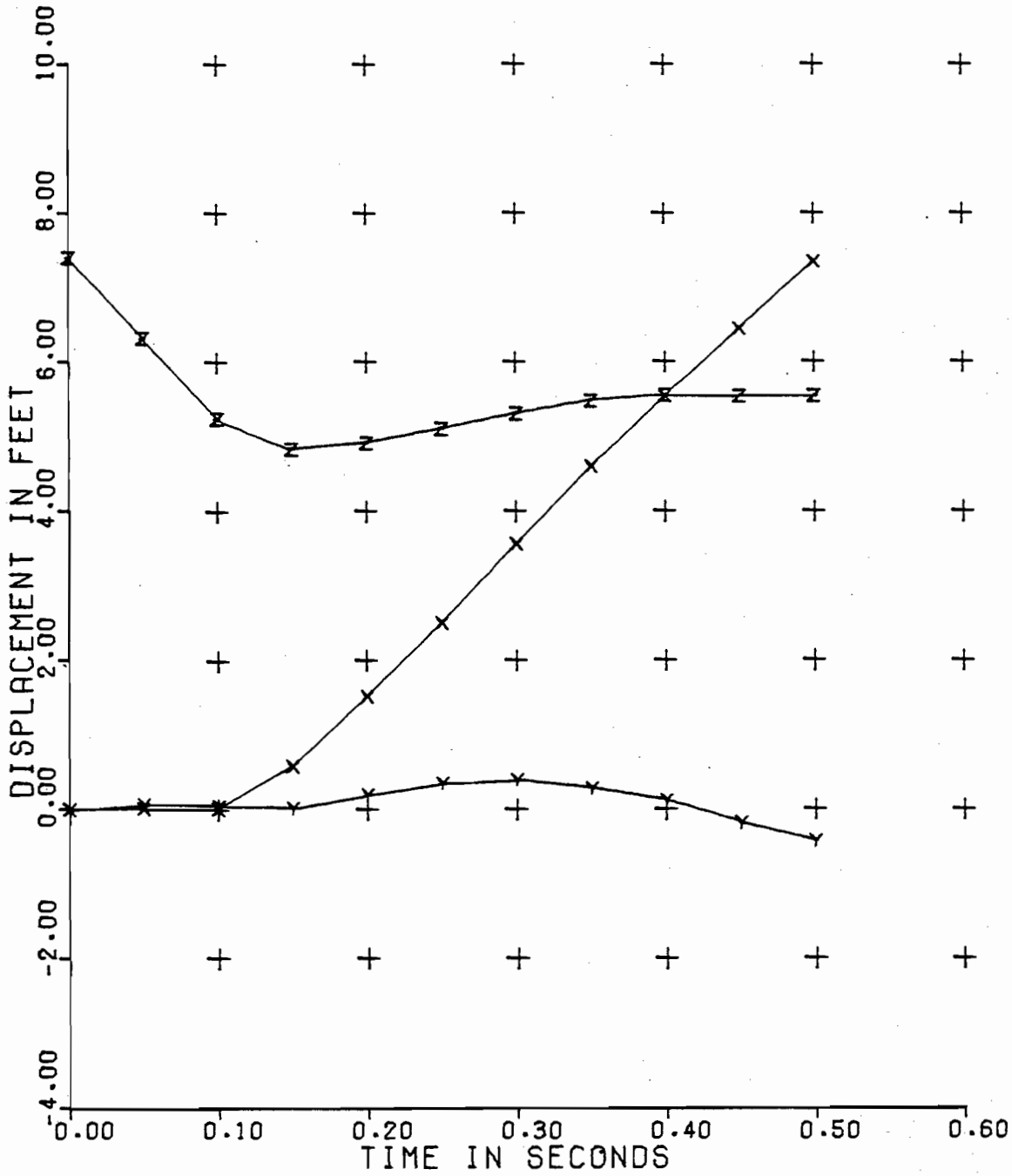

TEST NO. 2B APR 29, 1976 SERIES 3

BACK-UP DISTANCE 3.5 FT

SPEED AT IMPACT 14.9 MPH

KEY

X = HORIZONTAL DISPLACEMENT

Y = VERTICAL DISPLACEMENT

Z = HORIZONTAL DIFFERENCE

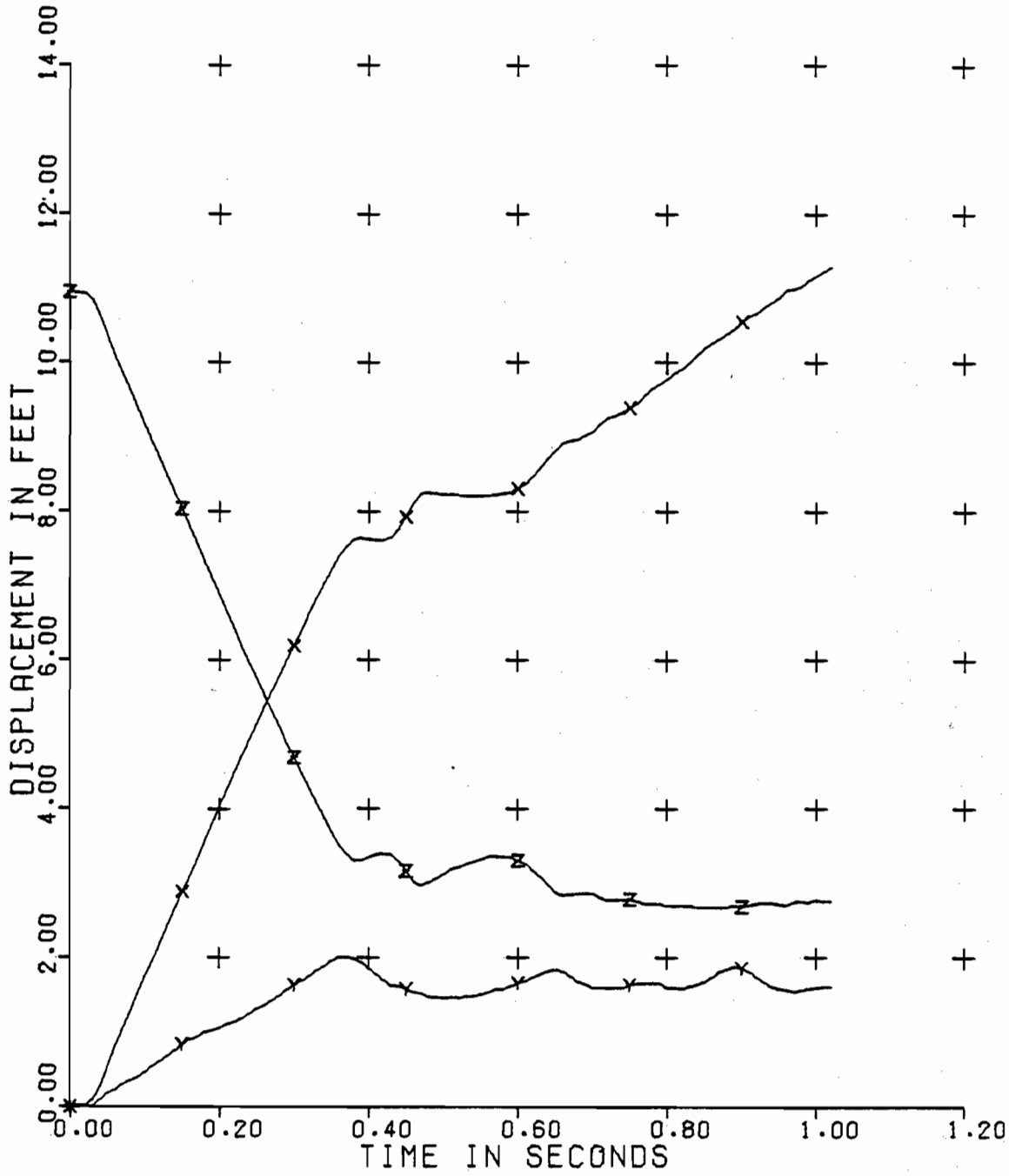

TEST NO. 3A MAY 6, 1976 SERIES 3

BACK-UP DISTANCE 3.5 FT

SPEED AT IMPACT 16.5 MPH

KEY

X = HORIZONTAL DISPLACEMENT

Y = VERTICAL DISPLACEMENT

Z = HORIZONTAL DIFFERENCE

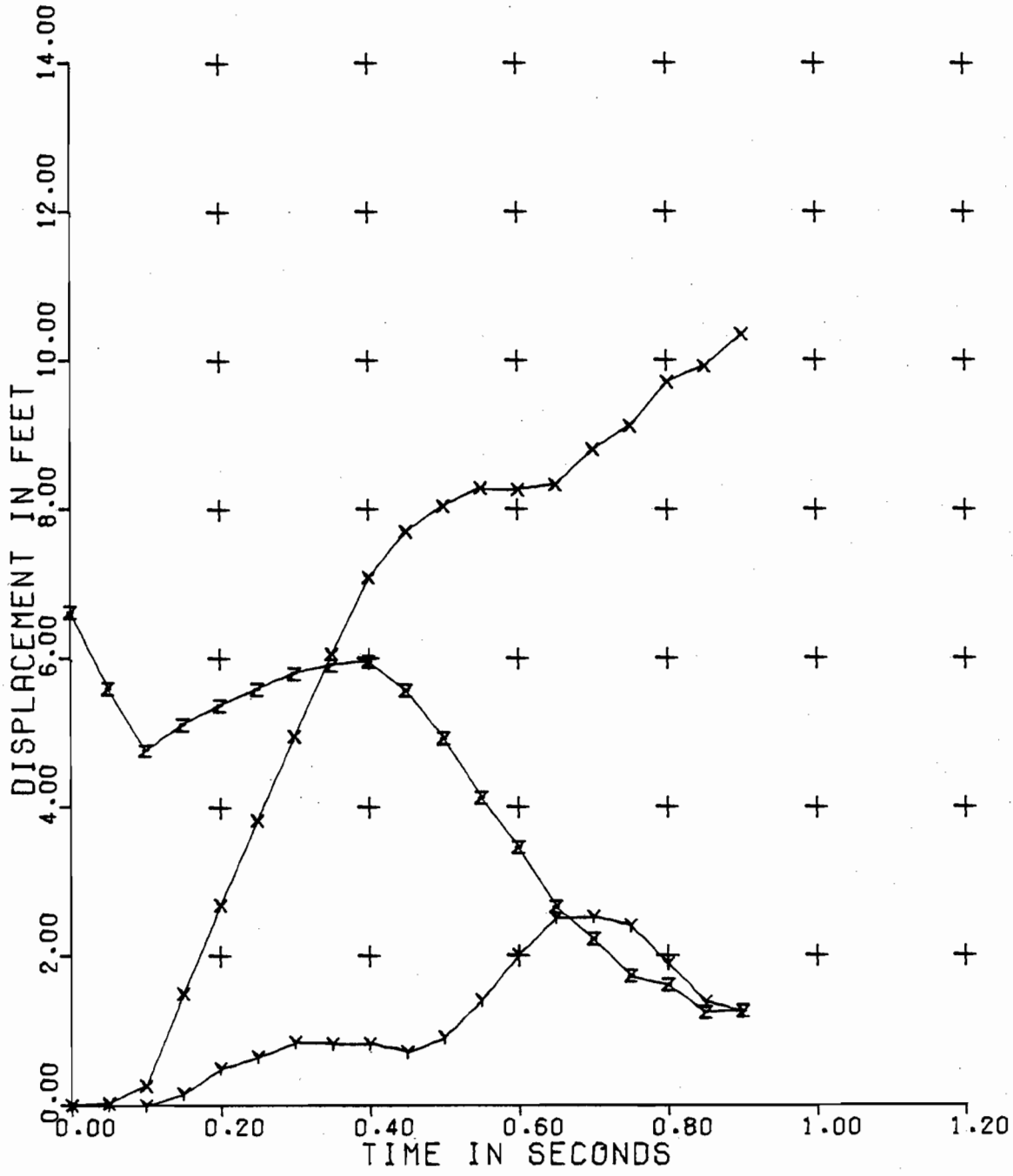

TEST NO. 3B MAY 6, 1976 SERIES 3

BACK-UP DISTANCE 3.5 FT

SPEED AT IMPACT 16.5 MPH

KEY

X = HORIZONTAL DISPLACEMENT

Y = VERTICAL DISPLACEMENT

Z = HORIZONTAL DIFFERENCE

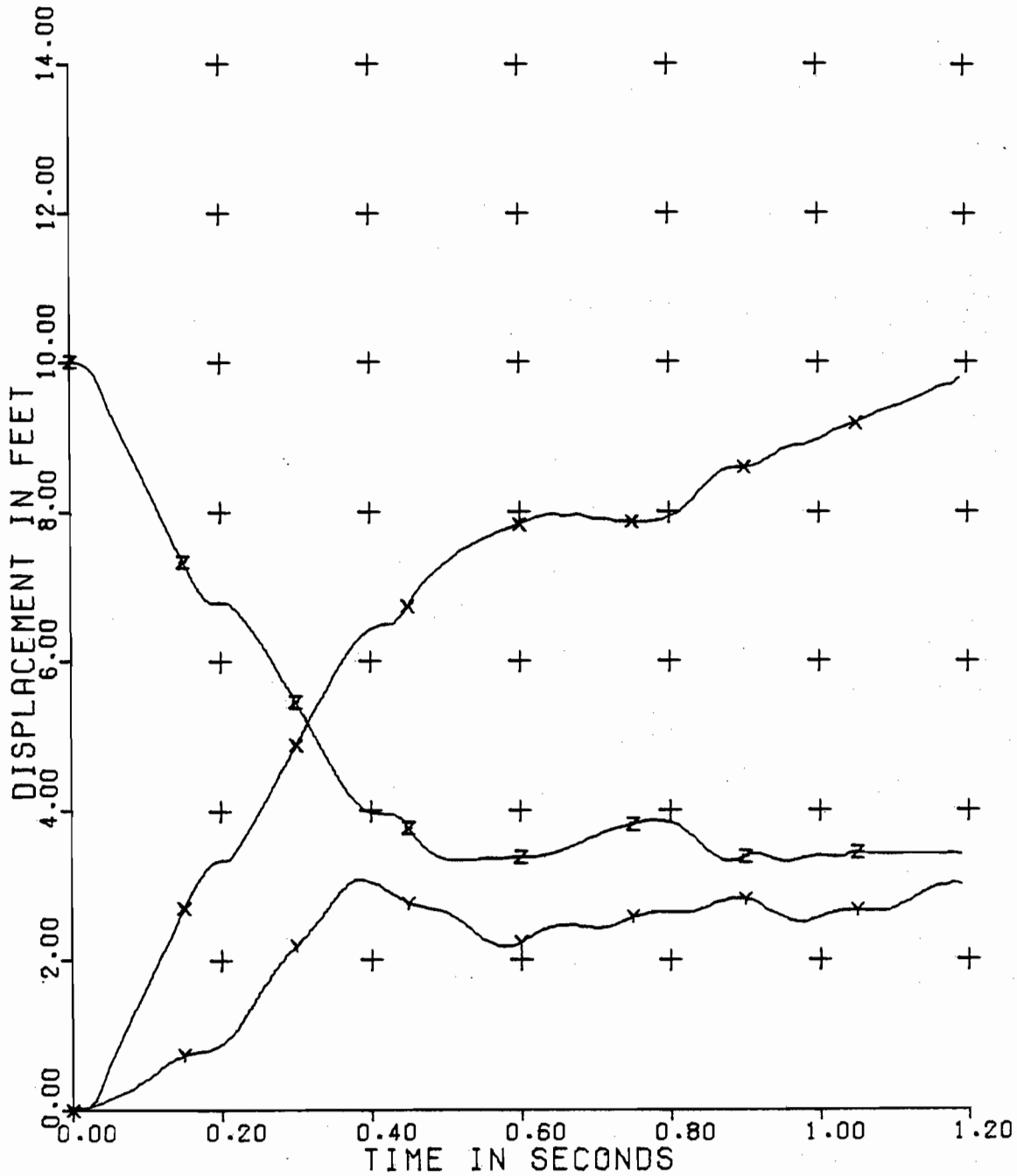

TEST NO. 4A MAY 20, 1976 SERIES 3

BACK-UP DISTANCE 2.5 FT
SPEED AT IMPACT 15.4 MPH

KEY
X = HORIZONTAL DISPLACEMENT
Y = VERTICAL DISPLACEMENT
Z = HORIZONTAL DIFFERENCE

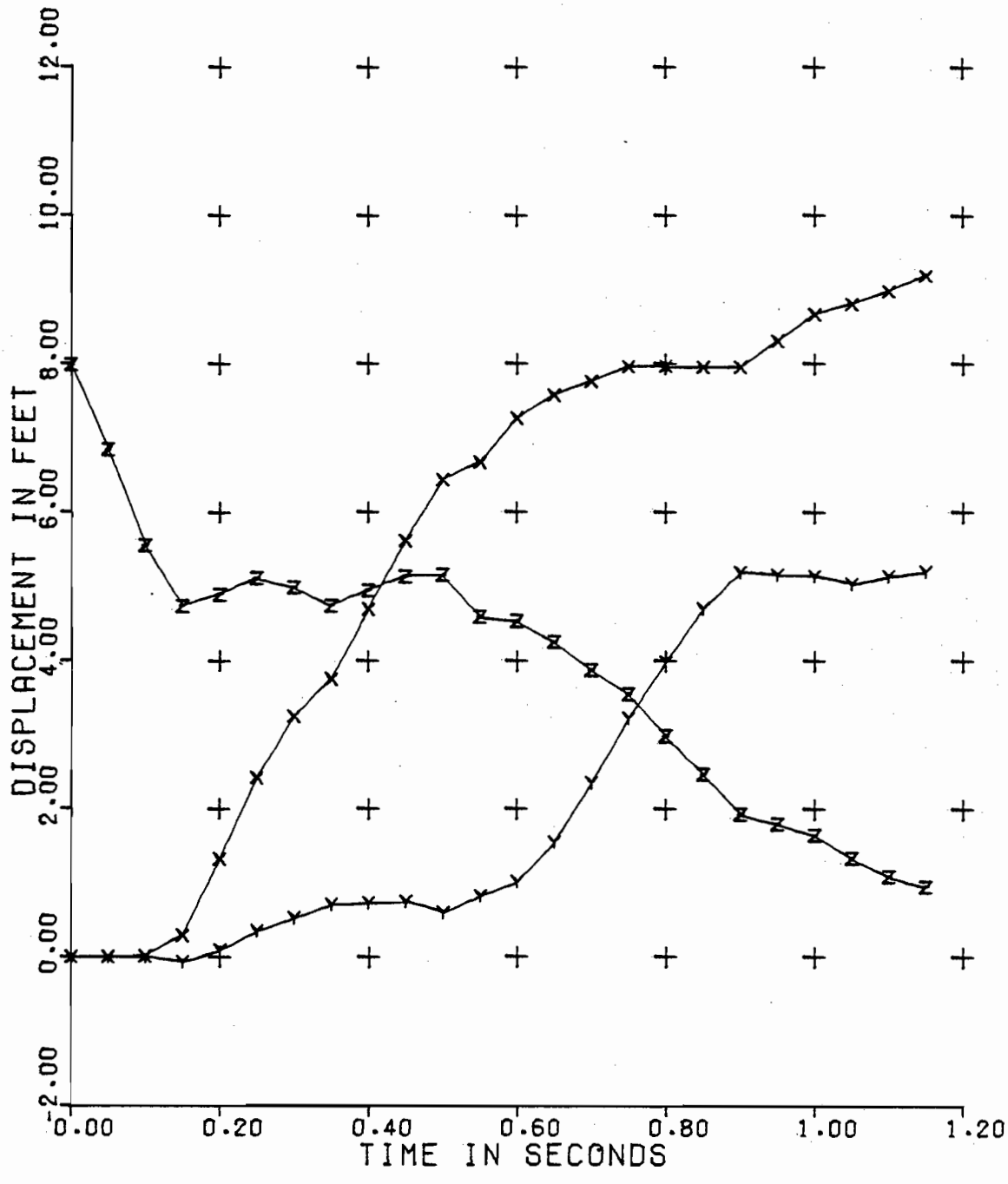

TEST NO. 4B MAY 20, 1976 SERIES 3

BACK-UP DISTANCE 2.5 FT

SPEED AT IMPACT 15.4 MPH

KEY

X = HORIZONTAL DISPLACEMENT

Y = VERTICAL DISPLACEMENT

Z = HORIZONTAL DIFFERENCE

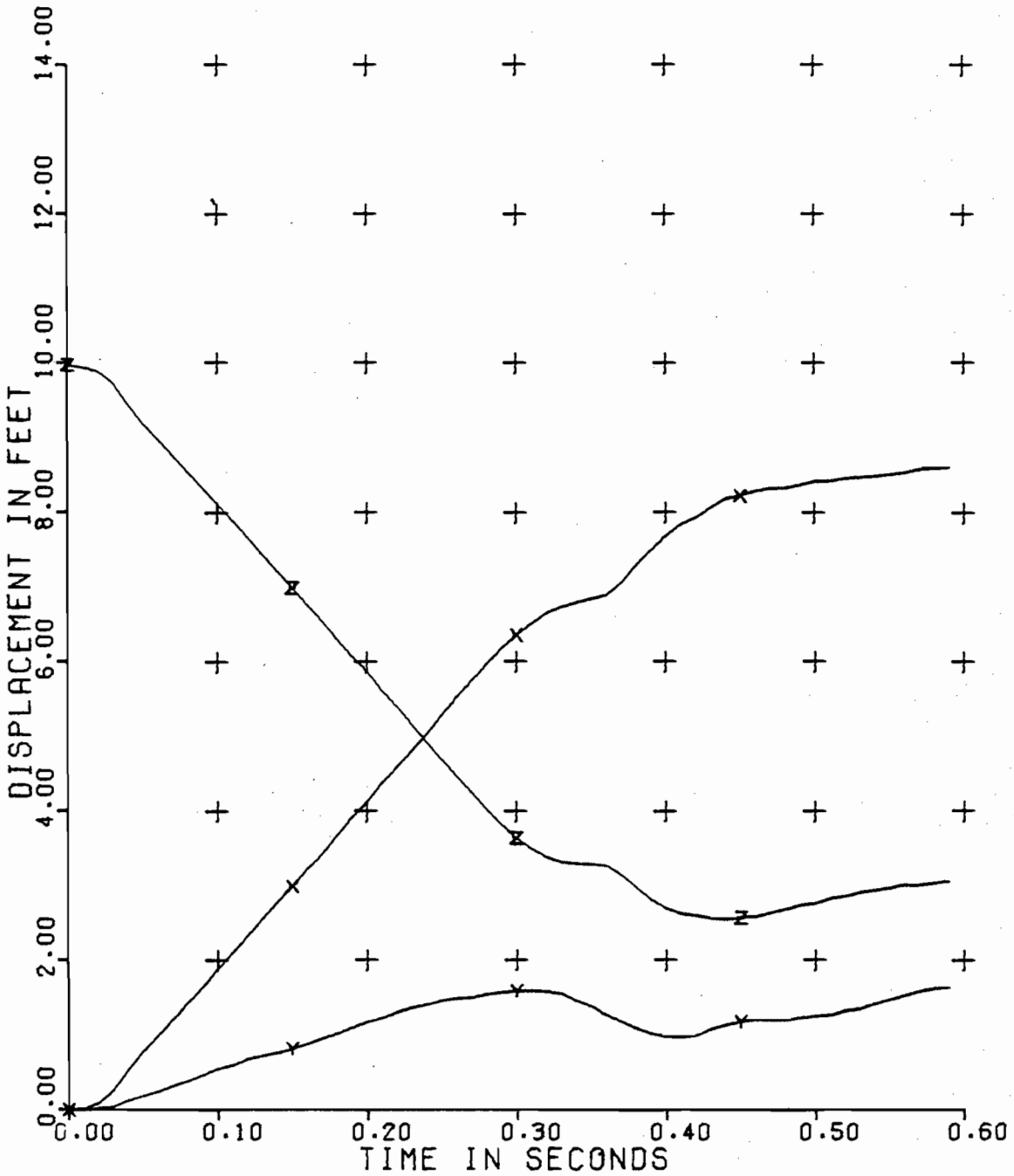

TEST NO. 5A MAY 27, 1976 SERIES 3

BACK-UP DISTANCE 2.5 FT
SPEED AT IMPACT 16.9 MPH

KEY
X = HORIZONTAL DISPLACEMENT
Y = VERTICAL DISPLACEMENT
Z = HORIZONTAL DIFFERENCE

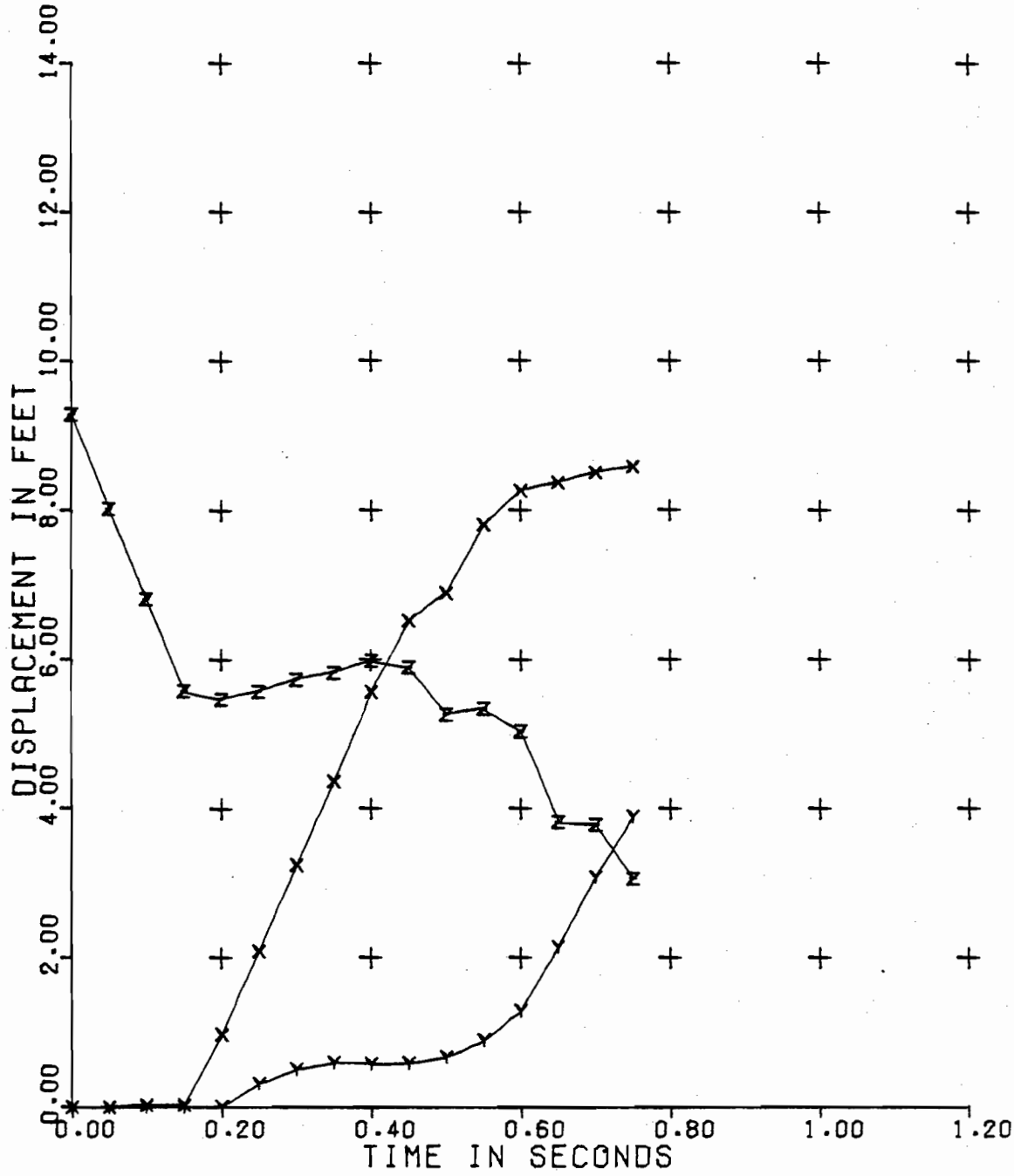

TEST NO. 5B MAY 27, 1976 SERIES 3

BACK-UP DISTANCE 2.5 FT

SPEED AT IMPACT 16.9 MPH

KEY

X = HORIZONTAL DISPLACEMENT

Y = VERTICAL DISPLACEMENT

Z = HORIZONTAL DIFFERENCE

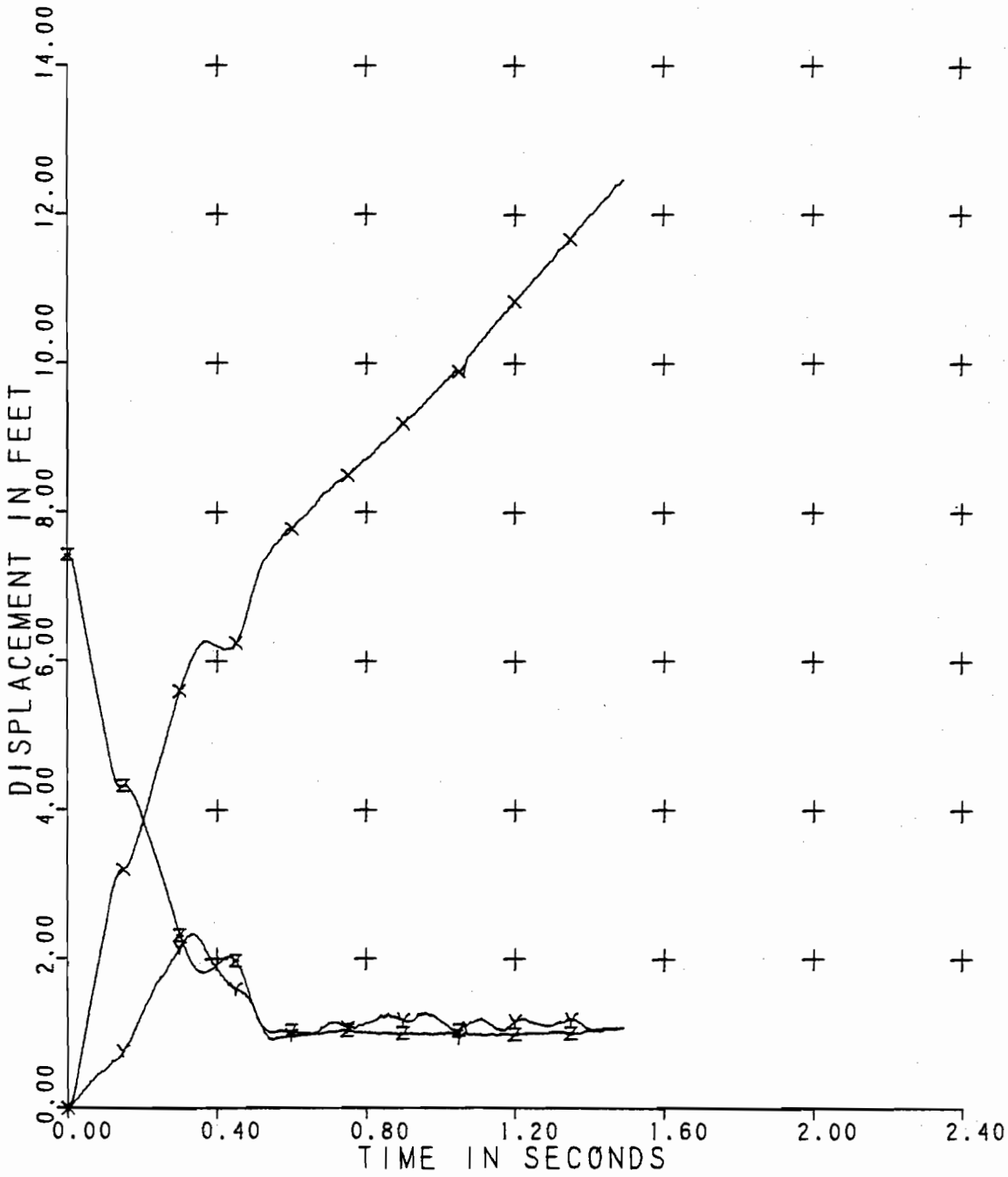

TEST NO. 1A JULY 8, 1976 SERIES 4

BACK-UP DISTANCE 2.5 FT
SPEED AT IMPACT 18.7 MPH

KEY
X - HORIZONTAL DISPLACEMENT
Y - VERTICAL DISPLACEMENT
Z - HORIZONTAL DIFFERENCE

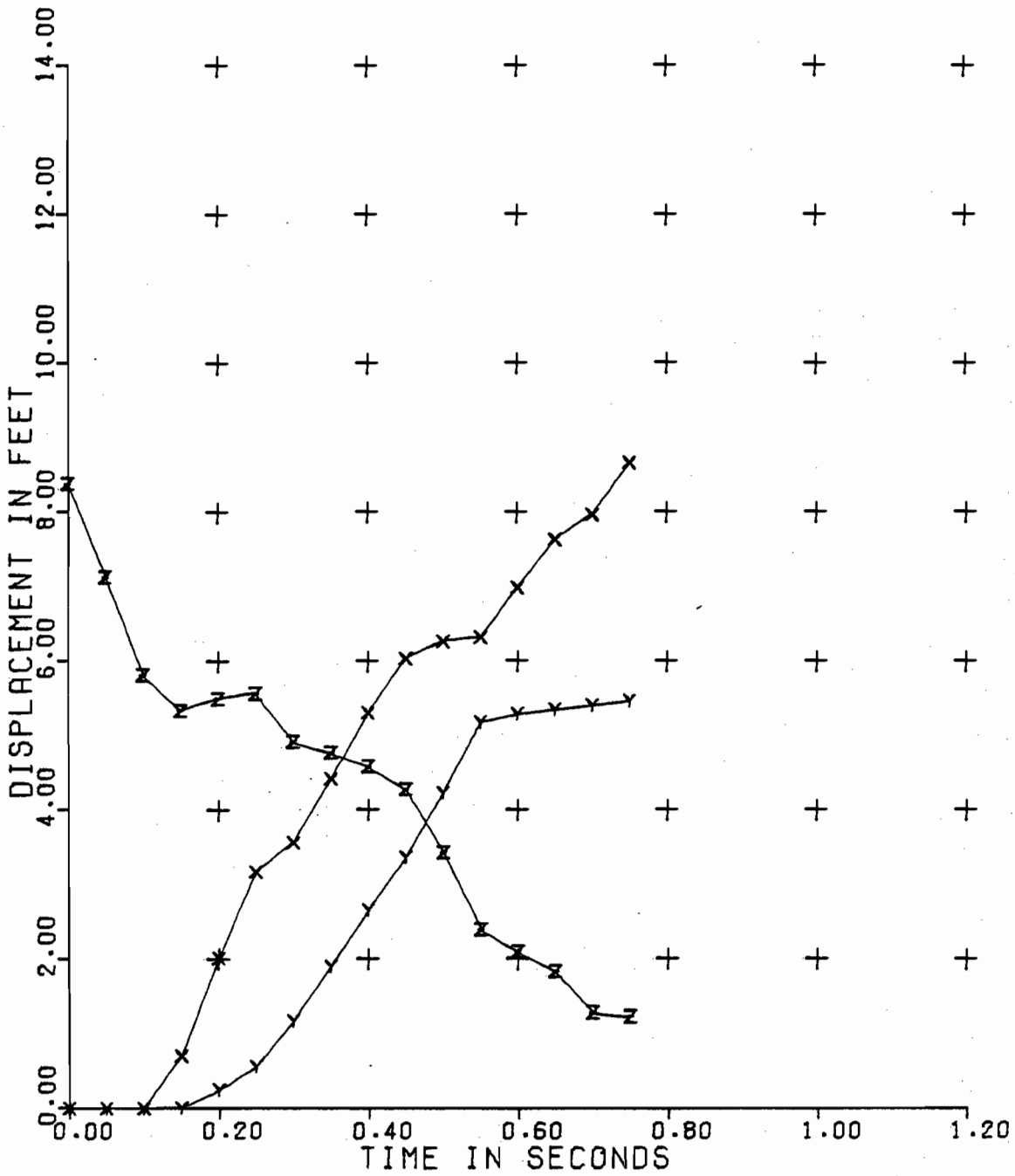

TEST NO. 1B JULY 8, 1976 SERIES 4

BACK-UP DISTANCE 2.5 FT

SPEED AT IMPACT 18.7 MPH

KEY

X = HORIZONTAL DISPLACEMENT

Y = VERTICAL DISPLACEMENT

Z = HORIZONTAL DIFFERENCE

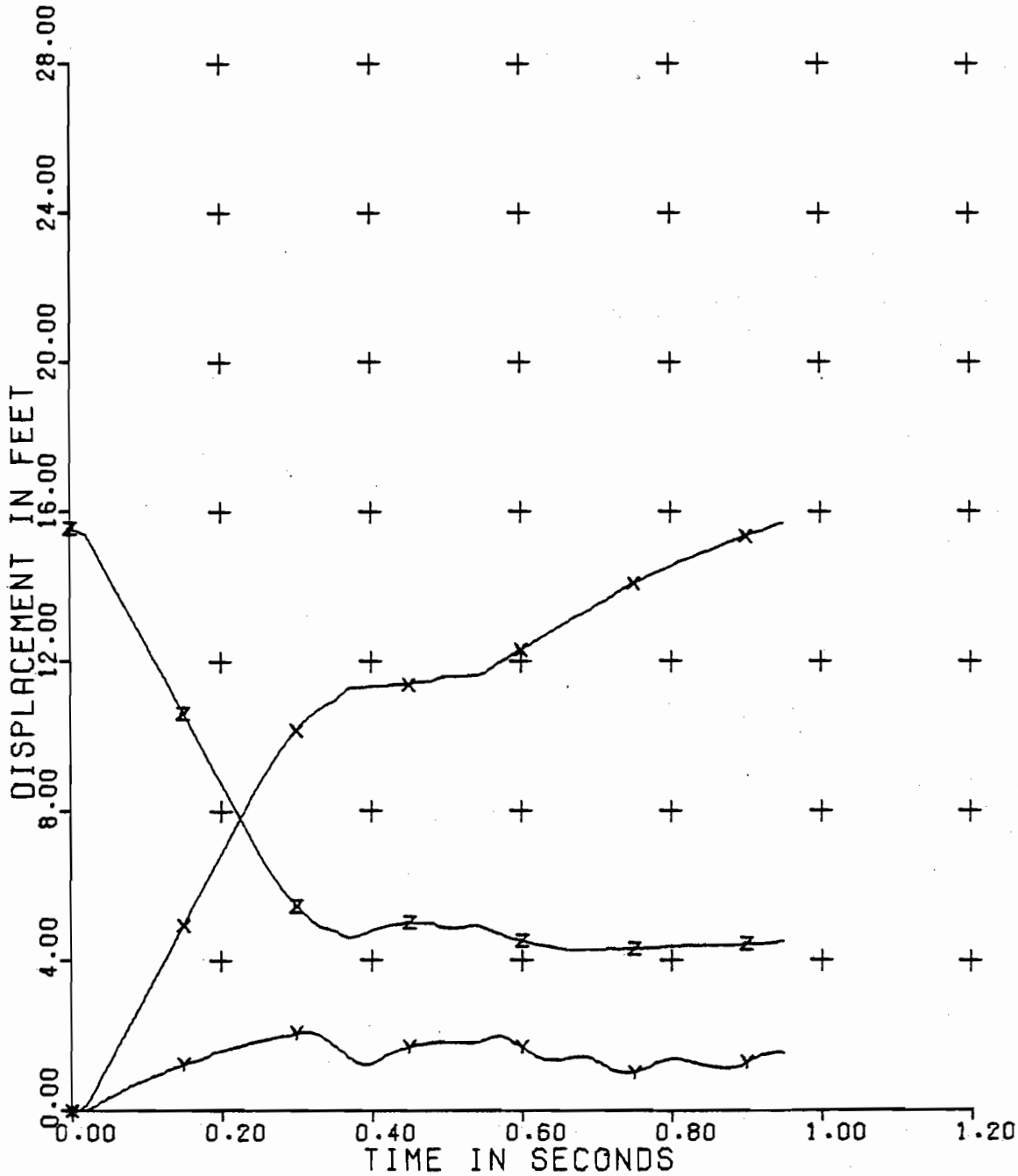

TEST NO. 2A SEP 2, 1976 SERIES 4

BACK-UP DISTANCE 3.5 FT

SPEED AT IMPACT 19.2 MPH

KEY

X = HORIZONTAL DISPLACEMENT

Y = VERTICAL DISPLACEMENT

Z = HORIZONTAL DIFFERENCE

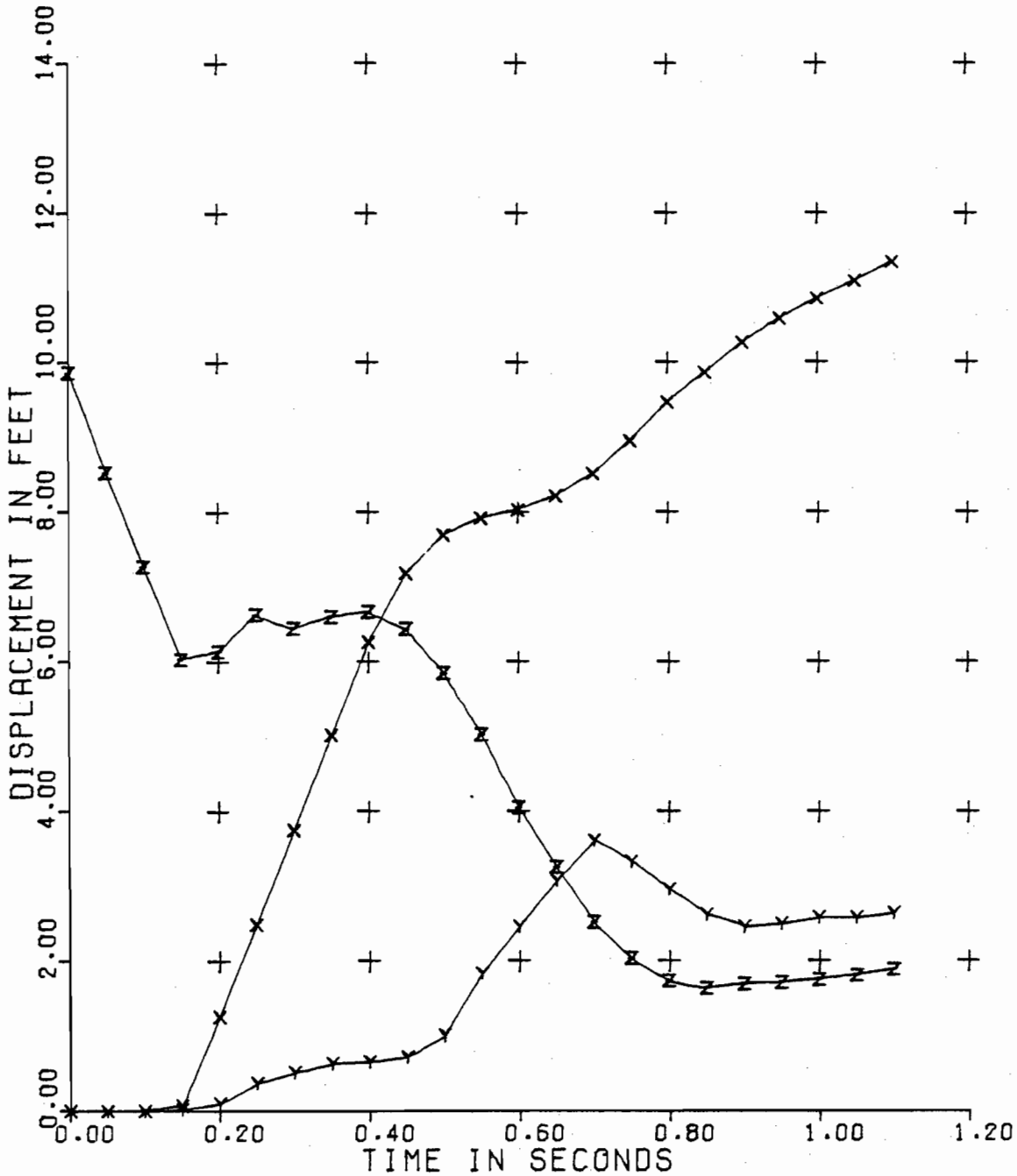

TEST NO. 2B SEP 2, 1976 SERIES 4

BACK-UP DISTANCE 3.5 FT

SPEED AT IMPACT 19.2 MPH

KEY

X = HORIZONTAL DISPLACEMENT

Y = VERTICAL DISPLACEMENT

Z = HORIZONTAL DIFFERENCE

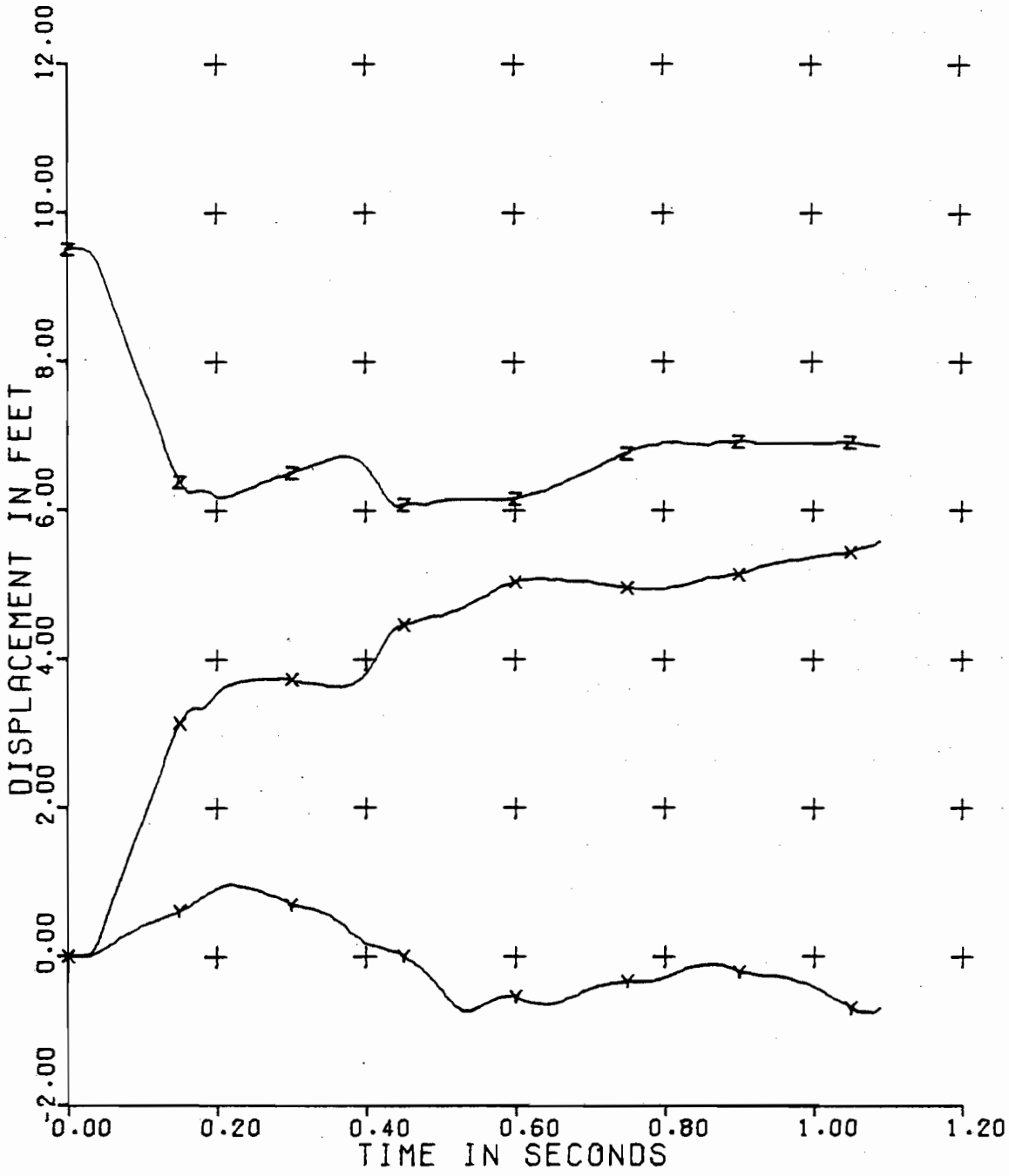

TEST NO. 1A AUG 5, 1976 SERIES 5

BACK-UP DISTANCE 2.5 FT

SPEED AT IMPACT 19.4 MPH

KEY

X = HORIZONTAL DISPLACEMENT

Y = VERTICAL DISPLACEMENT

Z = HORIZONTAL DIFFERENCE

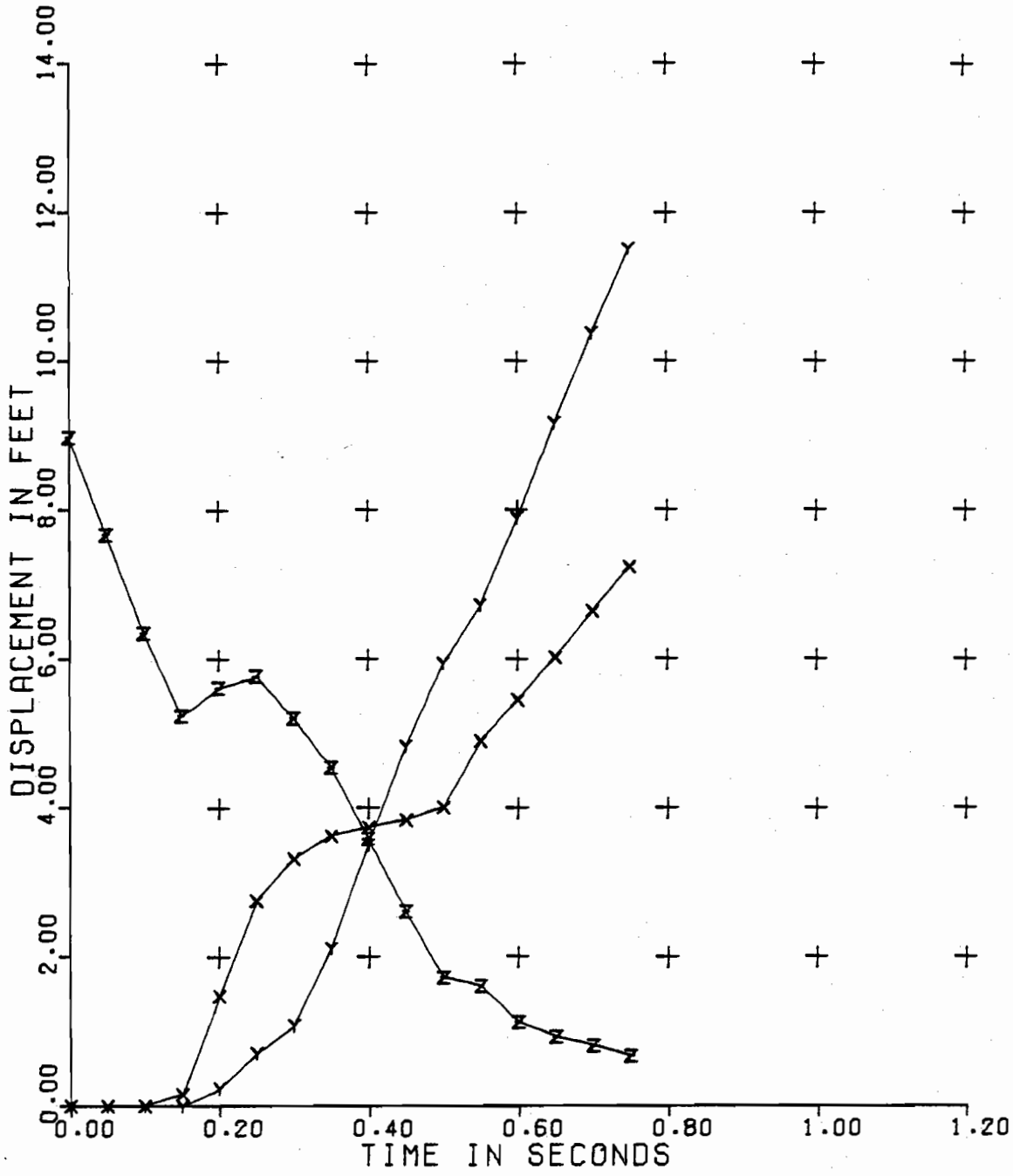

TEST NO. 1B AUG 5, 1976 SERIES 5

BACK-UP DISTANCE 2.5 FT

SPEED AT IMPACT 19.4 MPH

KEY

X = HORIZONTAL DISPLACEMENT

Y = VERTICAL DISPLACEMENT

Z = HORIZONTAL DIFFERENCE

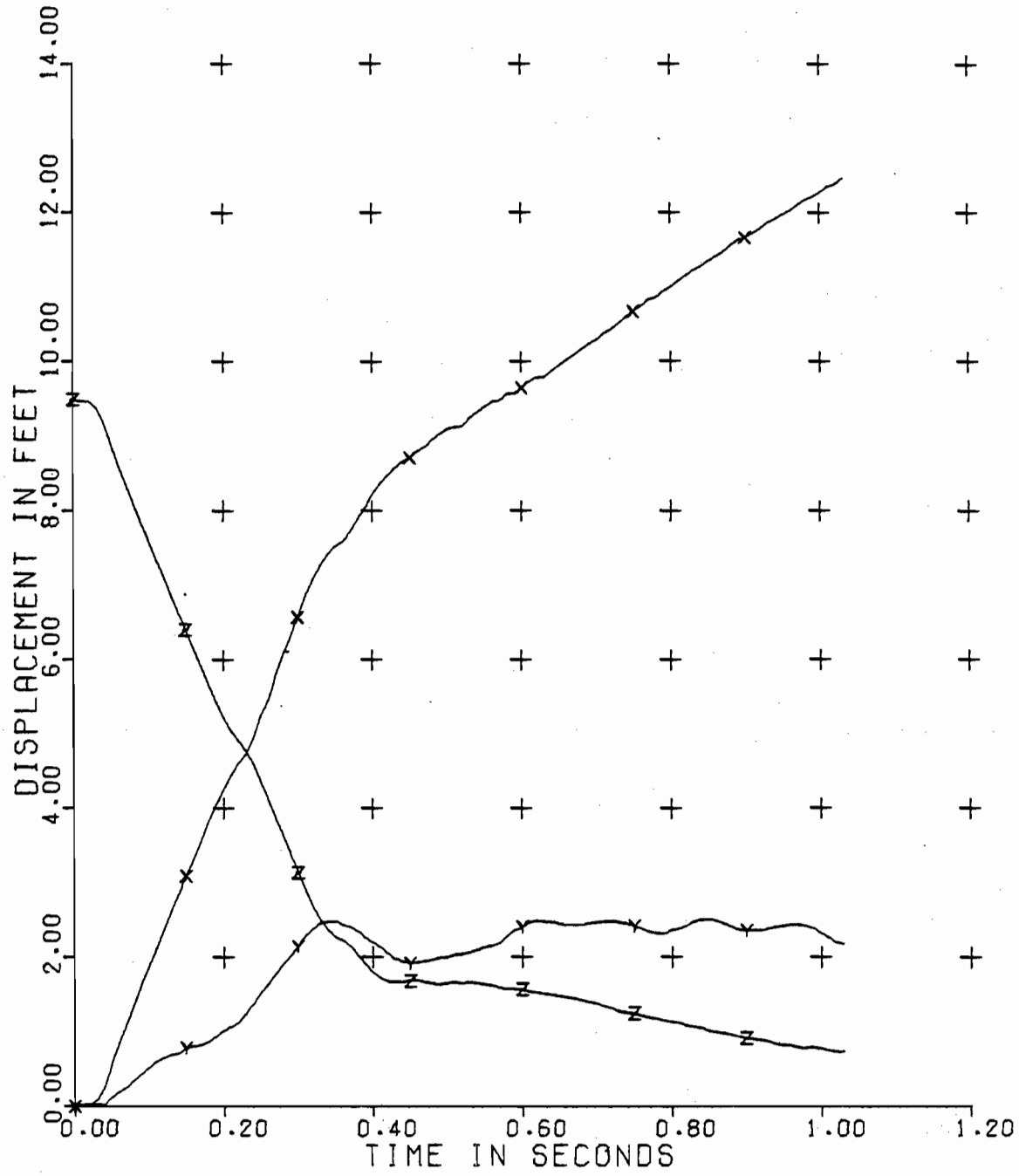

TEST NO. 2A AUG 17, 1976 SERIES 5

BACK-UP DISTANCE 3.75 FT

SPEED AT IMPACT 19.0 MPH

KEY

X = HORIZONTAL DISPLACEMENT

Y = VERTICAL DISPLACEMENT

Z = HORIZONTAL DIFFERENCE

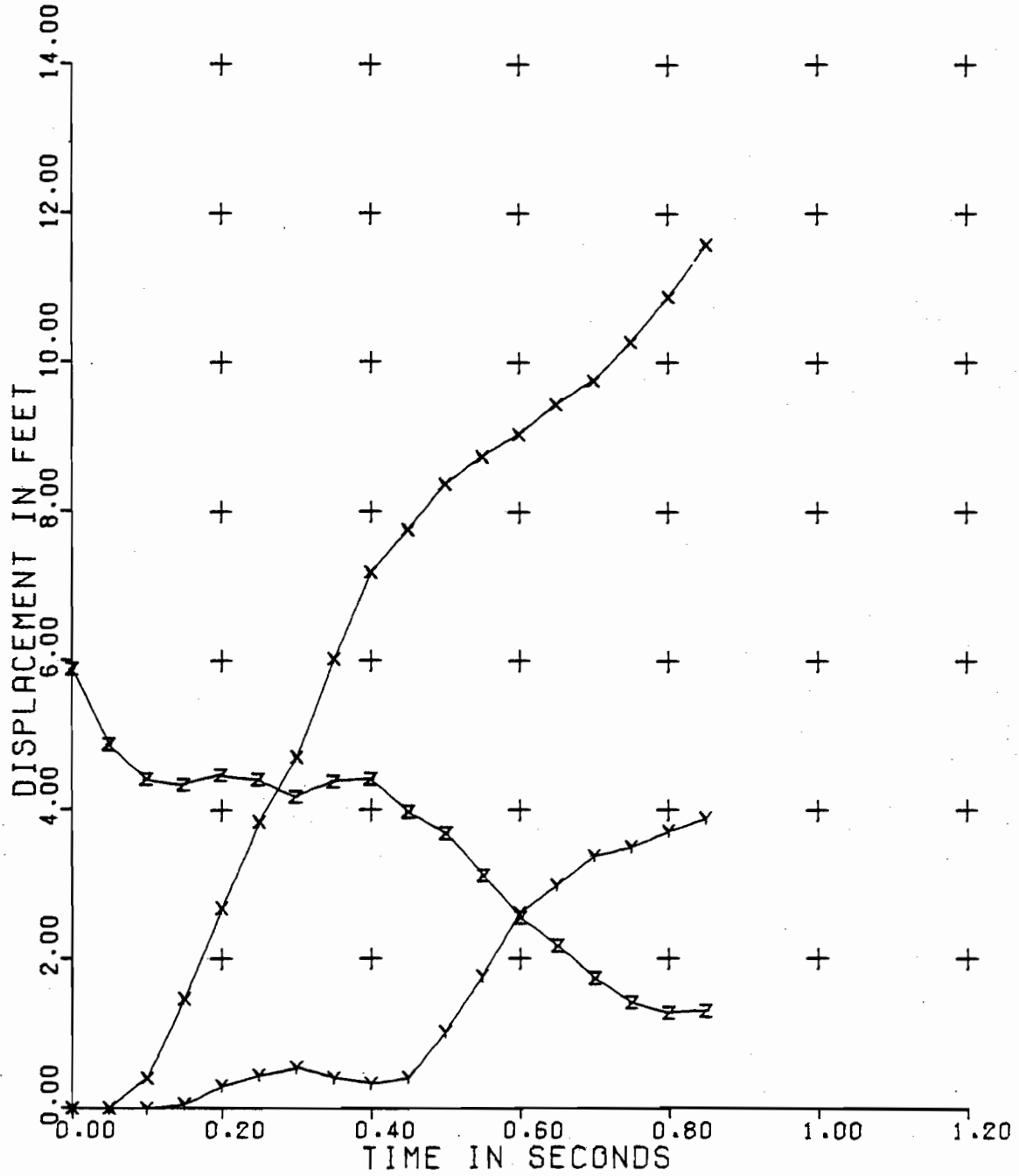

TEST NO. 2B AUG 17, 1976 SERIES 5

BACK-UP DISTANCE 3.75 FT

SPEED AT IMPACT 19.0 MPH

KEY

X = HORIZONTAL DISPLACEMENT

Y = VERTICAL DISPLACEMENT

Z = HORIZONTAL DIFFERENCE

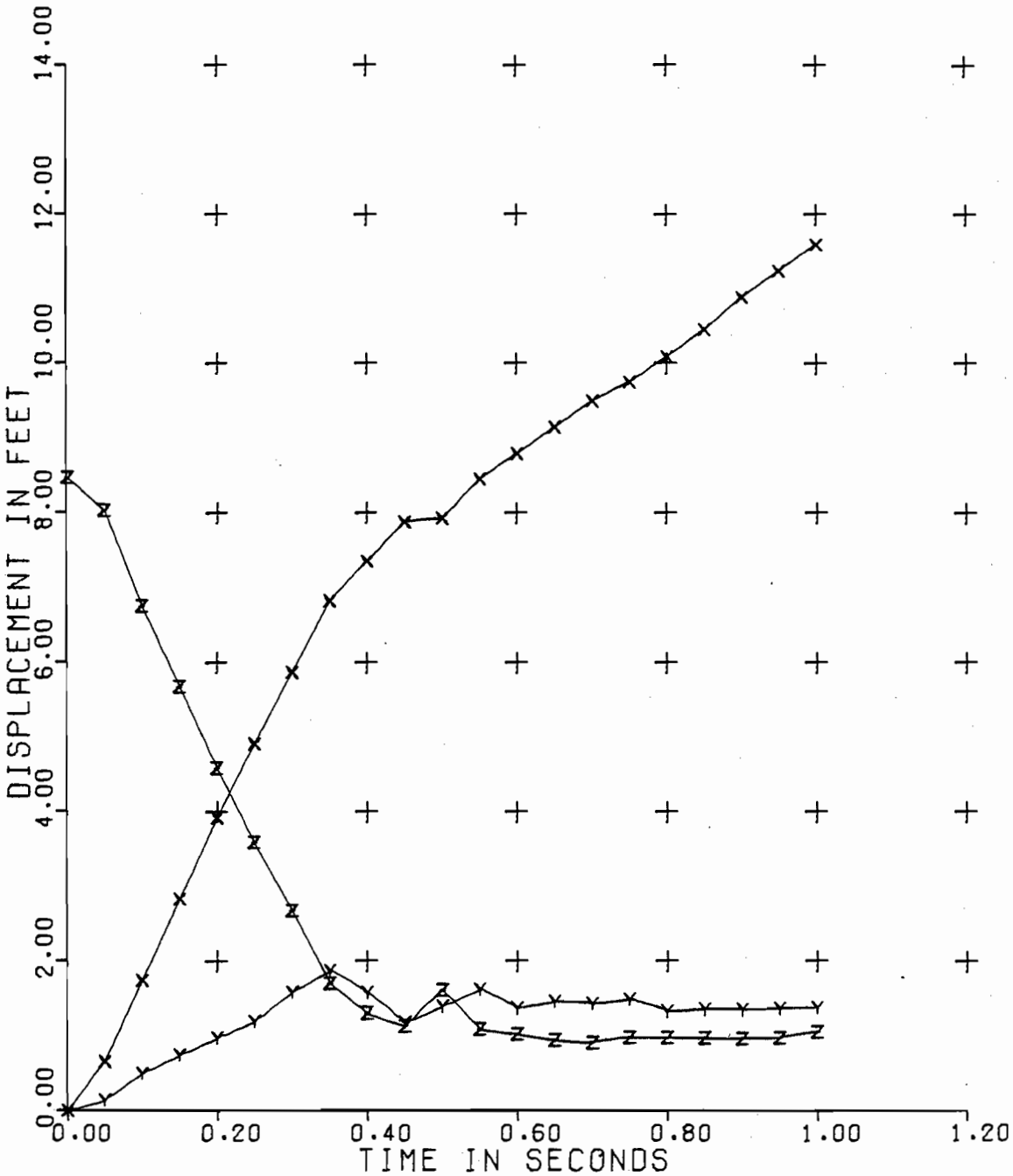

TEST NO. 1A OCT 13, 1976 SERIES 6

BACK-UP DISTANCE 2.92 FT
SPEED AT IMPACT 14.2 MPH

KEY
X = HORIZONTAL DISPLACEMENT
Y = VERTICAL DISPLACEMENT
Z = HORIZONTAL DIFFERENCE

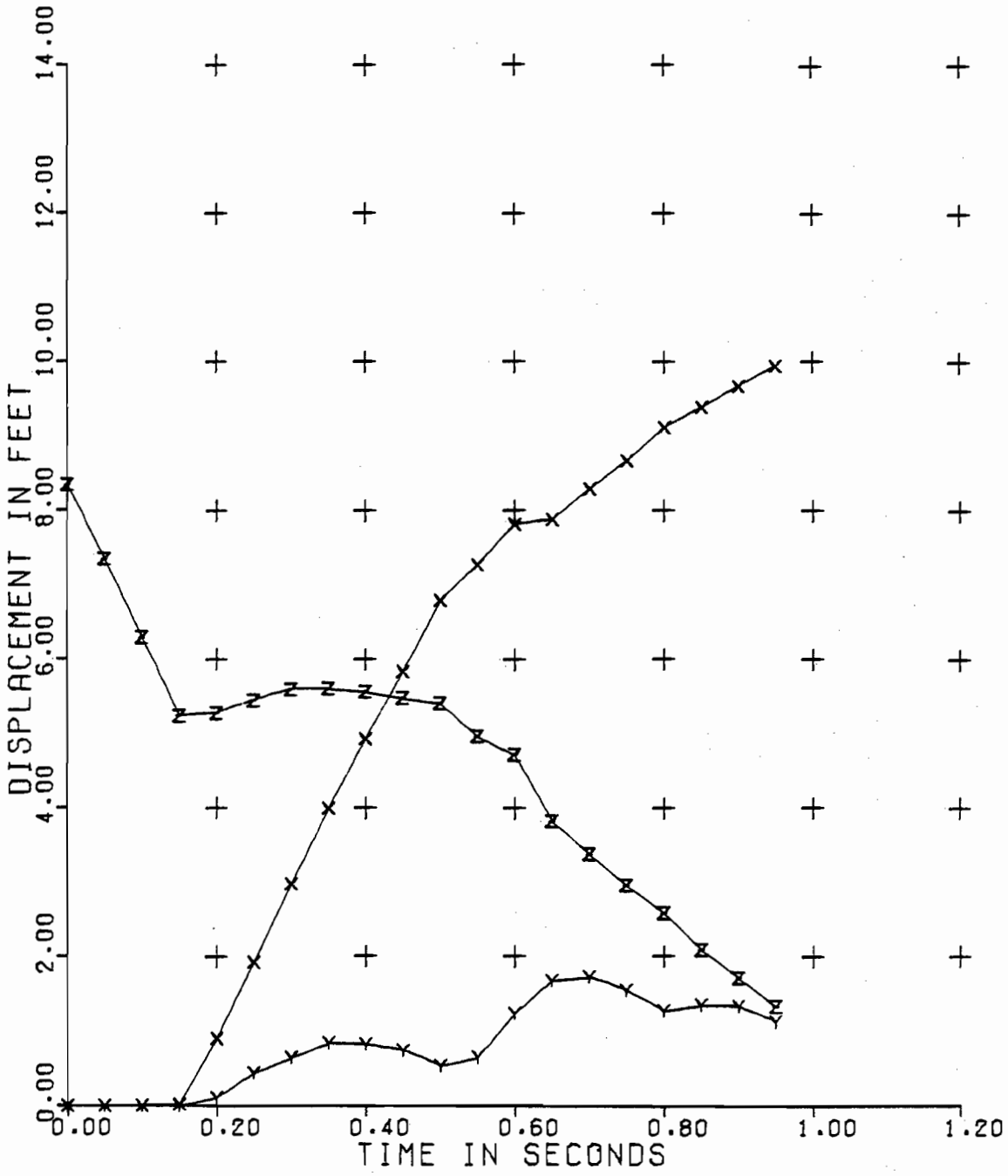

TEST NO. 1B OCT 13, 1976 SERIES 6

BACK-UP DISTANCE 2.92 FT

SPEED AT IMPACT 14.2 MPH

KEY

X = HORIZONTAL DISPLACEMENT

Y = VERTICAL DISPLACEMENT

Z = HORIZONTAL DIFFERENCE

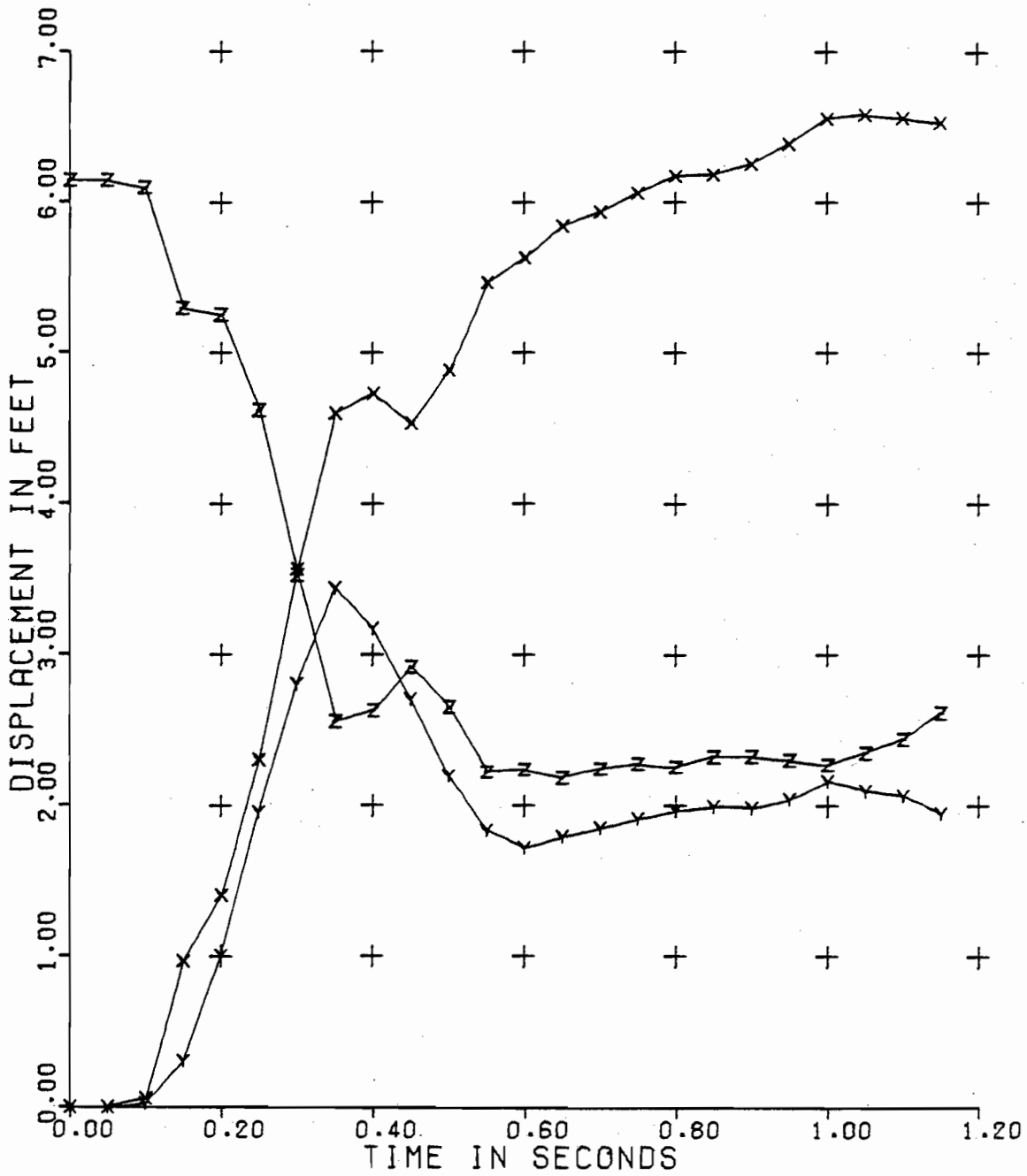

TEST NO. 1A SEP 17, 1976 SERIES 7

BACK-UP DISTANCE 0.0 FT

SPEED AT IMPACT 18.1 MPH

KEY

X = HORIZONTAL DISPLACEMENT

Y = VERTICAL DISPLACEMENT

Z = HORIZONTAL DIFFERENCE

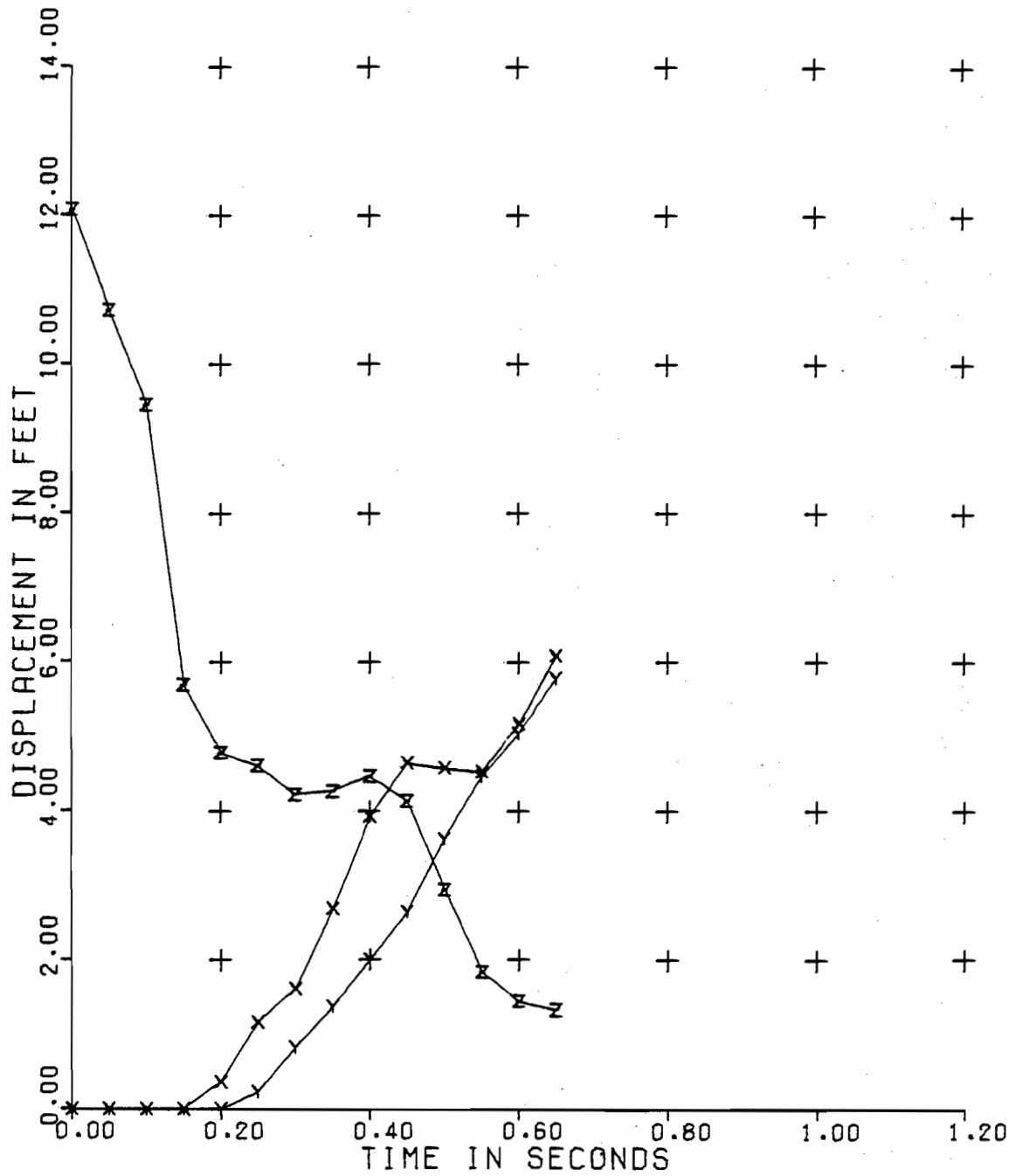

TEST NO. 1B SEP 17, 1976 SERIES 7

BACK-UP DISTANCE 0.0 FT

SPEED AT IMPACT 18.1 MPH

KEY

X = HORIZONTAL DISPLACEMENT

Y = VERTICAL DISPLACEMENT

Z = HORIZONTAL DIFFERENCE

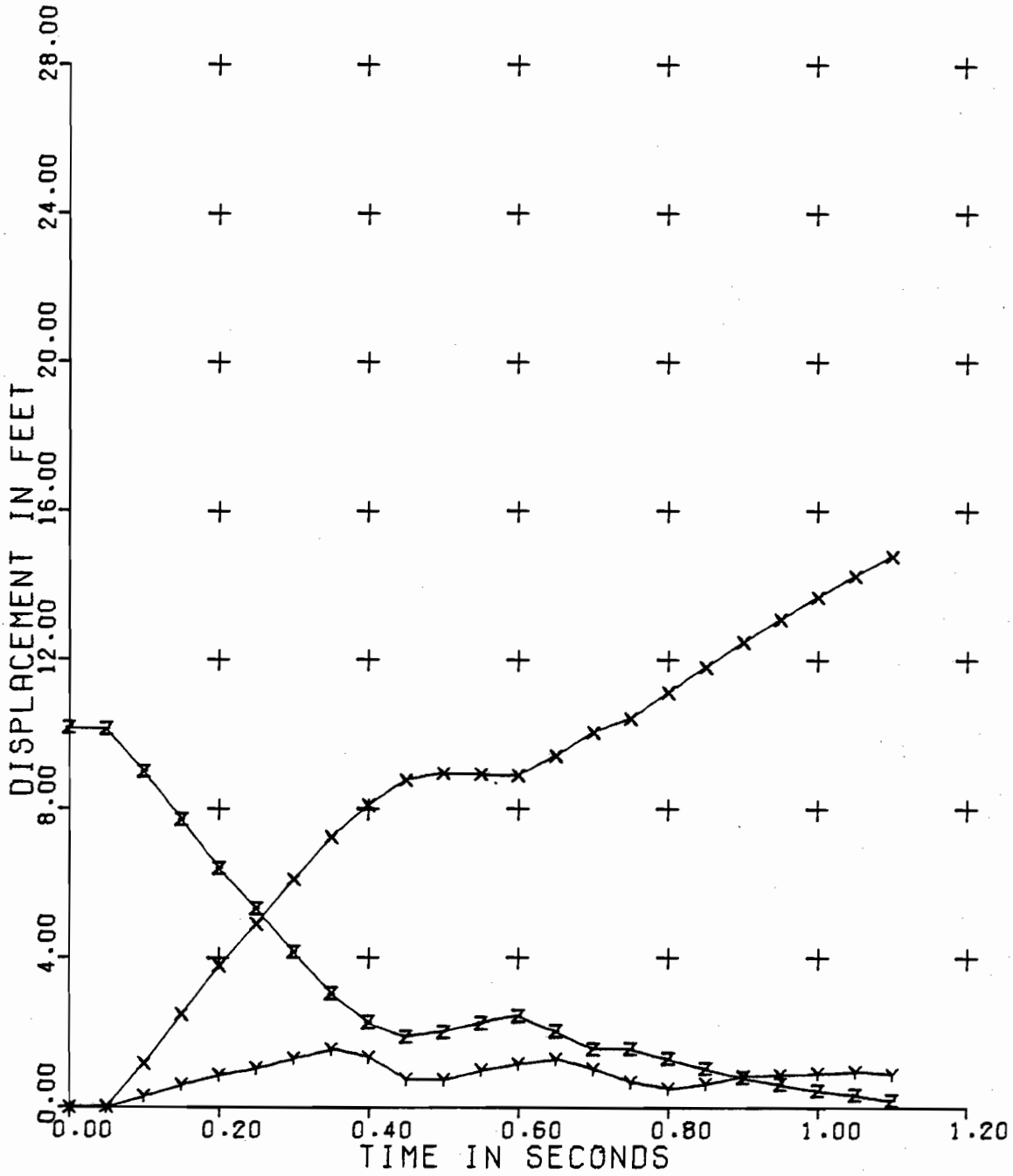

TEST NO. 1A NOV 23, 1976 SERIES 10

BACK-UP DISTANCE 3.75 FT

SPEED AT IMPACT 17.1 MPH

KEY

X = HORIZONTAL DISPLACEMENT

Y = VERTICAL DISPLACEMENT

Z = HORIZONTAL DIFFERENCE

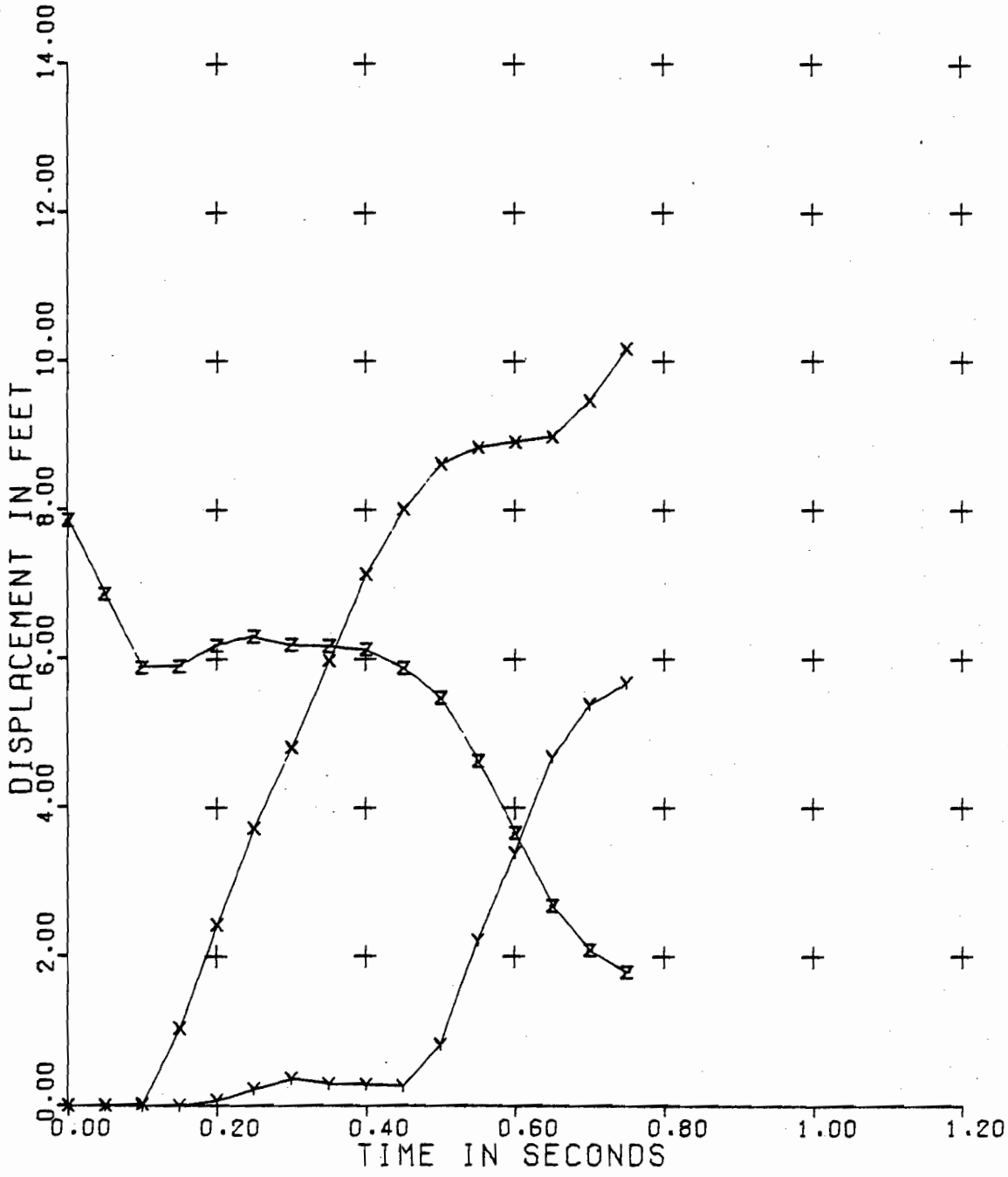

TEST NO. 1B NOV 23, 1976 SERIES 10

BACK-UP DISTANCE 3.75 FT

SPEED AT IMPACT 17.1 MPH

KEY

X = HORIZONTAL DISPLACEMENT

Y = VERTICAL DISPLACEMENT

Z = HORIZONTAL DIFFERENCE

APPENDIX D

ONE-DIMENSIONAL COLLISION MODELS

D.1 STANDARD COLLISION ENERGY

Assume that masses m_1 and m_2 are traveling at speeds U_1 and U_2, respectively, and are located at positions X_1 and X_2, respectively, at a given instant (Figure D-1). Then the energy available for absorption during subsequent collision of m_1 amd m_2 can be derived as follows. From the instantaneous position of the system center of mass,

$$X_c = \frac{m_1 X_1 + m_x X_2}{m_1 + m_2} \qquad \text{(D-1)}$$

it is easily shown that the velocity of the center of mass is:

$$U_c = \frac{dX_c}{dt} = \frac{m_1 U_1 + m_2 U_2}{m_1 + m_2} \qquad \text{(D-2)}$$

the collision energy is then given by the difference between the system total energy and the energy associated with the center of mass:

$$E_c = \tfrac{1}{2} m_1 (U_1)^2 + \tfrac{1}{2} m_2 (U_2)^2 - \tfrac{1}{2} (m_1 + m_2) (U_c)^2 \qquad \text{(D-3)}$$

After some manipulation, Eq. D-3 can be reduced to:

$$E_c = \tfrac{1}{2} \left(\frac{m_1 m_2}{m_1 + m_2} \right) (U_1 - U_2)^2 \qquad \text{(D-4)}$$

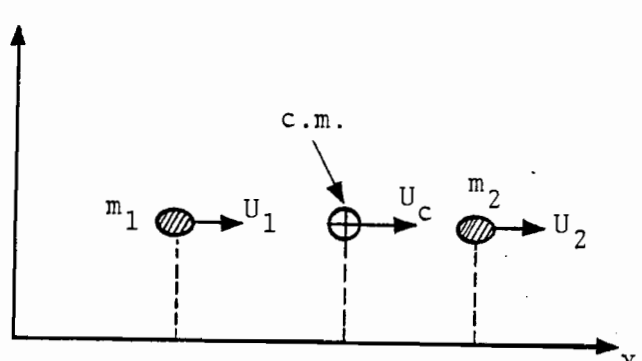

FIGURE D-1. TWO-MASS MODEL

D.2 DYNAMICS OF TWO-MASS MODEL

Now assume that masses m_1, m_2 collide, after which their velocities are U_1' and U_2'. Also, assume that an amount of energy, E, is absorbed inelastically during the collision. Convervation of momentum requires that:

$$m_1U_1 + m_2U_2 = m_1U_1' + m_2U_2' \qquad \text{(D-5)}$$

Conservation of energy is usually expressed as:

$$m_1(U_1)^2 + m_2(U_2)^2 = m_1(U_1')^2 + m_2(U_2')^2 + 2E \qquad \text{(D-6)}$$

However, since no external agencies are involved, the kinetic energy associated with the system center of mass remains constant, and can be subtracted from both sides of Eq. D-6 to yield:

$$\frac{m_1m_2}{m_1+m_2}\ (U_1-U_2)^2 = \frac{m_1m_2}{m_1+m_2}\ (U_1'-U_2')^2 + 2E \qquad \text{(D-7)}$$

Hence,

$$U_1' - U_2' = \pm\ (U_1-U_2)\ \sqrt{1-e} \qquad \text{(D-8)}$$

where e is the nondimensional energy-absorption coefficient:

$$e = E/E_c \qquad \text{(D-9)}$$

Obviously, e = 0 corresponds to a perfectly elastic collision,

while e = 1 corresponds to a completely inelastic collision. The correct sign to select from Eq. D-8 is the negative sign, which corresponds to the rebound characteristic of the collision, i.e.,:

$$U_1' - U_2' = - (U_1-U_2) \sqrt{1-e} \qquad \text{(D-10)}$$

Simultaneous solution of Eqs. D-5 and D-10 then leads to the following expressions for the post-impact velocities:

$$U_1' = U_1 + \frac{m_2}{m_1+m_2} (U_2-U_1)(1 + \sqrt{1-e}) \qquad \text{(D-11)}$$

$$U_2' = U_2 - \frac{m_1}{m_1+m_2} (U_2-U_1) (1 + \sqrt{i-e}) \qquad \text{(D-12)}$$

Let $\varepsilon = 1 + \sqrt{1-e}$ (i.e., $\varepsilon = 2$ for perflectly elastic impact, and $\varepsilon = 1$ for completely inelastic impact), and consider the special case $U_1 = 0$. Then the above results reduce to:

$$U_1' = \frac{m_2 \varepsilon}{m_1+m_2} U_2 \qquad \text{(D-13)}$$

$$U_2' = \left[1 - \frac{m_1 \varepsilon}{m_1+m_2}\right] U_2 \qquad \text{(D-14)}$$

D.3 SLOSHING/SLACK-ACTION MODEL

Assume that mass m_2 contains an internal independent mass, m_4, that may travel back and forth relative to m_2. For a single tank car, m_2 represents the carbody, trucks and part of the lading. For a multiple-car consists, m_2 represents the lead car, while m_4 represents the remaining cars.

The model is shown conceptually in Figure D-2, where it is seen that two states are possible. In the primary state, m_2 and m_4 have velocities U_2 and U_4, with $U_4 > U_2$ so that m_4 will eventually collide with the forward end of m_2. This collision produces the secondary state, in which the velocities are U_2'' and U_4'', with $U_4'' < U_2''$ so that m_4 will eventually collide with the rear end of

m_2 and will thus restore the primary state.* We shall call m_2 the observed mass, since only the velocities U_2, U_2'' can be directly observed.

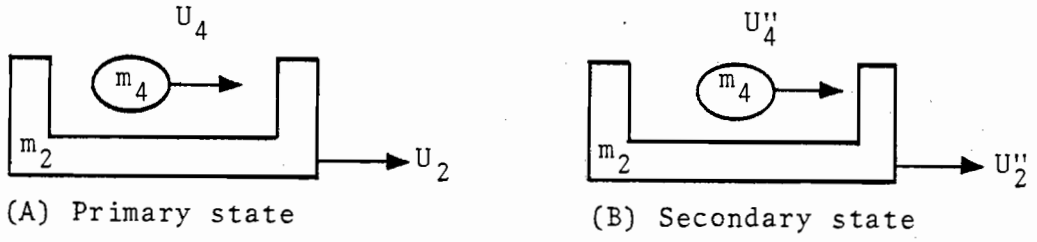

FIGURE D-2. SLOSHING/SLACK-ACTION MODEL

The primary and secondary states can be related by applying the results derived previously for the two-mass model. Let

$$U = \frac{m_2U_2 + m_4U_4}{m_2 + m_4} = \frac{m_2U_2'' + m_4U_4''}{m_2 + m_4} \qquad \text{(D-15)}$$

denote the center-of-mass velocity, and define

$$\Delta U = U_4 - U_2 \qquad \text{(D-16)}$$

Then the internal kinetic energy of sloshing or slack action is given by:

$$E_s = \frac{1}{2}\left(\frac{m_2m_4}{m_2+m_4}\right)(\Delta U)^2 \qquad \text{(D-17)}$$

and

$$U_2 = U - \frac{m_2}{m_2+m_4}\Delta U \qquad \text{(D-18)}$$

*For consists, the forward and rear-end impacts can be thought of as the remaining cars reaching full buff and full draft position, respectively.

$$U_4 = U + \frac{m_2}{m_2+m_4} \Delta U \qquad \text{(D-19)}$$

We shall assume for the sake of simplicity that the collisions between m_2 and m_4 are perfectly elastic. Therefore, $\Delta U'' = -\Delta U$, and:

$$U_2'' = U + \frac{m_4}{m_2+m_4} \Delta U = \frac{(m_2-m_4)\, U_2 + 2m_4 U_4}{m_2+m_4} \qquad \text{(D-20)}$$

$$U_4'' = U - \frac{m_2}{m_2+m_4} \Delta U = \frac{2m_2 U_2 + (m_4-m_2)\, U_4}{m_2+m_4} \qquad \text{(D-21)}$$

Now consider the effects of a collision between the sloshing/slack-action model and a third mass m_1 at rest, representing a loose standing car (Figure D-3). As indicated in the figure, two possible sequences must be analyzed, depending on whether the m_2/m_4 system is in its primary or secondary state when m_2 collides with m_1.

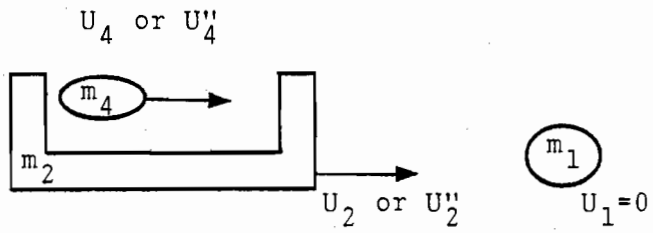

FIGURE D-3. COMPLETE SLOSHING/SLACK-ACTION MODEL

We consider first the case of the primary state. Assume that an amount of energy, E, is absorbed by the m_2/m_1 impact, and define:

$$e = \frac{E}{\frac{1}{2}\left(\frac{m_1 m_2}{m_1+m_2}\right)(U_2)^2} \qquad \text{(D-22)}$$

and $\varepsilon = 1 + \sqrt{1-e}$ as was done previously. Applying the results derived in subsection D.2, we then find:

$$U_1''' = \frac{m_2\varepsilon}{m_1+m_2} U_2 \tag{D-23}$$

$$U_2''' = \left[1 - \frac{m_1\varepsilon}{m_1+m_2}\right] U_2 \tag{D-24}$$

$$U_4''' = U_4 \tag{D-25}$$

$$U''' = \frac{m_2U_2''' + m_4U_4'''}{m_2+m_4} = \frac{\left[1 - \frac{m_1\varepsilon}{m_1+m_2}\right] m_2U_2 + m_4U_4}{m_2+m_4} \tag{D-26}$$

$$\Delta U''' = U_4''' - U_2''' = U_4 - \left[1 - \frac{m_1\varepsilon}{m_1+m_2}\right] U_2 \tag{D-27}$$

where $(\,)'''$ represents the state after m_2/m_1 impact. Note that the m_2/m_4 system is still in a primary state, but that its internal energy (as represented by $\Delta U'''$) has changed. We are assured that the state remains primary because U_4 has not changed, while $U_2''' < U_2$. Thus, the next event to occur will be a forward-end impact, resulting in a change of the velocity U_2''' to a value U_2' given by:

$$U_2' = U''' + \frac{m_4}{m_2+m_4} \Delta U''' = \left[1 + \left(\frac{m_4-m_4}{m_2+m_4}\right)\left(\frac{m_1\varepsilon}{m_1+m_2}\right)\right] U_2 + \frac{2m_4}{m_2+m_4} \Delta U \tag{D-28}$$

Thus far, nothing has been said about the time interval between m_2/m_1 and m_4/m_2 impact, and in fact this interval cannot be determined without making additional assumptions about the model. However, the most interesting characteristic of the model is obtained simply by conceiving a situation in which the interval is sufficiently short to allow the intermediate velocity U_2''' to escape observation. Such a situation is possible, for example, when the observed velocities are deduced from position-time plots prepared by examination of periodically selected frames taken from a high-speed motion picture film. Under these conditions, it will then be possible to obtain apparently anomalous results by

considering U_2, U_2' to be initial and final velocities associated with the collision of two rigid masses m_1 and m_2. Specifically, the obvious anomaly $U_2' > U_2$ results when (from Eq. D-28):

$$\frac{\Delta U}{U_2} \geq \frac{m_1(m_2-m_4)\varepsilon}{2m_4(m_1+m_2)} \tag{D-29}$$

Note in particular that this anomaly can occur even if there is no initial sloshing or slack action ($\Delta U=0$) whenever the independent mass m_4 is equal to or larger than the observed mass m_2.

Now consider the case the begins with m_2/m_4 in its secondary state. Assume that an amount of energy E" is absorbed inelastically in the m_2/m_1 impact, and define:

$$e'' = \frac{E''}{\frac{1}{2}\left(\frac{m_1 m_2}{m_1+m_2}\right)(U_2'')^2} \tag{D-30}$$

and $\varepsilon'' = 1 + \sqrt{1-e''}$. The intermediate state after m_2/m_1 is then given by:

$$U_1'' = \frac{m_2\varepsilon''}{m_1+m_2} \quad U_2'' = \frac{m_2\varepsilon''}{m_1+m_2}\left[U + \frac{m_4}{m_2+m_4}\Delta U\right] \tag{D-31}$$

$$U_2''' = \left[1 - \frac{m_1\varepsilon''}{m_1+m_2}\right]\left[U + \frac{m_4}{m_2+m_4}\Delta U\right] \tag{D-32}$$

$$U_4''' = U_4'' = U - \frac{m_2}{m_2+m_4}\Delta U \tag{D-33}$$

$$U''' = \frac{\left[m_2\left(1 - \frac{m_1\varepsilon''}{m_1+m_2}\right) + m_4\right]U - \left(\frac{m_2 m_4}{m_2+m_4}\right)\left(\frac{m_1\varepsilon''}{m_1+m_2}\right)\Delta U}{m_2+m_4} \tag{D-34}$$

$$\Delta U''' = \frac{m_1\varepsilon''}{m_1+m_2}U - \left[1 - \left(\frac{m_4}{m_2+m_4}\right)\left(\frac{m_1\varepsilon''}{m_1+m_2}\right)\right]\Delta U \tag{D-35}$$

At this point, the m_2/m_4 system may be in either a primary or a secondary state, depending upon the sign of $\Delta U'''$. Without loss of generality, we can consider the primary sub-case ($\Delta U''' > 0$), which leads after m_4/m_2 impact to the final velocity:

$$U_2' = \left[1 + \left(\frac{m_4 - m_2}{m_2 + m_4}\right)\left(\frac{m_1 \varepsilon''}{m_1 + m_2}\right)\right] U_2 + \left(\frac{2m_4}{m_2 + m_4}\right)\left(\frac{m_4 - m_2}{m_2 + m_4}\right)\left(\frac{m_1 \varepsilon''}{m_1 + m_2}\right)\Delta U \tag{D-36}$$

In a manner similar to the case of a primary initial state, U_2' can exceed U_2'' when:

$$\frac{\Delta U}{U_2} > \frac{\frac{m_1 \varepsilon''}{m_1 + m_2}}{1 - \left(\frac{2m_4}{m_2 + m_4}\right)\left(\frac{m_1 \varepsilon''}{m_1 + m_2}\right)} \tag{D-37}$$

However, if U_2'' escapes observation in this case, the apparent anomaly will be that the speed reduction $U_2'' - U_2'$ will be less than predicted by the two-mass model.

APPENDIX E

TWO-DIMENSIONAL COLLISION MODELS

E.1 TWO-MASS MODEL WITH THREE DEGREES OF FREEDOM

The simplest form of a two-dimensional collision model accounts for the offset of a two-mass impact from the center of one of the masses. The model is illustrated schematically in Figure E-1. Consideration is restricted to cases in which the mass m_1, representing a loose standing car, is initially at rest. Mass m_1 is assumed to have a rotary inertia I_1 about its center of mass, and acquires an angular velocity ω^1 as a result of the offset impact.

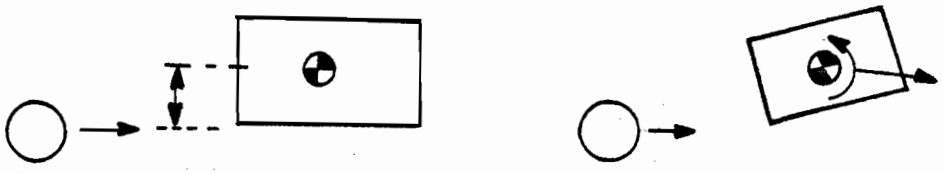

FIGURE E-1. TWO-MASS/THREE-DEGREE-OF-FREEDOM MODEL

A dynamical description of the above model requires an expression for conservation of angular momentum, as well as the conservation laws for energy and linear momentum. The momentum conservation laws are:

$$m_2 U_2 = m_1 U_1' + m_2 U_2' \qquad \text{(E-1)}$$

$$m_2 h U_2 = I, \omega_1' + m_2 h U_2' \qquad \text{(E-2)}$$

Energy conservation is expressed by:

$$m_2 (U_2)^2 = m_1 (U_1')^2 + m_2 (U_2')^2 + I, (\omega_1')^2 + 2E \qquad \text{(E-3)}$$

where E is the amount of energy assessed to be absorbed inelastically. Using Eqs. E-1 and E-2 to eliminate U_1' and U_2' from Eq. E-3 and solving the resulting quadratic equation for ω_1' then leads to:

$$\omega_1' \quad \frac{\frac{I_1U_2}{h} \pm \sqrt{\left(\frac{I_1U_2}{h}\right)^2 - 2EI_1\left[1 + \frac{(m_1+m_2)\ I_1}{m_1m_2h_2}\right]}}{I_1\left[1 + \frac{(m_1+m_2)\ I_1}{m_1m_2h^2}\right]} \qquad \text{(E-4)}$$

Equation E-4 suggests a natural definition for an energy-absorption coefficient, e, such that $0 \leq e \leq 1$ covers the range from perfectly elastic to completely inelastic impacts:

$$e = \frac{E}{\frac{1}{2}\left[\frac{m_1m_2h^2I_1}{m_1m_2h^2 + (m_1+m_2)\ I_1}\right](U_2/h)^2} \qquad \text{(E-5)}$$

Substitution of Eq. E-5 in Eq. E-4 and use of the parameter $\varepsilon = 1 + \sqrt{1-e}$ then leads to:

$$\omega_1' = \left(\frac{m_1m_2h^2\varepsilon}{m_1m_2h^2 + (m_1+m_2)I_1}\right)\left(\frac{U_2}{h}\right) \qquad \text{(E-6)}$$

The inadequacy of this model is easily demonstrated by comparing the observed angular velocities with the predictions of Eq. E-6. For this purpose, the total rail-weight mass is used for the hopper car, m_1, while effective masses for the striking consist have been estimated based on Table 7. The relevant data are summarized in Table E-1. The value of the offset, h, is estimated by assuming that the center of mass of the trucks is at axle height, i.e., 16.5 inches (1.375 ft) above the rails. Thus*:

$$\text{System C.M. Height} = \frac{1.375\text{x}14.92 + 4.759\text{x}22.84}{37.76} = 3.422 \text{ ft}$$

$$h = \text{C.M. Height} - \ell \cong 3.422 - 2.04 - 1.382 \text{ ft}$$

The results, summarized in Table E-1, show that the predicted an-

*See Figure 11 for component weights.

gular velocities are one order of magnitude greater than the observations, and do not reproduce the observed inconsistency of sign.

TABLE E-1. ASSESSMENT OF TWO-MASS/THREE-DEGREE-OF-FREEDOM MODEL

Series and Test Number	ω_1 (KIPS)	$W_2^{(eff)}$ (KIPS)	U_2 (ft/sec)	ω_1 (rad/sec)	
				Predicted	Observed
3.2	37.5	288.96	21.9	.407	.0547
3.3	37.5	288.96	24.2	.450	-.0194
3.4	37.5	287.05	22.6	.420	.0650
3.5	37.5	287.05	24.8	.461	.0024
4.1	37.5	303.91	27.3	.510	-.0564
4.2	37.5	311.40	28.2	.528	.0703
5.1	37.5	308.7	28.5	.533	-.0994
5.2	37.5	308.7	27.9	.522	.1408
6.1	40.4	350.14	20.6	.417	-.0258
7.1	40.1	351.58	26.6	.535	.2030
10.1	37.8	523.94	25.1	.495	.1107

E.2 CARBODY/TRUCK INTERACTION MODEL

The prediction for angular velocity can be improved, and a vertical-motion mode can be included by considering a model that treats first impact from the viewpoint of a three-mass system. The three-mass model is illustrated schematically in Figure E-2. As was done with the sloshing/slack-action model (Appendix D), we consider a compound sequence in which tank car/hopper carbody impact and carbody/truck interaction are treated separately, but we assume that only initialand final states are observed.

Equations E-1 through E-3 apply to the first impact in the sequence, except that the offset, h, is replaced by offset ℓ.

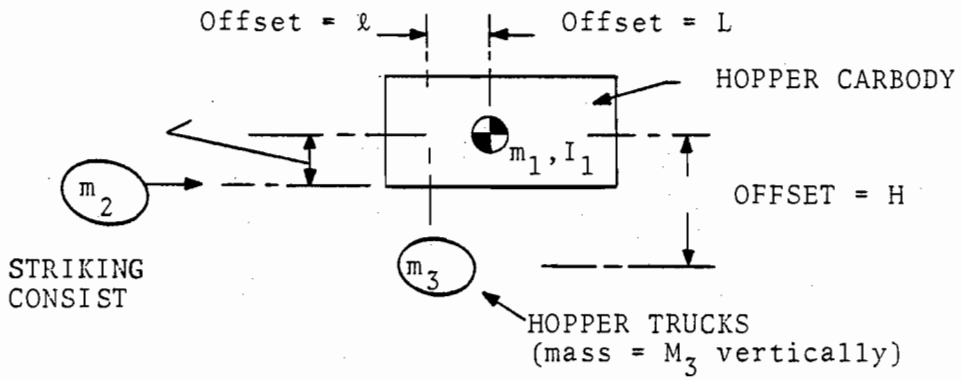

(A) Definitions of Inertias and Offsets

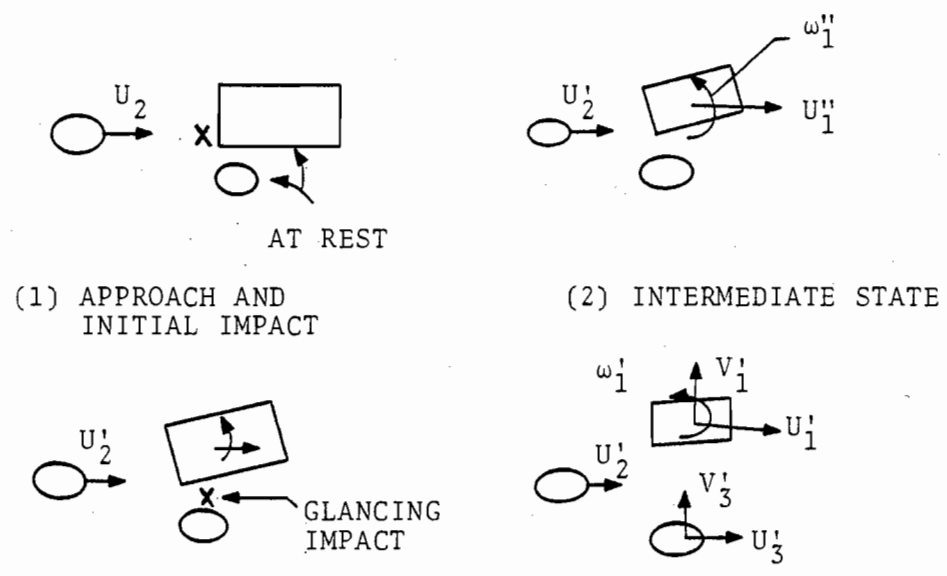

(1) APPROACH AND INITIAL IMPACT

(2) INTERMEDIATE STATE

(3) CARBODY/TRUCK INTERACTION

(4) FINAL STATE

(B) COMPOUND IMPACT SEQUENCE

FIGURE E-2. CARBODY/TRUCK INTERACTION MODEL

The complete solution for intermediate state is given by:

$$U_1''/U_2 = \frac{I_1\varepsilon}{m_1\ell^2} \Big/ \left[1 + \frac{(m_1+m_2)I_1}{m_1m_2\ell^2}\right] \tag{E-7}$$

$$U_2''/U_2 = \left[1 + \frac{(2-\varepsilon)I_1}{m_1\ell^2}\right] \Big/ \left[1 + \frac{(m_1+m_2)I_1}{m_1m_2\ell^2}\right] \tag{E-8}$$

$$\ell\omega_1''/U_2 = \varepsilon \Big/ \left[1 + \frac{(m_1+m_2)I_1}{m_1m_2\ell^2}\right] \tag{E-9}$$

where $\varepsilon = 1 + \sqrt{i-e}$ and

$$e = \frac{E}{\frac{1}{2}\left[\frac{m_1m_2\ell^2}{m_1m_2\ell^2 + (m_1+m_2)I_1}\right](U_2/\ell)^2} \tag{E-10}$$

is the inelastic energy-absorption coefficient.

Treatment of the carbody/truck interaction requires more careful consideration. An amount of energy, E", may be absorbed inelastically by suspension dismount, friction snubbing, wheel/rail interface friction, etc. We may visualize the interaction in terms of a glancing blow, e.g., between the carbody centerplate and the edge of the bolster bowl, as the carbody begins to move forward in the intermediate state. Thus, temporarily ignoring the angular momentum-transfer characteristics of the system, the carbody/truck interaction appears as shown in Figure E-3.

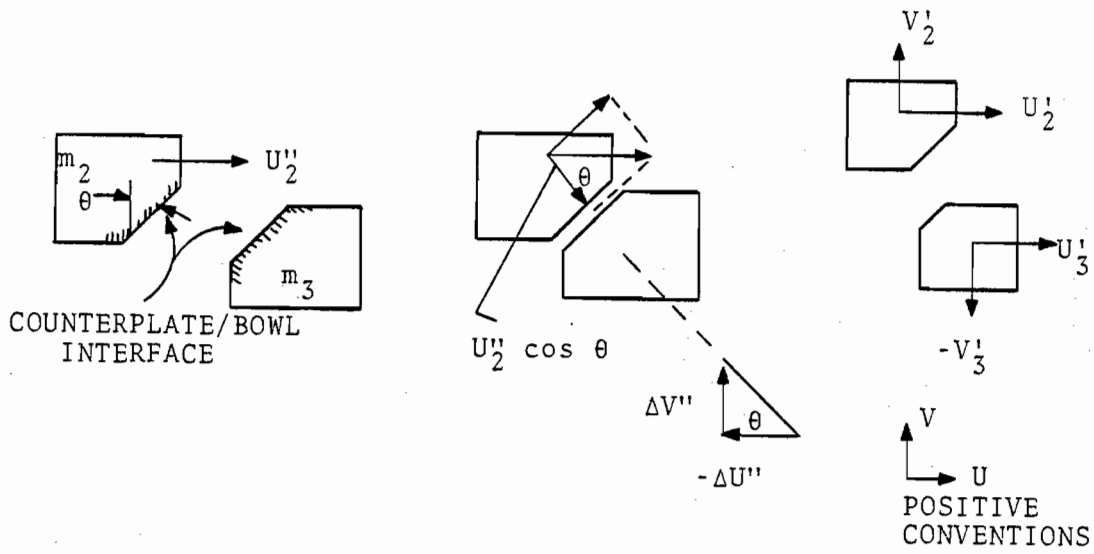

FIGURE E-3. GLANCING IMPACT CONCEPT

Suppose that the centerplate/bowl interface is inclined at an angle θ from the vertical. Then only the velocity component normal to the contact surface, $U_2''COS\theta$, is involved in the momentum/energy exchange. In other words, the changes in velocities from the ( )'' state to the ( )' state, denoted by ΔU'' and ΔV'', must combine to give a velocity vector parallel to $U_2''COS\theta$, i.e.:

$$-\frac{\Delta V''}{\Delta U''} = \tan\theta = \beta \qquad \text{(E-11)}$$

Treatment of the mass representing the trucks must also be considered with some care. Intuitively, we expect that the trucks will acquire a downward vertical velocity, as shown in Figure E-3. However, they will also interact with the earth through the track structure, and this interaction will occur essentially at the same time as the carbody/truck interaction. It will be convenient to account for the truck/ground interaction by imagining the model to have an effective mass, M_3, for vertical motion, such that M_3 is much larger than the actual truck mass, m_3.

Finally, the use of a single point mass to represent both trucks can be justified by recognizing that the horizontal location of the two actual masses, $m_3/2$ each, is immaterial in the m_3 angular momentum term, and that M_3 represents an effective truck/ground mass at its proper location (the impact end of the hopper car).

The equations relating the intermediate and final states can now be written in terms of the familiar conservation laws:

Horizontal momentum

$$m_1 U_1'' = m_1 U_1' + m_3 U_3' \tag{E-12}$$

Vertical momentum

$$0 = m_1 V_1' + M_3 V_3' \tag{E-13}$$

Angular momentum

$$I_1 \omega_1'' = I_1 \omega_1' + m_3 H U_3' - M_3 L V_3' \tag{E-14}$$

Energy

$$m_1 (U_1'')^2 + I_1 (\omega_1'')^2 = m_1 (U_1')^2 + m_1 (V_1')^2 + I_1 (\omega_1')^2 + m_3 (U_3')^2 + M_3 (V_3')^2 + 2E'' \tag{E-15}$$

where E'' is the energy absorbed inelastically during carbody/truck interaction. To the above four equations we can now add the geometrical constraint by recognizing that $\Delta V'' = V_1'$ and $\Delta U'' = U_1' - U_1''$. Hence, Eq. E-11 becomes:

$$V_1' = B\,(U_1'' - U_1') \tag{E-16}$$

By using Eqs. E-12 through E-14 and Eq. E-16 to eliminate U_2', U_3', V_1' and V_3', Eq. E-15 is transformed to a quadratic equation in ω_1':

$$a\,(\omega_1')^2 - 2b\omega_1' + c = 0 \tag{E-17}$$

where

$$a = I_1 + \left(\frac{I_1}{H + \beta L}\right)^2 \left[\frac{1+\beta^2}{m_1} + \frac{1}{m_3} + \frac{\beta^2}{M_3}\right] \tag{E-18}$$

$$b = \omega_1'' \left(\frac{I_1}{H+\beta L}\right)^2 \left[\frac{1+\beta^2}{m_1} + \frac{1}{m_3} + \frac{\beta^2}{M_3}\right] - \frac{I_1 U_1''}{H+\beta L} \tag{E-19}$$

$$c = \left(\frac{I_1 \omega_1''}{H+\beta L}\right)^2 \left[\frac{1+\beta^2}{m_1} + \frac{1}{m_3} + \frac{\beta^2}{M_3}\right] - I_1 (\omega_1'')^2 + \\ - \frac{2 I_1 U_1'' \omega_1''}{H+\beta L} + 2E'' \tag{E-20}$$

Of the possible solutions,

$$\omega_1' = \frac{b \pm \sqrt{b^2 - ac}}{a} \tag{E-21}$$

it is apparent that the negative square root must be chosen, by examining the special case $U_1'' = E'' = 0$ and requiring that $\omega_1' < \omega_1''$.

Also, Eqs. E-18 through E-20 suggest the definition of the following effective mass parameter for convenience:

$$1/\bar{M} = \frac{1+\beta^2}{m_1} + \frac{1}{m_3} + \frac{\beta^2}{M_3} \tag{E-22}$$

The solution for ω_1' then becomes:

$$\omega_1' = \frac{1}{I_1 + \dfrac{I_1^2}{\bar{M}(H+\beta L)^2}} \left[\frac{I_1^2 \omega_1''}{\bar{M}(H+\beta L)^2} - \frac{I_1 U_1''}{H+\beta L} + \right. \\ \left. - \sqrt{I_1^2 \left(\omega_1'' + \frac{U_1''}{H+\beta L}\right)^2 - 2E'' \left[I_1 + \frac{I_1^2}{\bar{M}(H+\beta L)^2}\right]}\right] \tag{E-23}$$

Equation E-23 in turn suggests the definition of a natural energy-absorption coefficient e", such that e" = 0 for perfectly elastic impact and e" = 1 for completely inelastic impact:

$$e'' = \frac{E''}{\frac{1}{2}\left[\dfrac{I_1 \bar{M}(H+\beta L)^2}{I_1 + \bar{M}(H+\beta L)^2}\right]\left(\omega_1'' + \dfrac{U_1''}{H+\beta L}\right)^2} \tag{E-24}$$

Substituting these results back into expressions for the other ( )' velocities and defining $\varepsilon'' = 1+\sqrt{1-e''}$ in the usual manner then leads to the following set of relations between the intermediate and final states:

$$\frac{U_1'}{(H+\beta L)\omega_1''} = \frac{U_1''}{(H+\beta L)\omega_1''} - \frac{\left[1 + \frac{U_1''}{(H+\beta L)\omega_1''}\right]\frac{I_1\varepsilon''}{m_1(H+\beta L)^2}}{1 + \frac{I_1}{\bar{M}(H+\beta L)^2}} \qquad \text{(E-25)}$$

$$\frac{V_1'}{(H+\beta L)\omega_1''} = \frac{\left[1 + \frac{U_1''}{(H+\beta L)\omega_1''}\right]\frac{I_1\beta\varepsilon''}{m_3(H+\beta L)_2}}{1 + \frac{I_1}{\bar{M}(H+\beta L)^2}} \qquad \text{(E-26)}$$

$$\frac{U_3'}{(H+\beta L)\omega_1''} = \frac{\left[1 + \frac{U_1''}{(H+\beta L)\omega_1''}\right]\frac{I_1\varepsilon''}{m_3(H+\beta L)^2}}{1 + \frac{I_1}{\bar{M}(H+\beta L)^2}} \qquad \text{(E-27)}$$

$$\frac{V_3'}{(H+\beta L)\omega_1''} = -\frac{\left[1 + \frac{U_1''}{(H+\beta L)\omega_1''}\right]\frac{I_1\beta\varepsilon''}{m_3(H+\beta L)^2}}{1 + \frac{I_1}{\bar{M}(H+\beta L)^2}} \qquad \text{(E-28)}$$

$$\frac{\omega_1'}{\omega_1''} = \frac{\frac{I_1}{\bar{M}(H+\beta L)^2} - \frac{U_1''}{(H+\beta L)\omega_1''} - \left[1 + \frac{U_1''}{(H+\beta L)\omega_1''}\right]\sqrt{1-e''}}{1 + \frac{I_1}{\bar{M}(H+\beta L)^2}} \qquad \text{(E-29)}$$

Note that we may now pass to the limit $M_3 \to \infty$ to represent the truck/ground mass as the mass of the earth. In the limit, $V_3' \to 0$ as should be expected, and

$$1/\bar{M} \to \frac{1+\beta^2}{m_1} + \frac{1}{m_3} \tag{E-30}$$

We now seek a set of relations between the initial and final states. These relations can be derived by combining Eqs. E-7, E-9 and E-25 through E-29. The results are:

$$U_1'/U_2 = \frac{\varepsilon}{A}\left[\frac{I_1}{m_1 \ell^2} - \frac{C(C-1)\varepsilon''}{B}\right] \tag{E-31}$$

$$V_1'/U_2 = \frac{\beta\varepsilon\varepsilon''C(C-1)}{AB} \tag{E-32}$$

$$\ell\omega_1'/U_2 = \frac{E}{A}\left[1 - \frac{C\varepsilon''}{B}\right] \tag{E-33}$$

$$U_3'/U_2 = \frac{m_1\varepsilon\varepsilon''C(C-1)}{m_3 AB} \tag{E-34}$$

$$V_3'/U_2 = -\frac{m_1\varepsilon\varepsilon''C(C-1)}{M_3 AB} \tag{E-35}$$

where

$$A = 1 + \frac{(m_1+m_2)I_1}{m_1 m_2 \ell^2}$$

$$B = 1 + \frac{I_1}{\bar{M}(H+\beta L)^2} \tag{E-36}$$

$$C = 1 + \frac{I_1}{\bar{M}\ell(H+\beta L)} \tag{E-38}$$

APPENDIX F

REGRESSION MODEL AND ANALYSIS

F.1 REGRESSION MODEL

The most useful results from the carbody/truck interaction model derived in Appendix E are Eqs. E-31 through E-33, relating the hopper carbody final velocities U_1', V_1', ω_1' to the initial speed, U_2, of the striking consist. Since the velocities, masses and dimensions are known quantities, these equations can be used to formulate a regression model for analysis of the unknown energy-absorption parameters ε, ε'' and contact geometry $\beta = \tan\theta$.

However, some manipulation is required to reduce the nonlinearities (and thereby the numerical sensitivity) of the regression model to a minimum. Of most concern in this respect is the need to eliminate $\bar{M}$, B and C (Eqs. E-30, E-37 and E-38) because of the complex dependence of these parameters on β. The parameters $\bar{M}$, B, C and E" can be eliminated by multiplying Eq. E-31 by β and rearranging:

$$\beta\varepsilon\left(\frac{I_1}{Am_1\ell^2}\right) - \beta\,\frac{U_1'}{U_2} = \frac{\beta\varepsilon\varepsilon''C(C-1)}{AB} \qquad \text{(F-1)}$$

The right-hand side of Eq. F-1 is equal to V_1'/U_2 (see Eq. E-32). Hence, Eq. F-1 can be put in the form:

$$\beta\varepsilon - \beta x - y = 0 \qquad \text{(F-2)}$$

where

$$x = \left(\frac{Am_1\ell^2}{I_1}\right)\left(\frac{U_1'}{U_2}\right) \qquad y = \left(\frac{Am_1\ell^2}{I_1}\right)\left(\frac{V_1'}{U_2}\right) \qquad \text{(F-3)}$$

can be computed from the observed quantities.

A regression model for β and ε can now be formulated by minimizing the square error with respect to their average estimators $\hat{\beta}$, $\hat{\varepsilon}$:

$$\text{Square Error} = \sum_{i=1}^{N} (\hat{\beta}\hat{\varepsilon} - \hat{\beta}x_i - y_i)^2 \qquad \text{(F-4)}$$

where N is the total number of data points. This procedure leads to the following explicit expressions for the estimators:

$$\hat{\beta} = \frac{(\sum x_i)(\sum y_i) - N(\sum x_i y_i)}{N(\sum x_i^2) - (\sum x_i)^2} \qquad \text{(F-5)}$$

$$\hat{\varepsilon} = \frac{1}{N}\left[(\sum x_i) + \frac{1}{\hat{\beta}}(\sum y_i)\right] \qquad \text{(F-6)}$$

The estimates obtained from Eqs. F-5 and F-6 can then be combined with Eq. E-33 to estimate the average value of ε":

$$\hat{\varepsilon} = \frac{B(\hat{\beta})}{C(\hat{\beta})}\left[1 - \frac{A\ell}{N\hat{\varepsilon}} \sum_{i=1}^{N} (\omega_1'/U_2)_i\right] \qquad \text{(F-7)}$$

F.2 REGRESSION ANALYSIS

Regression analysis of the Switchyard Impact Test results was conducted with Eqs. F-5 through F-7, the typical hopper carbody properties given in Figure 11, and the effective weights of the striking consists given in Table E-1. Details of the calculations appear in Table F-1.

The results of the regression are as follows:

$$\hat{\beta} = 8.11 = \tan\hat{\theta} \qquad \hat{\theta} \cong 83°$$

$$\hat{\varepsilon} = 1.247 \qquad \hat{e} = 1 - (1 - \hat{\varepsilon})^2 = 0.939$$

$$\hat{\varepsilon}" = 1.016 \qquad \hat{e}" = 1 - (1 - \hat{\varepsilon}")^2 \cong 0.9997$$

The value of $\hat{\theta}$ represents a low-angle glancing impact ($90 - \hat{\theta} \cong 7°$), indicating that initial positive pitch of the carbody brings the forward edge of the "B"-end centerplate up from the bowl before carbody/truck interaction occurs. The values of $\hat{e}$ and $\hat{e}"$ indicate that the inelastic mechanisms absorb virtually all of the energy that is available to be absorbed in the two impacts.

TABLE F-1. SUMMARY OF REGRESSION DATA (N=11)

SERIES and TEST NUMBER	U_2 (ft/sec)	U_1' (ft/sec)	V_1' (ft/sec)	$Am_1\ell^2/I_1$	x_i	y_i	x_iy_i	x_i^2	ω_1' (rad/sec)	ω_1'/U_2
3.2	21.9	20.6	4.30	1.1711	1.1016	.22994	.25330	1.2135	0.547	.002498
3.3	24.2	28.2	7.66	1.1711	1.3647	.37069	.50588	1.8624	-.0194	$-.0_3802$
3.4	22.6	27.05	5.98	1.1720	1.4028	.31011	.43502	1.9678	.0650	.002876
3.5	24.8	22.3	6.20	1.1720	1.0539	.29300	.30879	1.1107	.0024	$.0_597$
4.1	27.3	26.0	5.84	1.1646	1.1091	.24913	.27631	1.2301	-.0564	-.002066
4.2	28.2	27.5	6.59	1.1616	1.1328	.27145	.30750	1.2832	.0703	.002493
5.1	28.5	28.5	7.67	1.1627	1.1627	.31291	.36382	1.3519	-.0994	-.003488
5.2	27.9	32.0	7.79	1.1627	1.3336	.32464	.43294	1.7785	.1408	.005047
6.1	20.6	19.8	6.32	1.1481	1.1035	.35223	.38869	1.2177	-.0258	-.001252
7.1	26.6	23.15	15.73	1.1477	0.9988	.67870	.67789	0.9976	.2030	.007632
10.1	25.1	34.0	5.48	1.1121	1.5064	.24280	.36578	2.2695	.1107	.004410
REGRESSION STATISTICS					Σx_i= 13.2699	Σy_i= 3.6356	Σx_iy_i= 4.31592	Σx_i^2= 16.2829	AVG ω_1''/U_2 =+.001586	
					$(\Sigma x_i)^2$= 176.09024	$\Sigma x_i \Sigma y_i$= 48.244	$\frac{N}{2}\Sigma x_iy_i$= 23.73756	$N\Sigma x_i^2$= 179.1119		

APPENDIX G

ENERGY ABSORPTION BY COUPLERS AND CARBODY

G.1 COUPLER SHANK BENDING

Severe bending of the coupler shanks provides another possible mechanism for absorption of collision energy before the head of a tank car is truck. This mechanism is of particular interest for tank cars equipped with shelf-E couplers, which may prove to be more successful than standard-E couplers at engaging the couplers of a loose car.

First, consider the coupler shank material in terms of its ability to absorb energy per unit volume. This property can be estimated from a bilinear approximation to the elastic-plastic stress-strain curve (Figure G-1) as:

$$E^* = \frac{1}{2}\left[(s_y+s_u)\,\varepsilon_u - \frac{s_y s_u + 2s_y^2}{K}\right] \qquad \text{(G-1)}$$

where s_y is the material yield strength, s_u the ultimate strength, ε_u the ultimate strain, and K the elastic Young's modulus. The following values are typical for a low-strength AISI-1020 hot-rolled steel [34], which should reasonably represent coupler shank material:

$s_y = 43 \times 10^3$ psi $s_u = 65 \times 10^3$ psi

$\varepsilon_u = 0.36$ $K = 30 \times 10^6$ psi

Substitution of these values in Eq. G-1 leads to:

$$E^* \cong 19 \times 10^3 \text{ in.lb/in.}^3 \qquad \text{(G-2)}$$

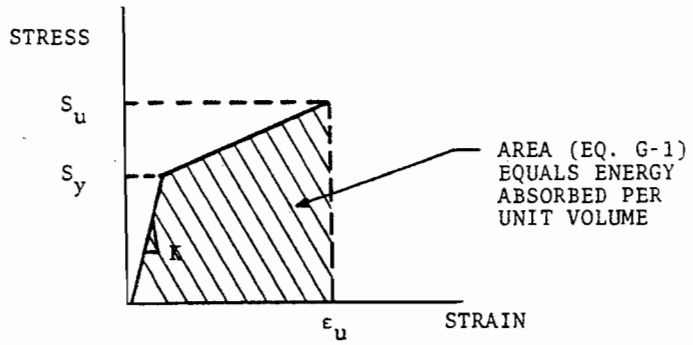

FIGURE G-1. APPROXIMATE STRESS-STRAIN CURVE

When engaged couplers failed by bending in the Switchyard Impact Tests, the bending was observed to be nonuniform, a plastic hinge usually occurring toward the knuckle-end of the shank. Figure G-2 illustrates the approximate dimensions of a type B-E67-HT standard-E coupler shank [28], and indicates the approximate location and extent of the plastic hinge region. The volume of this region is found to be 92.8 cubic inches.

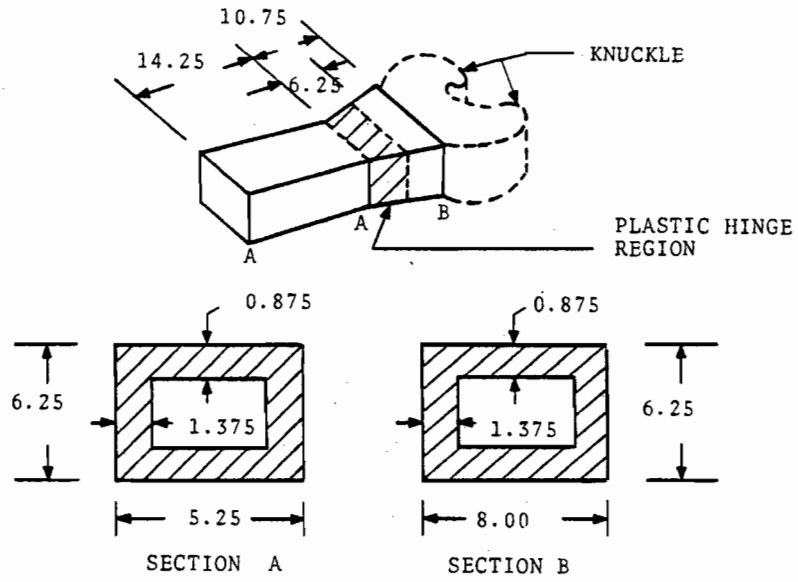

FIGURE G-2. STANDARD-E COUPLER SHANK (INCHES)

Combination of the foregoing estimates leads to the following energy-absorption estimate, assuming that two shanks are severely bent:

$$E = 2E^* \text{ (Volume)} \cong 2\text{x}19\text{x}10^3\text{x}92.8 = 3.53\text{x}10^6 \text{ in.lb}$$
$$E \cong 2.94\text{x}10^5 \text{ ft lb} \qquad \text{(G-3)}$$

On the other hand, a typical "severe" switchyard impact might be represented by a 16 mph (23.5 ft/sec) collision with a tank car weighing 329 KIPS, i.e., an initial kinetic energy of:

$$E_i = \frac{1}{2}\left(\frac{W_2}{g}\right)(U_2)^2 = \frac{3.29\text{x}10^5 \text{ x } (23.5)^2}{2\text{x}32.2} = 2.82\text{x}10^6 \text{ ft lb}$$

Thus, it is seen that:

$$E/E_i = \frac{2.94 \text{ x } 10^5}{2.82 \text{ x } 10^6} \cong 0.104$$

i.e., at most about 10 percent of the initial kinetic energy of the striking car can be absorbed by breaking one pair of coupler shanks.

G.2 CARBODY BUCKLING

Buckling of the hopper carbody can be characterized as a large-deflection/small-strain phenomenon, with strains of the order of 0.01 inch/inch. However, the large volume of material that participates in the process makes carbody buckling a much more significant mode of energy absorption than the bending of coupler shanks.

This can be demonstrated with an order-of-magnitude estimate by assuming that the entire weight of carbody material (22.84 KIPS) experiences 0.01 strain during buckling:

$$\text{Volume} = \frac{22.84 \text{ x } 10^3 \text{ lb}}{0.28 \text{ lb/in.}^3} \cong 8.16 \text{ x } 10^4 \text{ in.}^3$$

$$E^* \cong 43\text{x}10^3 \text{ psi x } 0.01 = 4.3\text{x}10^2 \text{ in.lb/in.}^3$$

$$E = E^* \text{ (Volume)} \cong 3.51\text{x}10^7 \text{ in.lb} = 2.92\text{x}10^6 \text{ ft lb}$$

Thus, it is seen that the energy which may be absorbed by inelastic buckling of the hopper carbody is the same order of magnitude as the initial kinetic energy of a striking car.

110 copies